Designer peptide markers towards multifunctional nanoprobes for cellular targeting at the nanoscale

Paulina Dominika Rakowska

Department of Chemistry
University College London
&
Bioengineering
National Physical Laboratory, UK

Thesis submitted for the degree of
Doctor of Philosophy at the University College London

June 2014

The work presented in this thesis is my own. Where information has been obtained from other sources, this has been clearly indicated in the methodology section of the thesis.

Paulina D. Rakowska

ACKNOWLEDGMENTS

I would like to thank my supervisors, Dr Maxim Ryadnov from National Physical Laboratory and Dr Stefan Howorka from UCL for their guidance throughout this project. I would like to acknowledge everyone, who contributed to this research with their work, expertise and advice – big 'thank you' to Eleonora Cerasoli, Santanu Ray, Mateusz Szymanski, Lloyd Ryan, Angelo Bella, Haibo Jiang, Jascindra Ravi, Alice Payne, Bill Cooley, Mark Turmaine and Prof. Chris Grovenor. I would like to thank Prof. Ian Gilmore for being such a wonderful friend. I am grateful to my partner Mariusz for his love and support. Finally, the biggest 'thank you!' to Baptiste Lamarre – a true scientist, for his enthusiasm, curious spirit and never-ending willingness to listen, discuss and help.

ABSTRACT

The project investigated the development of peptide-based nanotools for applications in cell biology. Differential intracellular and membrane targeting was probed using rationally designed cell penetrating and antimicrobial peptides.

The interaction of the peptides with bacterial and mammalian membranes was imaged using a combination of atomic force microscopy (AFM) and high-resolution secondary ion mass spectrometry (NanoSIMS). This approach provided unique information on the topography of peptide-treated membranes, obtained from AFM images, suggesting membrane changes as a result of peptide structuring and pore formation. The data was complemented by chemical imaging performed on the same samples with NanoSIMS, which revealed the precise localisation of peptide molecules in the membranes.

In parallel, multidimensional protocol for tag-free quantification of cellular uptake of cell penetrating peptides, based on chromatographic separations and followed by isotope dilution mass spectrometry was developed. The amount of the designed peptide, internalised by human dermal fibroblasts was evaluated and compared to the uptake of a broadly studied and well characterised naturally occurring peptide. The results were compared to the peptide uptake quantified using confocal fluorescence microscopy.

The studied synthetic peptides were also investigated as model systems to functionalise metallic nanoparticles (NPs). Characterisation and functionalisation of the NPs were carried out. To prevent a non-specific physisorption of molecules, the surface of NPs was passivated by coating with lipid bilayer or polyethylene glycol. Finally, using cross-linking chemistry, the designed peptides were conjugated to the coated particles and their interaction with mammalian and microbial cells was investigated by transmission electron microscopy.

The results of this work indicate that rationally designed peptides carry the potential for being employed in the development of nanoscale, multifunctional probes for differential and specific intracellular and extracellular targeting.

TABLE OF CONTENTS

LIST OF FIGURES

ABBREVIATIONS

ACCA	α-cyano-4-hydroxy-cinnamic acid
AFM	Atomic Force Microscopy
AgNPs	Silver Nanoparticles
AMP	Antimicrobial Peptide
ASV	Anodic Stripping Voltammetry
AU	Absorbance Units
AuNPs	Gold Nanoparticles
ACN	Acetonitrile
CD	Circular Dichroism
CID	Collision Induced Dissociation
CPP	Cell Penetrating Peptide
DHB	2,5-dihydroxybenzoic acid
DIPEA	Diisopropylethylamine
DLPC	1,2-dilauroyl-*sn*-glycero-3-phosphocholine
DLPE	1,2-dilauroyl-*sn*-glycero-3-phosphoethanolamine
DLPG	1,2-dilauroyl-*sn*-glycero-3-phospho-(1'-rac-glycerol)
DLS	Dynamic Light Scattering
DMPC	1,2-dimyristoyl-*sn*-glycero-3-phosphocholine
DNA	Deoxyribonucleic acid
DPPTE	1,2-dipalmiotyl-*sn*-glycero-3-phosphotioethanol
ESI	Electrospray Ionisation
FA	Formic Acid
HDFa	Human Dermal Fibroblasts
HPLC	High-Performance Liquid Chromatography
HSI	Hue Saturation Intensity
IEX	Ion Exchange Chromatography
LD	Linear Dichroism
MALDI MS	Matrix-Assisted Laser Desorption / Ionisation Mass Spectrometry
MDLC-MS	Multidimensional Liquid Chromatography – Mass Spectrometry
MS	Mass Spectrometry
NA	Nucleic Acid

NanoSIMS	High Resolution Secondary Ion Mass Spectrometry
NP	Nanoparticle
PBS	Phosphate Buffer Saline
PEG	Polyethylenglycol
RP-HPLC	Reversed-Phase High Performance Liquid Chromatography
SA	Sinapinic Acid
SEC	Size Exclusion Chromatography
SIMS	Secondary Ion Mass Spectrometry
SMCC	Succinimidyl 4-[N-maleimidomethyl]cyclohexane-1-carboxylate
Sulfo-SMCC	Sulfosuccinimidyl 4-(N-maleimidomethyl)cyclohexane-1-carboxylate
TCEP	Tris(2-carboxyethyl)phosphine
TEM	Transmission Electron Microscopy
TFA	Trifluoroacetic Acid
UV Vis	Ultraviolet and Visible

CHAPTER 1

BACKGROUND

This chapter is based on extracts from two review articles: (1) “Peptidome analysis: tools and technologies”; P D Rakowska, M G Ryadnov in Amino Acids, Peptides and Proteins; E Farkas, M G Ryadnov; *RSC Publishing* 2013, 38, 172-202; and (2) “Nano-enabled biomarker discovery and detection”; P D Rakowska and M G Ryadnov; *Biomarkers in Medicine*, 2011, 5(3), 387-96. Full versions of the articles can be found in ‘Publications from the project’ section of this thesis.

1.1. Introduction

In the era of ‘-omics’ strategies the information that can be obtained from the peptide content of biological systems has become of a great importance. The peptidome of a cell, tissue or even entire organism comprises all kinds of peptides, which occur either as ‘stand-alone’, functional species such as growth factors, hormones or metabolic products originating from protein precursors, or are products of metabolic processes and proteolytic degradation.

Peptidomics presents an area of thorough, comprehensive and systematic qualitative and quantitative analyses of peptides. The analyses are varied and include peptide identity, quantity, structure and function. They span from simplest biochemical methods to advanced multidimensional separations and bioinformatics-empowered mass spectrometry.

Peptides can serve as biomarkers but can also be used as templates in chemical biology for creation of novel peptide-based tools. The acquired knowledge, together with recent advancements in nanotechnology, provides opportunities to establish novel, sensitive, and selective methods for a wide range of bioanalytical platforms.

Below is a brief overview of well-established peptidomic processing and introduction to tools, methods and approaches for the characterisation of peptides from biological media. Particular attention is given to the development of nanotechnology-enabled platforms for peptide analyses as well as synthetic

peptides as a means for constructing specially engineered tools for peptide-mediated cellular targeting.

1.2. Naturally occurring peptides

Peptides present the most abundant class of molecules in biological systems. They can be defined as amino-acid assemblies, which contain no more than around 50 amino-acid residues and with molecular weights up to 8 kDa.[1] These low-molecular weight bio-regulators are critical to many biomolecular processes.

Naturally biosynthesised peptides can be divided in to two classes: (1) Protein precursor derived peptides, formed in all organisms by proteolysis and subsequent posttranslational modifications, such as acylation, amidation or epimerisation of inactive protein precursors;[2-5] (2) Those that are produced by synthetases,[6-8] specialised enzymes, that use amino- or hydroxyl-acid building blocks, which allows for the incorporation of unusual amino-acid residues, into the peptide structure, that are not encoded genetically.[9, 10]

Each tissue consists of a limited set of peptide compounds. Also, the content of protein components in the tissue shows relative specificity of proteolysis. The proteolysis of protein sets of a given tissue will result in a large group of peptides, defined as a "tissue-specific peptide pool."[11, 12]

Research shows that extensive number of a given pool components can present noticeable activity both *in vitro* and *in vivo*. This points to the potential regulatory role of peptides in an organism. Generally, there is hardly a process that does not involve a presence or could not be influenced by a peptide.[13] Also, the peptide composition undergoes changes as a result of tissue pathology, stress impact, treatment with drugs or genetic modifications. Based on the above, the thorough understanding of the effects on the peptide pools, caused by malfunctioning biological systems becomes extremely vital. As a result, the biological potential of peptides attracts an increasing attention in academia and industry and prompts the continuous development of new strategies and tools to enable peptidomic analysis of specific biological matrices.

Peptides can provide excellent biomarkers. This is the case even when their biological activity is unambiguous or not apparent. Being mere products of proteolytic degradation peptides can be indicative of a particular pathology or

a developing process, whilst being highly specialised molecules they can possess different functions at different levels of molecular recognition and organismal development. For example, antimicrobial peptides (AMPs), which are evolutionarily conserved host defence effector molecules, not only can recognise and kill microorganisms but also elicit immunomodulatory effects and serve as stand-alone protein transduction domains. AMPs have been shown to play inhibitory and mediatory roles in combating and containing various disorders ranging from atopic dermatitis,[14, 15] inflammations[16-18] and wound healing[19, 20] to autoimmunity[21, 22]and cancers.[23-26]

1.3. Synthetic peptides

Peptides can be seen as unique and powerful chemical tools. It is not only due to the natural diversity of amino-acid building blocks, but also due to the different types of modifications that are possible at an individual residue level.[27]

As opposed to proteins, peptides are relatively easier to work with as they do not pose a higher order or complex secondary structures. Therefore, virtually complete exposure of their reactive groups to solvent is possible. This allows for straightforward modifications of the reactive sites, such as group-specific labelling or for chemical depletion approaches. These modifications can affect the chemical structure of a peptide, its conformation and activity. Being able to introduce post translational and chemical modifications to the peptides makes their use very attractive in the entire range of biology-based research.[27]

It is possible, nowadays, to chemically synthesise complete, functional peptides such as hormones or antibiotics. The development of synthetic peptides can be, for example, used to create novel, alternative diagnostic assays, such as the widely used peptide microarrays (peptide chips)[28, 29] or as the one described by Real-Fernández et al.[30], who produced ferrocenyl glycopeptides, which can be used as electrochemical probes to characterise autoantibodies as biomarkers of multiple sclerosis, demonstrating that the autoantibodies are detectable with sensitivity comparable to ELISA methods. Here synthetic peptides are not targeted biomarkers as it would be for endogenous peptides but rather an auxiliary means for the detection and capture of other biomarkers, be these proteins, lipids or carbohydrates. Given that capturing peptides act as baits or epitopes and are

usually displayed on surfaces or used as conjugates with molecular reporters, their role in peptidome analyses is that of a probe. This type of probe can be defined as a known entity with known specific function, deliberately introduced into a peptidome to target and reveal a molecular mechanism or endogenous biomarker or to capture and help isolate the latter.

Uses of peptide-based probes and tools are various and include targeted drug and gene delivery,[31, 32] antimicrobials, neurodegenerative and neuroendocrinology research, regenerative medicine and synthetic biology.[174, 175] The main challenge facing scientists in this field is to be able to rationally design peptides in order to gain control over their physical properties. This requires detailed understanding of the intended application as well as depth knowledge of the peptide at its all length scales.

One of the most efficient approaches in synthetic biology is to emulate naturally occurring motifs. Here, available set of the first design principles is used and extended, linking peptide structure and function. Additional manipulations to the amino acid sequence are based on further or refined rules, provided by through intuitive and empirical designs as well as computational analyses. Targeting specific function determines the nature and structure of a given design, but often it is the delineation of closely related functions that require subtle tuning in the sequence, backbone or side chains. For example, generic peptide sequences can be designed to provide cell penetrating and gene delivery properties, thus promoting the uptake and intracellular release of DNA and enabling expression of target proteins,[32] and can be tailored for differential membrane binding enabling related functions of endosomal release and antimicrobial responses.[33]

Endogenous antimicrobial peptides are often used as biomarkers in peptidomics (wound healing monitoring, inflammatory responses). They present an evolutionarily conserved class of the host defence effector molecules. Apart from being promising candidates for next-generation antimicrobials, in the light of emerging antimicrobial resistance, the peptides are extensively being used as structural templates for mechanistic and structural studies at the cellular and systems level, providing convenient interfaces between systems biology and peptidome analysis. Recently, high resolution imaging techniques are being employed to address fundamental questions of peptide interactions with their targets in real time and with nanoscale precision. *De novo* design and nanoscale

imaging, used in combination, were shown to reveal mechanisms that could not be understood using more traditional approaches in structural biology including NMR and crystallography.[33] Somewhat reverse to this approach is the use of *de novo* engineered peptides as tools for targeting native antimicrobial peptides. These peptides cannot bind to membrane surfaces, microbial or mammalian, and are anionic in contrast to cationic antimicrobial peptides, which allows them to bundle with the antimicrobial counterparts into functionally inert coiled-coil heterooligomers (Figure 1).[34] In this format, the peptides act as antagonists of antimicrobial peptides or anti-antimicrobial peptides and can be used as means for capturing endogenous antimicrobial biomarkers.

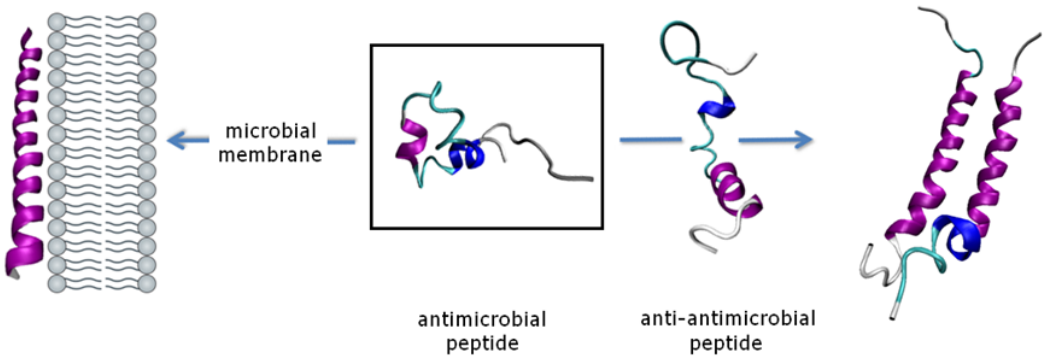

Figure 1. Examplar engineered peptide, portraying two scenarios of antimicrobial peptide action: an antimicrobial peptide binds to microbial membranes and forms membrane-disrupting helical structures (left) or when challenged by an anti-antimicrobial peptide it forms a biologically inert helical complex (right). Adapted with permission from Rakowska, et al., in Amino Acids, Peptides and Proteins; Eds. *RSC Publishing*, 2013, 38, 172-202.[35] Copyright © 2013 Royal Society of Chemistry.

By designing and using such systems one can expand proteome analysis. The elucidation of antimicrobial resistance at the level of specific peptide-lipid interactions with correlative studies of resistant and wild-type bacterial membranes in situ, in vitro and potentially in vivo can be enabled. Importantly, peptidome analysis takes a proactive role in the search of resistance mechanisms from the bottom up, from relatively simple scenarios, such as the expression of neutralising sequences, to more complex routes leading to membrane modifications or re-building.[34]

1.4. Peptidomics

As described above, peptides play central role in physiological processes. They can serve as excellent biomarkers and can be also used as templates in chemical biology for construction of molecular probes. Therefore, there is a need for the continuous development of technologies, which would enable comprehensive analyses of the entire peptidomes of cells, tissues and, in principle, whole organisms. Peptidomics – the area of comprehensive studies of peptides, is strongly related to proteomics, where protein analyses mostly rely on obtaining protein-derived peptide fragments, their analysis and sequencing.[36, 37]

Peptidomics and proteomics share many of the scientific objectives, technologies and techniques. Nevertheless, there are several key differences between these fields. These differences result from the size of peptides, origin, specific modifications and activity. Therefore, the same methods, which are well established to "mine" the proteome, unless altered to the analysis of naturally occurring peptides, often cannot be easily applied for peptidomes. For example, most of proteomic studies use proteolytic enzymes such as trypsin to obtain well defined fragments that can be subsequently analysed by mass spectrometry (MS). In contrast, in peptidomic studies digestive enzymes are scarcely employed as this is the native form of the peptides that is of scientific interest and the size already allows the use of mass spectrometry. Sample preparation for peptidomic studies can be more straightforward without proteolysis; however, data analysis can be more difficult in this case, especially for the analysis of larger peptides and those with multiple post translational modifications or those that contain unusual amino acids. This can influence not only the sensitivity of MS experiments but also affect prediction methods and the understanding of peptide fragmentation patterns in mass spectra.

1.4.1 Peptidomic processing

The analysis of peptides in complex biological samples can prove challenging. One of the difficulties in analysing complex media comes from the wide dynamic concentration ranges of various components in biological matrices. Very often some of the most important analytes are present at very low levels and masked by high abundance biomolecules.[38-40]

A combination of several techniques is almost always required to enable analyses of obscured biomolecules. Several strategies, forming multi-step workflows, have been developed and combined together in order to overcome biological sample complexity. An example of such a workflow is given in Figure 2. It shows major techniques used in peptidomic sample processing. It starts with a sample depletion to remove most abundant proteins, such as albumin and immunoglobulins, which can interfere with the detection of less abundant molecules. This is followed by sample fractionation and purification using chromatographic separations to further reduce the complexity of the sample. Peptide detection and identification is finally carried out by mass spectrometry, supported by computational methods.

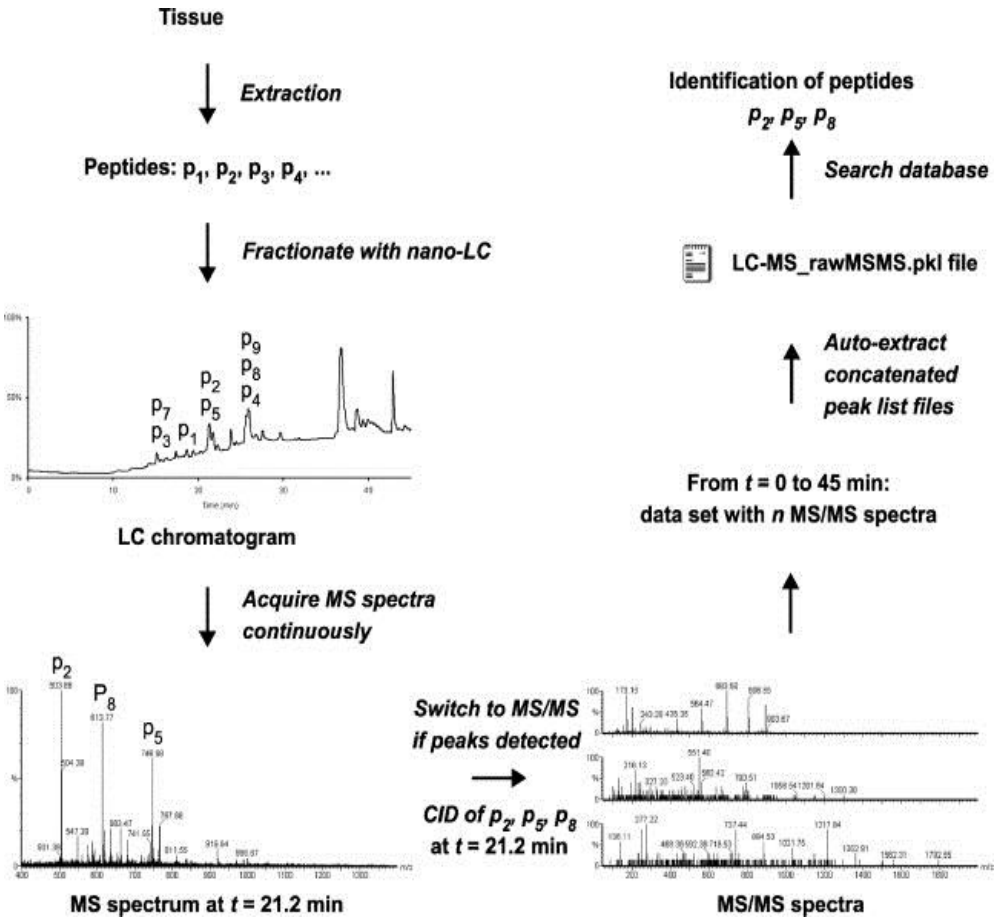

Figure 2. Flowchart of a typical peptidomic process: Tissue sample, after homogenisation and initial clean-up, is processed by nano-LC MS. Mass spectra are acquired continuously during the LC run and mass spectrometer software uses the MS spectrum to decide on peak selection for fragmentation using collision induced dissociation (CID) and MS/MS analysis. The obtained fragmentation spectra are converted to peak lists which are then used for query of a database. Reprinted from Baggerman, et al., *J Chromatogr B*, 2004[41] with permission from Elsevier.

1.4.2 Liquid chromatography – mass spectrometry interfaces

Mass spectrometric techniques are well suited for peptidomic studies. They allow obtaining accurate and reliable information, often in a high-throughput manner. The techniques enable the detection of low-molecular-weight peptides at very low concentrations with adequate resolution and sensitivity which makes them a useful tool for peptidome profiling.

MS techniques can be applied to almost any kind of biomolecules including proteins, lipids, nucleotides and amino acids. However, to be sufficiently sensitive, they require relatively pure samples in certain buffer / solvent compositions. Therefore, multidimensional strategies are nearly always essential in the analysis of biological samples.

Sample clean-up presents, usually, the first step in multidimensional peptidomic analyses. Size-based separations are occasionally employed for the separation of desirable peptide biomarkers or biomarker series. There are reports on successful approaches based on methods such as IEF, GE or even SEC.[42-45] However, they are not exclusive of drawbacks such as the amount of analyte necessary, usually relatively high for successful separations. Also, the nature of this kind of separations makes them efficient mainly for higher molecular weight components (>5 kDa).[46] Therefore, peptidome analyses are based, most often, on gel-free approaches. Additionally, there are many traditional procedures, which can be used, resulting in peptide-rich extracts, such as ultrafiltration,[47-49] the use of trifluoroacetic acid[50] and organic solvent extraction.[51, 52] The choice of a particular purification protocol needs to be carefully thought through and tailored to the specific target molecule.[53]

After initial extraction and enrichment, peptide pools are next introduced to liquid chromatography separations. A multidimensional chromatographic set-up is often employed. Ion exchange chromatography (IEX) presents a conventional method, which enables, in the first instance, separations based on pI values. Nevertheless, anything from immunoaffinity to chemical separations can be successfully applied, i.e. MS-preceding SEC analysis,[43] 2D-Hilic MS,[54] or two-dimensional 2D-HPLC run at basic pH (first dimension) followed by acidic pH (second dimension).[55]

Any salt-containing buffers used to pre-fractionate complex samples can hamper mass spectrometric detection. Therefore, the most common chromatographic step, directly preceding MS analysis, is a reversed-phased liquid chromatography (RP-LC). RP-LC is a MS-compatible technique as it allows setting elution gradients with the use of organic solvents such as acetonitrile with addition of proton donors i.e. trifluoroacetic acid or formic acid. These kinds of solvents are volatile and often promote analyte ionisation, enhancing MS sensitivity.

For the identification of peptides, individual RP-LC fractions are introduced to mass spectrometric analyses. Soft ionisation detection methods, such as MALDI and ESI MS, which rely on the precise measurement of the peptide mass, are preferred. Tandem mass spectrometry, i.e. nESI-TOF-MS/MS or MALDI-TOF/TOF-MS, can provide fragment spectra of the chosen parent ion, which is used to identify a corresponding peptide sequence.

1.4.3 MS-based quantification

Mass spectrometry is an essential tool in peptidomics for detection, identification and characterisation. It also presents the main tool for quantitative peptide analyses. Quantitative approaches can be divided into two categories, those that provide absolute and relative quantification and those that are label-based and label-free (Figure 3). [56, 57]

The strategies of relative quantification[58-60] are based on the comparison between the levels of individual peptides in a sample with those of an identical sample, in which the same compounds have been modified. In a typical experiment, peptides from two experimental samples are isotopically labelled, totally or at specific amino acid positions. Those two samples that contain the equal amounts of peptides are combined and can be analysed by LC-MS. Properties of the individual, differently labelled species coming from both samples remain identical, and hence they co-elute and are detected by MS at the same time. The intensities of corresponding heavy and light peptide ions are then compared for concentration differences.

Label-based methods

There are several methods enabling the use of peptide labels. They include:

- Metabolic labelling, the most common version of which may be stable-isotope labelling in cell culture (SILAC) (Figure 3(A)). This method involves in-vivo

incorporation, during cell growth and division, of a stable isotope labelled amino acid into the proteome/peptidome of the cells, which are added to cell culture media.[61-63] To carry out the relative quantification control cells grown in regular media are used. The main advantage of this method lies in its relatively simple protocol and the minimal manipulation of the probed systems. Nevertheless, this method is almost only appropriate to cell samples and may not be applicable to those that are sensitive towards changes in culture medium composition.

- Chemical labelling (Figure 3(B)) can be applied to samples that cannot be processed with metabolic labelling such as tissues or biological fluids, or when short experimental time is necessary. Many strategies involving chemical or enzymatic stable isotopic labelling have been developed, such as enzymatic labelling with ^{18}O, where tryptic digest is performed in water containing ^{18}O and another in water with ^{16}O. The mechanism of trypsin action incorporates the oxygen atoms at the C-termini of freshly digested peptides.[64, 65] This method however may not be suitable to study endogenous peptides or when the trypsin use is not appropriate. Stable isotope dimethylation is another example of chemical labelling, which involves the labelling of primary amines with deuterated methyl groups by formaldehyde in deuterated water.[66] ICAT (Isotope Coded Affinity Tag) is the most utilised of the cysteine tagging methods.[67, 68] This strategy requires a label composed of three parts: an isotopically labelled (deuterated) linker, biotin group and a cysteine reactant. Once peptides are labelled, they are subjected to column chromatography with immobilised avidin or streptavidin. Then biotin enables separation and enrichment and analysis of cysteine-containing peptides. This method is applicable to these species only.
- Isobaric tagging with reagents such as iTRAQ (Figure 3(C)).[69-71] It requires analysis with tandem mass spectrometry because isobaric tags have identical masses and chemical properties. Therefore, there is no distinction during the LC and MS runs. During MS/MS experiment, in the collision cell when the peptide parent ion collides with gas molecules, the tags are cleaved from the peptides. The peptide ions are sequenced and the tags are quantified. This allows the simultaneous determination of both the identity of the analytes and their relative abundance. Because the MS/MS is set up only for the tag detection unlabelled peptides are not quantified.

Label-free methods

Label-free quantification methods are used for both relative and absolute quantification.[59, 72, 73] These methods are also well suited for high-throughput screening and biomarker discovery experiments. They do not require control or differently labelled samples. Samples are prepared independently and analysed by LC-MS or LC-MS/MS. Nevertheless, the lack of controls imposes planned carefully, controlled and reproducible processes to avoid experimental variations.

In instances where ion signal intensity correlates with peptide concentration, as for example in electrospray ionisation experiments, the quantification of peptides can be performed taking into account ion intensity. These quantitative approaches are exclusively based on LC-MS and the relative levels of peptides between analysed samples can be directly estimated from the peak intensities (Figure 3 (E)).

Another type of label-free relative quantification is executed using spectral counts. This method requires tandem-MS set up and involves the comparison of the sum of MS/MS spectra originating from a peptide of interest across multiple samples, which correlates with the analyte abundance.

Absolute quantification[74-76] is possible by a label-free approach. This approach requires the preparation and incorporation of internal standards – isotopically labelled, heavy analogues of the probed peptide, which are spiked at known concentrations into the experimental sample (Figure 3(D)). The spiked sample is next subjected to processing by LC-MS. Though having different masses, chemically the peptides are identical. Therefore, they co-elute and are analysed by MS simultaneously. The abundance of the target peptide ion is compared to the abundance of its isotopically labelled analogue in the analysed sample and the quantification is performed with the use of a prior-built standard curve. A neat example is an isotope dilution approach for the quantification of cellular uptake of cell penetration peptides (CPPs) as described by Burlina, et al.[77] This method uses magnetic beads for peptide harvesting followed by direct peptide analysis by MALDI MS. Quantification is achieved using a deuterated analogue of the analysed CPP as a standard (Figure 4).

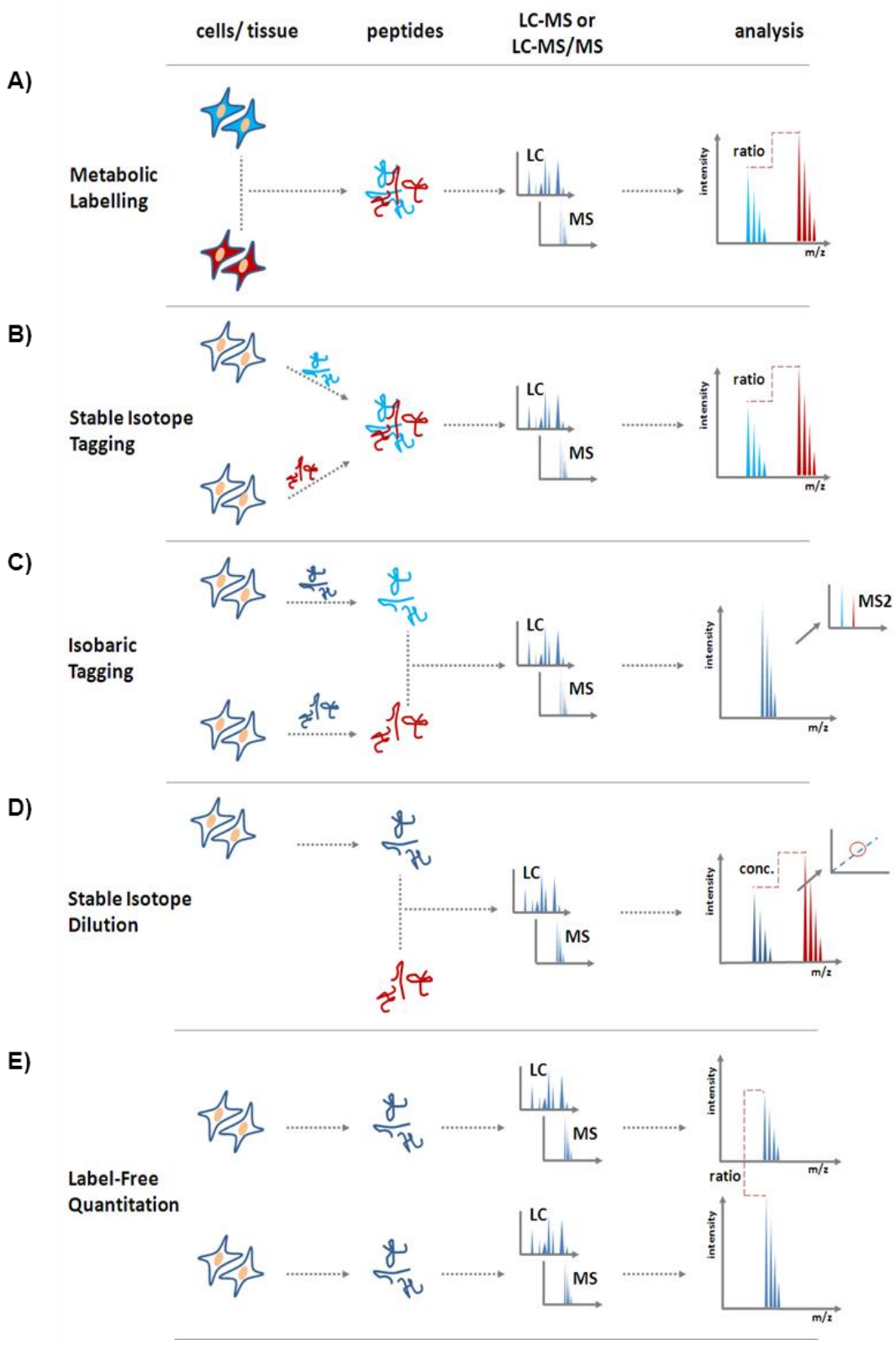

Figure 3. Overview of quantification workflows. The points, at which peptides are labelled, or at which isotopically labelled analogues are used, are indicated by colours blue and red (heavy). Metabolic labelling takes place *in vivo.* Reprinted with permission from Rakowska, et al., in Amino Acids, Peptides and Proteins; Eds. *RSC Publishing*, 2013, 38, 172-202.[35] Copyright © 2013 Royal Society of Chemistry.

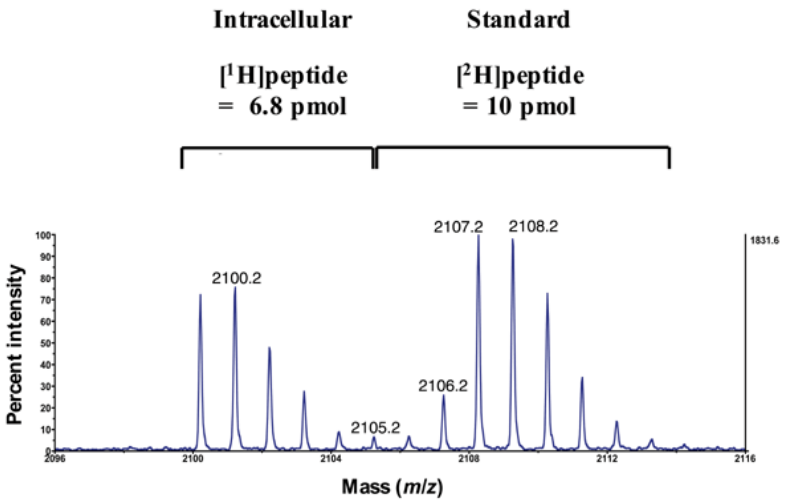

Figure 4. MALDI mass spectra presenting the results of isotope dilution-based quantification. The first isotope of the signals is identified for both [1H]peptide (m/z = 2,100.2) and [2H]peptide including the component with eight deuteriums (m/z = 2,108.2) and the non-completely deuterated components (m/z = 2,105.2, 2,106.2 and 2,107.2). Signals including all isotopes as delimited in the figure are taken into account in the quantification. Adapted with permission from Burlina, et al., *Nat Protoc,* 2006.[77] Copyright © 2006 Nature Publishing Group.

Absolute peptide quantification would be an ideal outcome. However, the relative quantification approaches are used more often. There are several reasons for that. This method is mainly limited to analysis of one analyte at a time and does not allow monitoring changes in abundance of several compounds in one sample simultaneously. Often time-consuming assay development has to be carried out for any peptide of interest and fabrication of isotopically labelled reference molecules can be often expensive due to costly reagents. Nevertheless, the choice of quantification method is dictated by the molecule in question and the type of biological samples to be analysed. Where the analyte to be quantified is well defined, such as the example of the detection of a single peptide biomarker, or when a defined marker is introduced to the system (as described further), methods based on isotopic labelling seem to be most advantageous. Firstly, the application of absolute quantification can be performed. But most importantly, when probing biological samples in the search for real answers, it is often crucial to retain the physico-chemical properties of both the analyte and the analysed samples. Isotopic labelling, regardless of the choice of the set up (label-free versus label-based), when properly designed and executed, should have no influence and should not invoke

any alterations to the natural behaviour of the analysed system, as is often the case with other tagging ligands.

1.5. Systems biology

Together with genome sequencing and the emergence of high-throughput analytical technologies an area of systems biology has emerged. This inter-disciplinary field seeks to explain biological processes using frameworks of complex interactions describing biochemical and cellular modules within an individual cell or an organism. 'Omics' technologies, which encompass genomics, transcriptomics, proteomics, metabolomics, lipidomics, glycomics and many others, existing and emerging, make it possible to collect and analyse comprehensive data sets on intricate biological processes.

Some see peptidomics as a complementary branch of proteomics. As aforementioned, many similarities between these two fields exist. However, it is best to see peptidomics as a discipline that complements proteomics by creating a bridge between proteomics through degradomics to metabolomics, even though endogenous peptides are not necessarily associated with proteome degradation. For other related "-omics" approaches, for example peptidoglycans and lipopeptides, which can fall under glycomics and lipidomics, respectively, the emphasis is equally split between the variabilities of glycans and lipids and the peptide sequence constitution. It is therefore common to relate different "-omics" capabilities with appropriate weighing of information obtained by a specific discipline.

There are obvious overlaps as well as links between different complex "-omics" disciplines. One example could be the combination of lipidomics studies with peptidomics, addressing molecular processes underlying the action of membrane-active peptides. Lipidomics data, concerned with the composition of biological membranes, aid understanding of how the peptides distinguish between mammalian and bacterial cells and how the lipid spectrum and membrane architecture influence the primary role of those peptides.

Systems biology addresses the links between "-omics" disciplines. It integrates complex data from multiple experimental sources. Starting from the understanding of the genetic information through the variations in the code, gene expression,

nucleic acid-protein binding, to molecule-molecule interactions, the networks of relations and dependence can be built, which would enable a deeper understanding of the underlying molecular biology of a given physiological state or process.[78, 79]

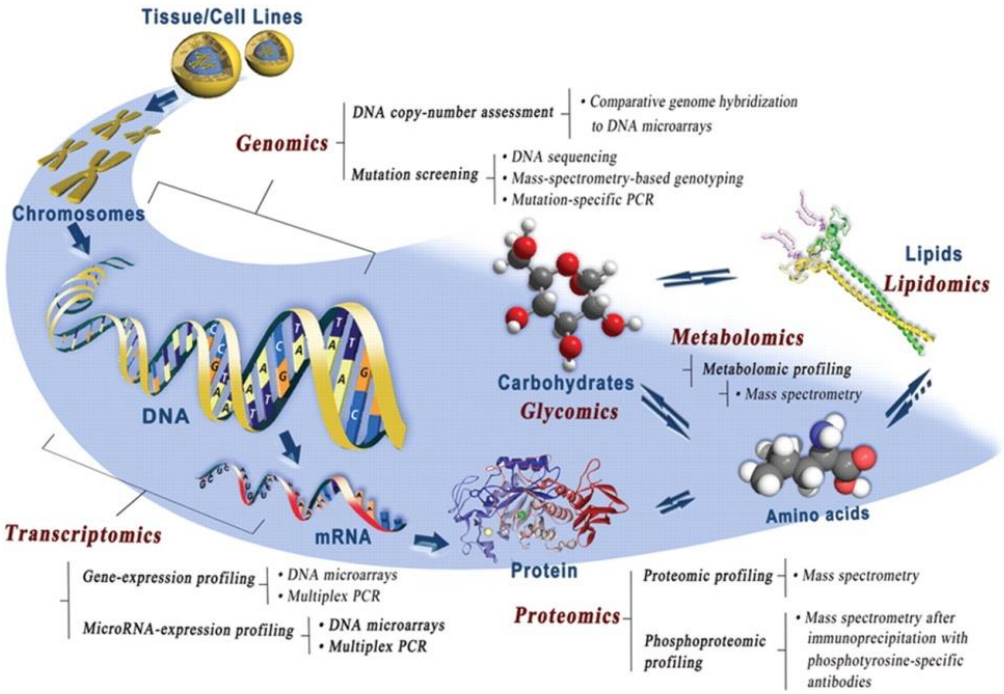

Figure 5. Schematic representation of a model of the "-omics" technologies landscape including examples of corresponding analytical subjects, and applied methods; DNA (genomics) undergoes transcription to mRNA (transcriptomics), which is next and translated into protein (proteomics). Proteins assist catalytic reactions resulting in metabolites (metabolomics), glycoproteins and carbohydrates (glycomics), and various lipids (lipidomics). Reprinted with permission from Wu et al., *J Dent Res*, 2011.[78] Copyright © 2011 Int. & American Associations for Dental Research.

1.6. Nanotechnology-enabled tools

With the growing demand for high-throughput methods, applications based on nanotechnology have a great exploitation potential and are resulting in a development of new technologies in different sectors of life science, including the diagnostic and peptidomic / proteomics fields.

Nanomaterials offer efficient agents to overcome persistent deficiencies of conventional methods in, for example molecular diagnostics and medical imaging. The interest for nanomaterial use and further development has been steady over the last two decades and has just begun its expansion into other areas including

peptidomics and proteomics. Clearly, the variety and repertoire of nanomaterials that can facilitate peptide / protein biomarker detection, to the point of clinical implementation, is not limited to one single class. Examples may include nanoscale particles, wires and tubes and their nano arrays. Primary attention here is given to the ability of a specific nanotechnology to refine or extend detection limits, which would otherwise require complex and cost-ineffective optic or immuno-based technologies. In this respect, the chemistry and morphology of a particular material play an auxiliary role and are important from the perspective of a specific experimental set-up. For example, carbon nanotube arrays assembled on the tips of molecular-imprinting sensors used in combination with electrochemical impedance spectroscopy can detect proteins with subpicogram per litre sensitivity,[80] whilst nanowire gated transistors or label-free nanomechanical cantilever sensors can be constructed for the detection of multiple and real-time binding events, which can enable multiplex biomarker detections.[81, 82]

1.6.1 Nanoparticles

Among the nanoscale materials the use of nanoparticulate systems appears to be predominant. Because of their universal and unique physico-chemical properties, nanoparticles are most attractive candidates for proteomics.[83-86] Specifically, their large surface-to-volume ratios ensure much faster reaction rates when compared to those of polymeric, colloidal, inorganic bulk or monolithic materials. The porosity of porous particles can be controlled to substantially enhance adsorption, and their surfaces can be tailored by chemical modifications to allow the fabrication of selective adsorbents.[87-90] These properties combined facilitate the capture and detection of specific analytes from biological fluids at subnanomolar concentrations.

Two main strategies are being followed for the development of nanoparticle-based analytical probes.[91] The first strategy relies on surface-tailored nanoparticles aiming at simplifying complex samples prior to analysis (Figure 6 (a)). This can be done with the help of nanoparticles coated with either porous materials or ionic functional groups enabling size- and charge-dependent fractionation of multi-component samples, respectively.[91-93] The nanoparticle fraction, carrying the captured molecules, is separated from the depleted fraction of the sample. In this format, either fraction may contain the target analytes, which are easier to

identify. However, isolating molecules of interest from media tends to be favoured, particularly given that the captured analytes can be directly eluted from the nanoparticles for subsequent analysis by mass spectrometry or electrophoresis. Alternatively, nanoparticles can be analysed directly and in some instances, for example in laser desorption ionisation mass spectrometry (LDI MS) methods, the direct measurement of nanoparticles can improve the signal-to-noise ratios.[94-97]

The second strategy (Figure 6 (b)) encompasses the covalent conjugation affinity tags to nanoparticles in order to selectively target individual analytes. Tagged nanoparticles have shown promise in various applications including molecular therapy, diagnostics and catalysis. Owing to their intrinsic polyvalency and relative uniformity in size and morphology these nanoparticles can provide a variety of functions ranging from direct traversal across biological membranes to multiple targeting and amplified sequestration.[98-101]

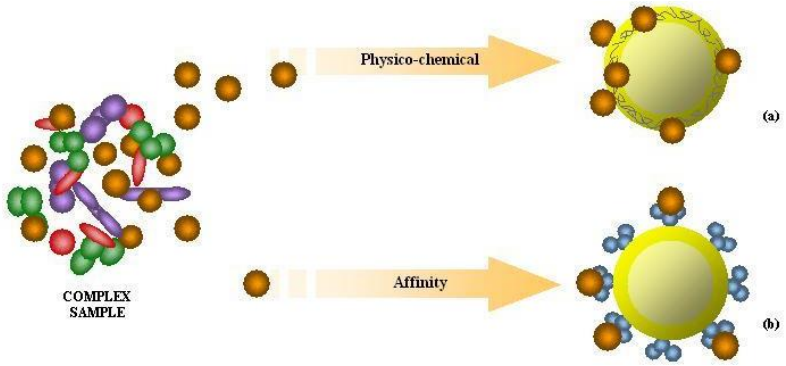

Figure 6. Cartoon portraying biomarker harvesting from a complex sample by surface-tailored (a) and affinity tagged (b) nanoparticles. Reprinted with permission from Rakowska et al., *Biomarkers in Medicine*, 2011.[102] Copyright © 2011 Future Medicine Ltd.

The use of nanoparticles imposes certain drawbacks. Most nanoparticles used for analyte capture or detection are polymeric or metallic colloids whose surfaces may adsorb plasma proteins leading to aggregation or undesired phagocytosis, if performed in tissues or in vivo. Surface modifications by charged or lipidic moieties can be sufficient to circumvent these drawbacks. However, the challenge remains and in some cases there are requirements for oriented immobilisation of biomolecules in order to preserve and sustain their folding-mediated function. Nevertheless, recent successes in the development and application of nanoparticle-based platforms are notable and some of them highlighted below.

1.6.2 Nanoparticles for biomarker diagnostics

An excellent example to introduce the utility of nanoparticle-based technology is a platform developed by Liotta and co-workers.[103] The technology uses "smart" nanoparticles – hydrogel particles engineered to selectively harvest classes of biomolecules from biological fluids such as plasma and urine.[103-105] Highly porous particles constructed from poly(*N*-isopropylacrylamide) were shown to serve as molecular sieves discriminating sample components according to their size. The porosity of the particles was tuned to capture molecules with sizes < 20 kDa. Peptides and small proteins in this molecular weight range are not accessible in sufficient yields by electrophoretic or chromatographic methods. Such a cut-off in pore sizes corresponds to a certain degree of cross-linking within the particles, which can be empirically controlled. Hydrogel nanoparticles proved to exclude high abundance molecules (i.e. albumin) and to sequester proteins of smaller sizes. Although efficient and consistent with the design, poly(*N*-isopropylacrylamide) particles cannot guarantee the full depletion of sample solutions from target analyte because the analyte concentrations in the particles remain in equilibrium with those in the bulk solution. To address this, the particles were modified to incorporate affinity baits to prevent the escape of captured molecules back into solution (Figure 7).[103] By incorporating anionic tags it was possible to select cationic species, while enhancing their uptake leading to significantly higher concentrations in the particles. Thus, the system is particularly appealing since it can be tailored for specific requirements simply by varying its chemistry and the degree of cross-linking, and it can enable encapsulation and enrichment of low molecular weight fractions from complex samples and their simultaneous enzymatic protection against degradation during subsequent sample treatments. The platform has been validated for harvesting human growth hormone from urine samples[104] and platelet derived growth factor from serum.[105]

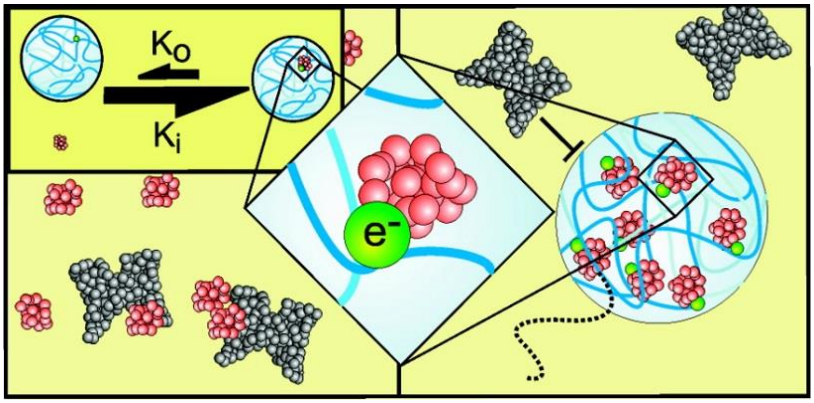

Figure 7. Concept of size- and charge-based biomarker harvesting by engineered gel nanoparticles. Only the passage of positively charged and low molecular weight molecules is endorsed. Reprinted with permission from Luchini, et al., *Nano Letters*, 2007.[103] Copyright © 2008 American Chemical Society.

Most recently, a different protocol for using hydrogel nanoparticles was proposed by Cerasoli, Rakowska *et al.*[106] The authors proposed direct mass-spectrometric analysis of analyte-loaded gel particles without eluting the captured molecules from the nanoparticles. The design of the MIS-MALDI (Microgel Selected MALDI) platform was set off from two main criteria: (1) to afford low detection levels of specific analytes in multi-component media, a physicochemical means for harvesting and enrichment had to be introduced, and (2) the chosen means had to allow on-probe analysis of captured analytes at standard MS conditions. Gel particles were able to extract target proteins, such as human growth hormone, from complex media according to their size (<30 kDa) and isoelectric points (protein pI <6.5).

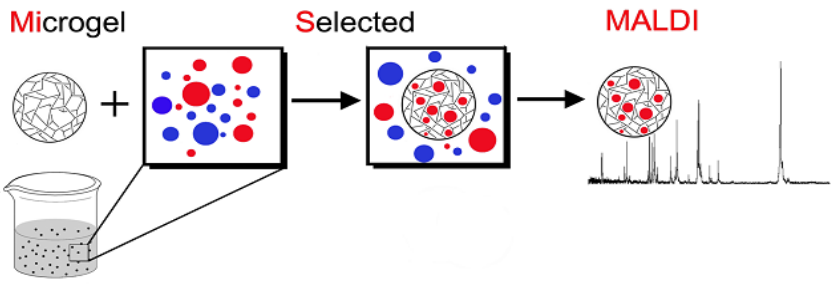

Figure 8. Diagram of MiS-MALDI. Microgel particles are dispersed in a multi-component protein solution to harvest protein biomarkers, which are selected by their size and charge (pI). The loaded particles are isolated and analysed by MALDI-ToF MS. Reprinted from Cerasoli, Rakowska, et al., *Mol Biosyst,* 2010[106] with permission from the Royal Society of Chemistry.

These types of approaches, allowing on-probe detection offer considerable throughput in areas such as biomarker discovery. However, the strategies work well only for the ‘‘class specific’’ selection of biomarkers. Nevertheless, they could be taken further, as the chemical composition of the gel particles can readily be tailored to meet more selective discrimination of different biomarker types. For example, nanoscale systems for a specific peptide binding can be designed using functionalised polymer particles possessing high affinity for biomacromolecular toxins (melittins) with simultaneous neutralisation of their toxic effects. Co-polymeric nanoparticles constructed from different functional monomers were shown to be able to capture and neutralise the toxicity of melittin even in a complex biological milieu (Figure 7). [107]

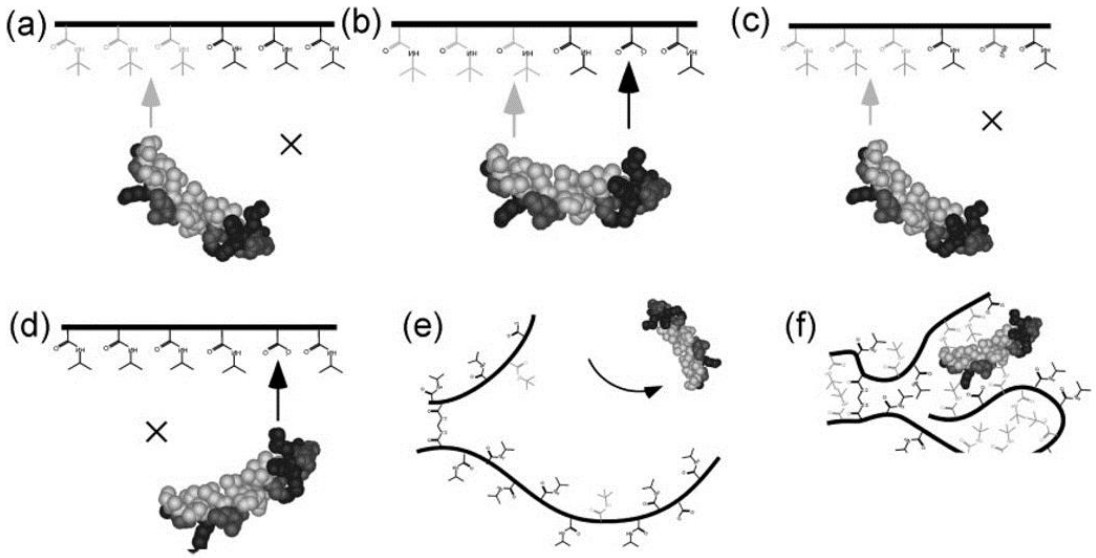

Figure 9. Melittin–NP interaction: Contributions of hydrophobic (light arrow) and electrostatic (dark arrow) interactions between melittin and NPs 7 (a), 6 (b), 2 (c), and 5 (d). Contributions of polymer density to interactions between melittin and NPs 9 (e) and 10 (f). Reprinted with permission from Hoshino, et al., *Small*, 2009.[107] Copyright © 2009 Wiley-VCH Verlag GmbH & Co. KGa, Weinheim.

1.6.3 Multimodal nanoprobes

There is little doubt that the number of similar to the described above technologies will be growing. However, it would be of considerable advantage to develop tools, which would carry more specialised functions. One example for the use of such technologies could be the identification of disease specific

biomarkers. Arguably, major progress has been made in the area of cancer. Two main directions can be identified in the application of nanoparticle-aided assays for cancer diagnostics: 1) the development of tumour-targeting functionalised nanoparticles and 2) nanoparticle-based sensors.

Metallic nanoparticles are an attractive alternative to the mainly "class specific" polymeric particles in the development of highly selective targeting tools. They present a diverse class of materials with size that can be tuned and surface chemistries, which allow their modifications and functionalisation with multiple ligands. In addition, the surface plasmon in metallic particles provides them with remarkable optical properties what yields a wide range of applications in the diagnostics and bio-medical fields.

Multi-modal nanoparticles or multi-modal nanoprobes are nanoparticles functionalised with multiple molecular motifs or tags, each carrying a specific function. Main uses for these particles include tumour targeting and contrast-enhanced imaging. For instance, nanoparticles containing strong contrast agents such as iodinated and gadolinium-based reagents can be used in magnetic resonance imaging or angiography.[108-110] Because contrast agents may be associated with cytotoxicity, their encapsulation is sought to minimise cytotoxic effects. In many instances, coating the particles with inert polymers or lipids proved to be equally efficient, and provided stable and biocompatible probes. The nanoparticle surfaces can then be modified with antimetabolites, integrin antagonists or micronutrients to target or accumulate at cancer sites. A representative example is shown in Figure 10.

The probes of this type can generate strong MRI signals at lower concentrations of contrast agents, efficiently compromise uptake into non-malignant cells, and exhibit increased circulation time and bioavailability. Similar probes can be made based on magnetic nanoparticles, which can provide dynamic contrast agents. When activated by an externally applied magnetic field, these probes can modulate the optical scattering properties of local tissue (tumour) microenvironments allowing local changes monitoring with a displacement sensitivity of a few tens of nanometres.[98, 109]

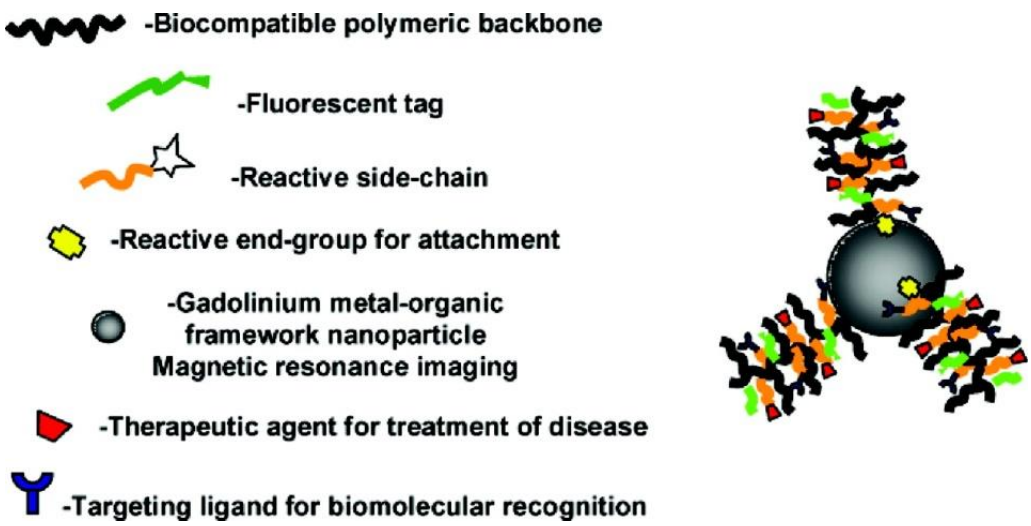

Figure 10. Schematic drawing of a multi-modal nanoparticle for tumour targeting and imaging. Reprinted with permission from Rowe, et al., *Biomacromolecules*, 2009.[111] Copyright ©2009 American Chemical Society.

Nanoparticle-based sensors can provide increased specificity in tumour detection. Metal nanoparticles conjugated to antibodies or ligands that are specific to cellular receptors such as integrins, integrin-associated and growth-factor receptors can discriminatively detect malignant cells, which shed the receptors in soluble forms in amounts exceeding those in normal or dysplastic cells.[112-114] Given that this directly correlates with enhanced invasiveness of malignant cells, nanoparticles with immobilised receptor-recognising moieties are deemed to be efficient tumour-targeting agents. Indeed, engineered nanoparticle sensors display higher (up to an order of magnitude) affinities to cancerous cells than to normal cells thereby making the detection of tumours possible merely by optical microscopy or surface plasmon resonance.[115, 116] If exposed to laser or thermal treatments (i.e. continuous argon ion lasers or alternating magnetic field) the nanoprobes accumulated in tumour sites require only half the energy needed to affect normal cells to destroy cancer cells.[115, 116] The large surface areas of nanoparticles can be exploited for finding optimal agonist-antagonist affinities using, for example, large libraries of receptor-specific peptide ligands diversifying thus both the choice and modalities of nanoparticulate sensors.[117, 118]

1.7. Conclusions

The increasing knowledge of peptidome content and analysis, together with advances in associated techniques, physicochemical strategies, bioinformatics and nanotechnology provides an important insight into the nature and role of peptides and peptide biomarkers in complex biological systems. It can also lead to the creation of new peptide-based technologies with a reach beyond traditional peptidomics applications. New possibilities exist for efficient peptidomic technologies. However, primary attention is still given to the discovery of new predictive peptide biomarker patterns and analyses of endogenous peptides.

Understanding peptidomes and, in particular, peptide-mediated interactions underlying their complexity and diversity, is critical for the development of more reliable and robust analytical platforms. The use of engineered synthetic peptides is still of lesser emphasis in the literature, primarily due to molecular diagnostics approaches and nanoscale technologies that are developed in parallel and inter-relate with peptidomics at the point of mutual applications – the tendency which can be anticipated to develop further. At the same time, there is little doubt, that being once of a specialist chemistry area, the principles of nanotechnology are now being adapted to generate powerful tools aiding various areas of research and medicine. Of immediate relevance in this respect are those approaches that concentrate on the platforms, which carry multiple functions such as multi-modal nanoprobes. The implementation of nanoscale strategies and developments of nano-enabled technologies hold promise for “smarter” tools with various areas of application in life sciences, diagnostics and medicine.

1.8. Aim of the study

Mimicking peptides or producing chemically modified peptide structures with certain properties can be crucial. It could aid the creation of new, nanoparticle-based diagnostic methods as well as targeted drug and gene delivery agents. The goal of the project is to study specialist cellular targeting, using rationally designed membrane-active peptides as ligands for a generic nanoprobe functionalisation. The project serves a long-term view of developing nanoscale peptide probes for applications in cell biology. The development of such probes

requires detailed understanding of functions and properties of their each component.

Firstly, *de novo* designed antimicrobial (AMPs) and cell penetrating (CPPs) peptides are investigated as model systems for differential cellular membrane interactions.

Antimicrobial peptides are postulated to disrupt microbial phospholipid membranes. The principal molecular model of their action is based on the formation of stable or transient pores although the direct observation of the fundamental processes is lacking. This project gives an insight to this process by using a novel approach of nanoscale imaging. The imaging of peptide interactions with microbial membranes, in the form of supported lipid bilayers, is conducted with two surface analysis techniques: atomic force microscopy (AFM) and high-resolution secondary ion mass spectrometry (NanoSIMS). This way topographical information obtained with AFM is complemented with chemical details provided by NanoSIMS.

Cell penetrating peptides can efficiently traverse mammalian cell membranes and deliver various cargo materials. Therefore, CPPs could be used as robust and specific delivery agents or employed create functionalised molecular probes for intracellular targeting. However, the functional efficiency of cargo often depends on the completeness of intracellular peptide uptake. Existing approaches rely on the use of radioactive and fluorescent labels or tags which allow colorimetric, fluorescent or spectrometric detection. Controversies remain regarding discordant results in different studies and the need for artificial labelling, which continue questioning the general applicability of these methods. Therefore, the quantification remains largely unconvincing. Peptidomic processing is implemented in this project to study the uptake of the model CPP. Two-dimensional chromatography followed by isotope dilution MADLI mass spectrometry is performed for the lysates of human dermal fibroblasts transfected with the CPP. The method offers a generic label- and tag-free approach for intracellular quantification, which can be used as a correlative measure for fluorescence-based imaging methods.

Secondly, the development of generic nanoprobes, functionalised with the studied synthetic peptides is carried out (Figure 11).

Nanoparticles can underpin creation of very specific and sensitive platforms. They present a diverse class of nanoscale materials. Their surfaces can be modified to create highly selective adsorbing species or to incorporate desirable molecules. However, issues arise from the reactive nature of nanoparticles. Many different molecules can easily react with particle surfaces, which present a particular challenge in terms of their application to complex biological systems. Therefore, before particles can be used for analysis in such samples their surfaces should be passivated to prevent those interactions.

To overcome non-specific physisorption, metallic nanoparticles are firstly coated with surface-passivation moieties (lipid bilayers and polyethylene glycol), to which designed model peptides of cell penetrating properties are next conjugated. Nanoparticles allow their direct imaging (without the need of additional tags or staining) by transmission electron microscopy. Therefore, the ability of the created probes to interact with mammalian cells is investigated by this technique.

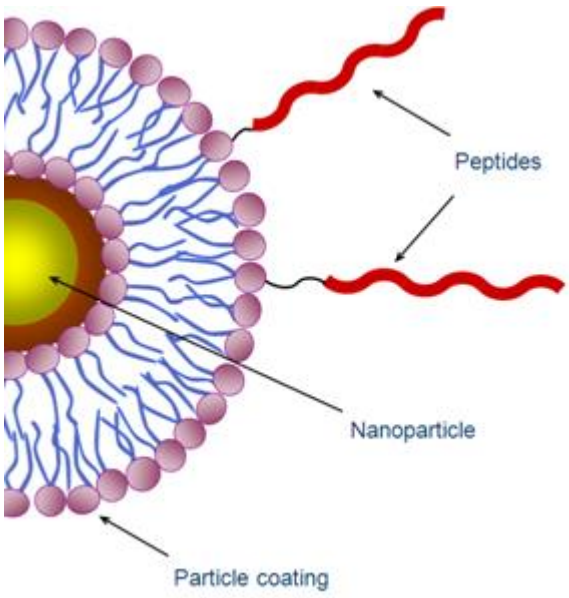

Figure 11. Drawing of a functionalised nanoparticle.

This project offers a basis for the fabrication of nanoprobes, which can be readily conjugated with peptidic moieties of desired properties and activities. Summary of the project is represented in Figure 12.

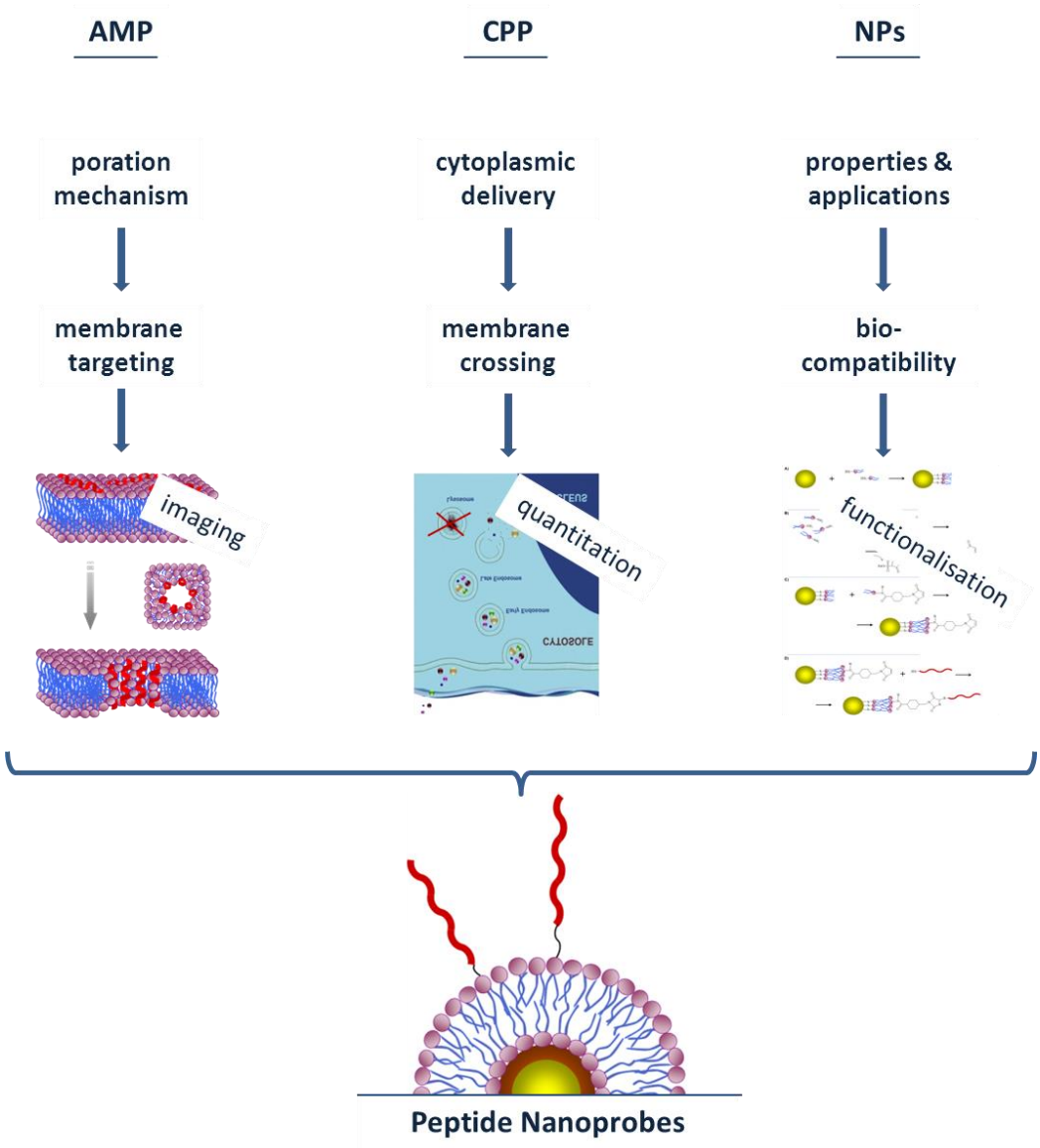

Figure 12. Graphical summary of the project subjects.

CHAPTER 2

MODEL PEPTIDES FOR CELLULAR TARGETING – ELUCIDATION OF MECHANISM OF ACTION

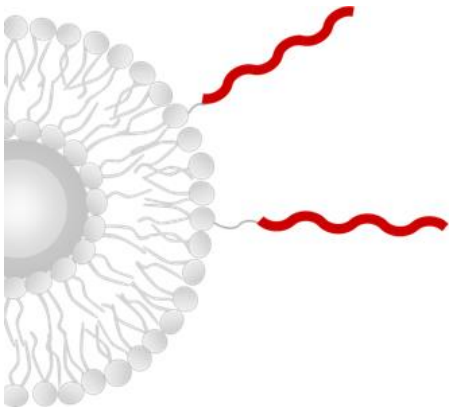

2.1. Summary

De novo designed, membrane-active peptides are investigated to probe specialist, selective cellular targeting. The ultimate aim is to use the peptides as model ligands in functionalisation of nanoparticle-based probes for extracellular binding and intracellular transport.

This chapter focuses on a novel approach to study the action mechanism of antimicrobial peptides. A combination of surface analysis techniques (AFM and NanoSIMS) is used to probe changes in supported lipid bilayers as a result of interactions with the designed peptides. Differential membrane targeting (bacterial versus mammalian) is chosen as model milieu. The work resulted in two publications: 1) 'Nanoscale imaging reveals laterally expanding antimicrobial pores in lipid bilayers', P D Rakowska, H Jiang, S Ray, et al.; *PNAS*, 2013, 110, 8918-8923; and 2) 'Stable isotope imaging of biological samples with high resolution secondary ion mass spectrometry and complementary techniques', H Jiang, E Favaro, C N Coulbourne, P D Rakowska, et.al.; *Methods*, 2014, 2014, 68

(2), 317-324. Full versions of the articles can be found in 'Publications from the project' section of this thesis.

2.2. Introduction

2.2.1 Antimicrobial peptides as model system

Antimicrobial peptides (AMPs) are endogenous effector molecules of the innate immune system of all multicellular organisms. Due to their high surface activity and remarkable biological properties these peptides are of increasing interest. Most of AMPs are membrane-active. Their amino acid composition, amphipathicity and size allow them to attach to and insert into membrane lipid bilayers or enable them to penetrate the cells and to bind to intracellular targets, crucial to cell living. They are attracting growing attention as potential drug candidates and efficient anti-infective agents as well as components in diagnostic probes and drug delivery systems. However, before they can be used as such, and on an industrial scale, a considerable effort has to be put to firstly understand the basis of their biological activity and mechanisms of action.

Bacterial membranes differ from mammalian membranes in lipid composition and architecture. Membrane-active peptides are able to interact with both kinds. However, a particular effect of the interaction is based on the membrane type. Interactions with microbial membranes are non-selective and aimed at the membrane disruption, leading to bacterial lysis. The understanding of how these peptides distinguish between bacterial and mammalian cell membranes, based on the membrane lipid composition, allows for the design of archetypal peptides, which can aid in the elucidation of the molecular mode of action of antimicrobial peptides and can underpin the future exploitation of these peptides. By further manipulating their properties towards selectivity to particular microbial species, classes of novel antibiotics or specific probes could be devised.

2.2.2 Poration

AMPs are designed to kill microbial cells, not necessarily specifically, but rapidly. Few of the naturally occurring AMPs have been studied to expose the molecular mechanism of action and several models have been proposed including barrel-stave

pore, toroidal pore and carpet models ().[119] However, the direct observation of the fundamental processes is needed.

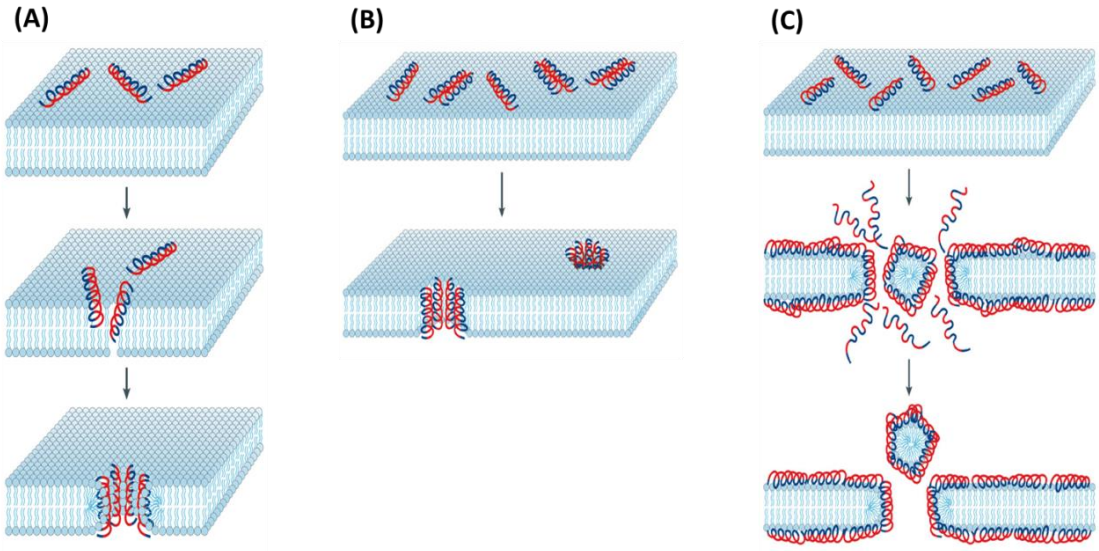

Figure 13. Current models of the action mechanism of membrane-active antimicrobial peptides: (A) toroidal pore model, (B) barrel-stave model, (C) carpet model. Adapted with modification from Brogden, *Nat Rev Micro*, 2005[119] with permission of Nature Publishing Group.

The prevailing molecular model for AMP action is based on the formation of stable or transient pores. In lipid vesicles[120, 121] and supported bilayers,[122] kinetic studies imply the formation of transient pores,[123] suggesting that antimicrobial peptides may expand through the monolayers of the lipid bilayers.[120-122, 124] Much research has also focused on small and stabilised pores.[120, 125-127] Growth arrest and uniform sizes of pores conform to the functional and structural rationale of specialised transmembrane proteins[128, 129] but may not be consistent with that of antimicrobial peptides. Heterogeneity in pore formation for AMPs may derive from the fact that, unlike the case of membrane proteins, there are no a priori topological constraints on assembled structures that the peptides must adopt in bilayers. Therefore, their pore sizes may be governed as much by progressive peptide aggregation as they are by local energetics.

In this light, poration can be described as a physical phenomenon accommodating peptide diffusion in the membrane matrix with no strict predisposition for a particular pore size, but with sufficient freedom of movement

for lateral expansion. To address this phenomenon in a sufficient molecular detail, the direct observation of pore architecture and dynamics is needed, but so far has been lacking.

One reason for the lack of direct observation is the intrinsic complexity of imaging poration in live cells. Membrane binding of AMPs is kinetically driven and, in live cells, occurs over timescales of microseconds to minutes. Pores need not expand substantially because cell death can occur concomitantly as a result of membrane leakage and swelling under osmotic pressure and because AMPs can reach and bind to intracellular targets or disrupt processes that are crucial to cell viability (protein, DNA, or cell wall syntheses) within the same timescales.

2.2.3 Imaging approach

Biological membranes are fluid structures, yet possessing a degree of lateral organisation, essential for their function. Probing and, especially, imaging variations in the lateral composition of those biological membranes, resulting from interactions between membrane components as well as from the actions of extracellular factors interacting with the membranes, presents a major challenge.

Membrane proteins and protein assemblies can be determined by techniques such as x-ray crystallography and atomic force microscopy. However, this does not allow the main components of the membranes, lipids, which are below the diffraction limits of light microscopy to be probed at molecular level. Fluorescence microscopy may help to overcome the issue. This technique is sensitive enough, though only to the fluorescently labelled components. Hence, the detection of only these components is possible. In addition, the introduction of a fluorophore may alter the properties of the labelled ligand as well as its interactions with membranes. Other techniques, such as infrared Raman spectroscopy can offer greater chemical specificity, yet again with limited sensitivity and lateral resolution.

Imaging with the use of high-resolution secondary ion mass spectrometry (NanoSIMS) brings an advantage over those methods. The great information content of this technique leads to unambiguous identification of molecules by their mass and to visualisation of the distribution of analytes in the sample. It facilitates imaging based on chemical fingerprint of molecules and allows for their label-free analyses. Nevertheless, due to both the similarity of chemical content of different

biomolecules as well as complexity of biological systems, labelling with stable isotopes often proves necessary in the analysis of biological processes. Stable isotopes are ideal labels for studying biological processes because they have little or no effect on the biochemical properties of target molecules. NanoSIMS is a tool that can image the distribution of stable isotope labels with up to 50 nm spatial resolution, with good quantification and high sensitivity (see 5.1.4). This combination of features has enabled several groups to undertake significant experiments on biological problems in the last decade.[130-133] In addition, combining the NanoSIMS with other imaging techniques enables obtaining not only chemical information but also the structural information needed to understand biological processes.[134]

Therefore, this is the combination of Atomic Force Microscopy (AFM) and NanoSIMS that makes it possible to image and probe membrane-related interactions at the nanoscale. AFM provides information about the topography of samples (see 5.1.3) and can help indicate and visualise changes such as the structuring / destructuring effects of AMPS on the membranes. AFM gives a very high degree of lateral information but, since there is no chemical information, it does not identify the localisation of AMPs. NanoSIMS is well suited for this purpose. By using isotopically labelled antimicrobial peptides, imaging of the peptide distribution with lateral resolution of 50 nm can be achieved. This approach provides exquisite chemical imaging, showing both the location of the AMPs and the associated disorder in the lipid bilayer. Data produced by these two methods enable to see, measure and characterise the mode of action of AMPs.

2.3. Imaging the action of AMPs

This section introduces the design of a model antimicrobial peptide (AMP), assessment of its interactions with cellular membranes and describes the application of correlative AFM and NanoSIMS analysis to directly image these interactions.

2.3.1 Model AMP design

A *de novo* antimicrobial peptide: AMP (sequence: KQKLAKLKAKLQKLKQKLAKL -am), was produced. The peptide was designed as an archetypal antimicrobial sequence,

capable of inserting into phospholipid bilayers in a transmembrane manner and stimulating pore formation. The sequence design is based on a repeated heptad pattern, which promotes the folding into amphipathic helices.[135-137] Three types of amino acids, in three heptads, are incorporated into the peptide sequence in a way to create the following repeat: CHNCHCN, where C comprises a cationic residue (Lysines), H – hydrophobic (Leucine) and N stands for neutral and polar (Alanine and Glutamine). This type of design allows the hydrophobic and polar residues to segregate into distinct regions (faces) upon the peptide folding during the interactions with anionic microbial membranes. Also, this arrangement allows for the formation of the helix spanning ~3.15 nm to match the thickness of the membrane lipid bilayer: ~3.2 nm[138, 139] (Figure 14).

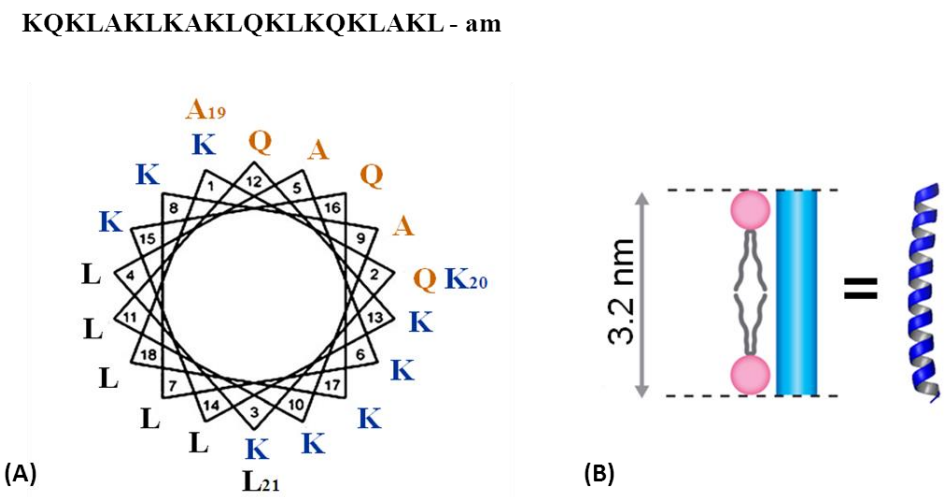

Figure 14. Representation of AMP folding; (A) Sequence of AMP introduced as an α-helical wheel, with 3.6 residues per turn, showing amino acid residues clustering into three regions: cationic (blue residues), hydrophobic (black residues) and neutral and polar (orange residues); (B) Upon contact with anionic membranes the peptide folds into an α-helix, with length matching the thickness of the lipid membrane.

2.3.2 AMP – membrane interactions

The interaction of the designed AMP with model lipid membranes was firstly evaluated by circular dichroism (CD) spectroscopy. CD is a convenient technique to probe the secondary and tertiary structure of proteins and peptides in solution. Different types of secondary structures give rise to characteristic spectra, such as

minima values of the CD signals at 208 nm and 222 nm, which are indicative of an α-helix (see 5.1.1).[140, 141]

AMP folding was probed with the use of neutral and anionic lipid vesicles, mimicking mammalian and microbial membranes, respectively. 1,2-dilauroyl-*sn*-glycero-3-phosphocholine (DLPC) was used to assemble neutral liposomes whereas its mixture with 1,2-dilauroyl-*sn*-glycero-3-phospho- (1'-rac-glycerol) (DLPG) at 3:1 ratio was used to assemble the anionic ones. The liposomes were titrated into the peptide aqueous solution and the changes in the AMP conformation were monitored. The CD analysis proved that the AMP, at micromolar concentrations, folds into an α -helix upon interactions with synthetic membranes mimicking microbial surfaces (anionic liposomes). In contrast, no change in the peptide conformation was detected in the absence of liposomes in the solution, nor in the presence of neutral liposomes (Figure 15).

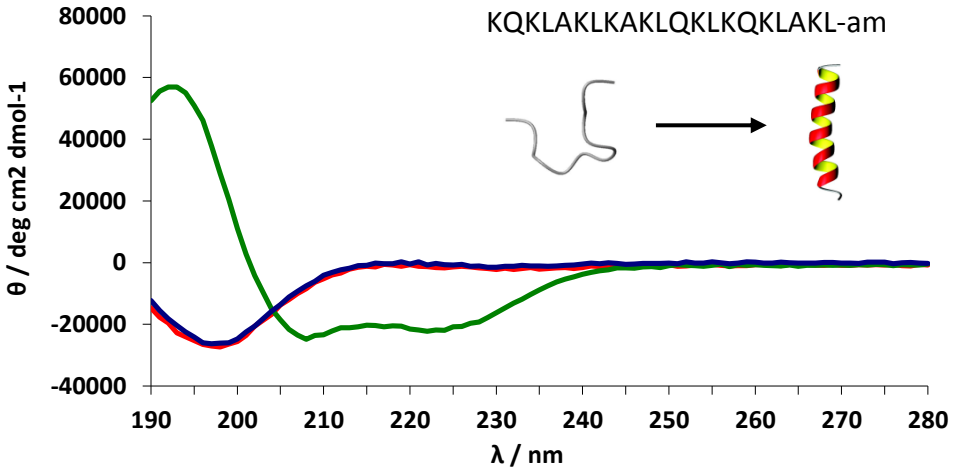

Figure 15. CD Spectra of AMP, revealing change in response, caused by folding of the peptide in to alpha-helical secondary structure upon the interaction with anionic membranes; Peptide in the in the absence of liposomes (red trace), in the presence of neutral membranes (blue trace), and in the presence of anionic membranes (green trace). Copyright © 2013, National Academy of Sciences, USA.

Linear dichroism (LD) spectroscopy was employed to assess the relative AMP orientation in the model microbial membranes. LD is a straightforward method used to investigate alignment of molecules in solution (see 5.1.2). It gave an indication for the peptide insertion into AUVs in a trans-membrane manner, by

showing band patterns comprising maxima at 190-195 nm and 220-230 nm, and a minimum at 205-210 nm.[142, 143] As a control Non-AMP peptide (sequence QIAALEQEIAALEQEIAALQ–am), which cannot bind and order in membranes, was also probed, for which no signal was observed (Figure 16).

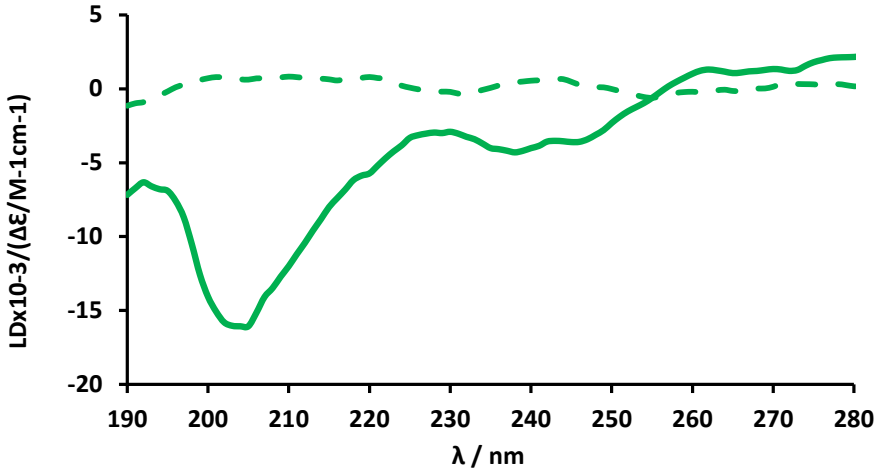

Figure 16. LD spectra, showing relative AMP orientation in membranes; Insertion into vesicles in trans-membrane manner (solid line), in contrast to the lack of signal observed for the non-AMP (dashed line). Copyright © 2013 National Academy of Sciences, USA.

The designed peptides were found to be selectively antimicrobial with minimum inhibitory concentrations being typical of AMPs.[144, 145] Given that in biological systems AMPs must respond to microbial challenge within their proteolytic life time (i.e. minutes), antimicrobial effects were monitored in real time by stain-dead assays using a culture of *Escherichia coli*. In these assays the fluorescence emission of propidium iodide (PI) was used as a dead cell marker and was measured after peptide addition as a function of time (Figure 17). As expected, just after few minutes increase in fluorescence in the bacterial culture treated with AMP was observed. In contrast, no fluorescence was observed for bacteria treated with a non-AMP used as a negative control (Figure 17).

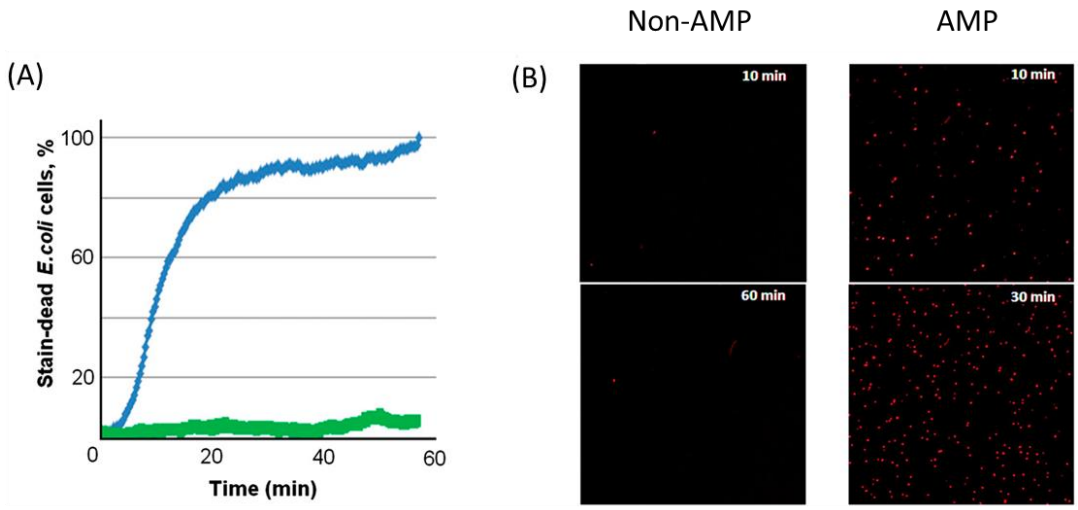

Figure 17. Results of stain-dead antimicrobial assay; (A) Average number of stain-dead cells incubated with the AMP (blue) and the non-AMP (green), as a function of time. (B) Fluorescence microscopy images of PI-stained *E. coli* cells.

Direct visualisation of AMP-treated bacterial cells by AFM revealed the surface corrugation of AMP-treated microbial cells. However, at this stage, more detailed analysis of the cell surface proved impractical due to its considerable roughness (Figure 18).

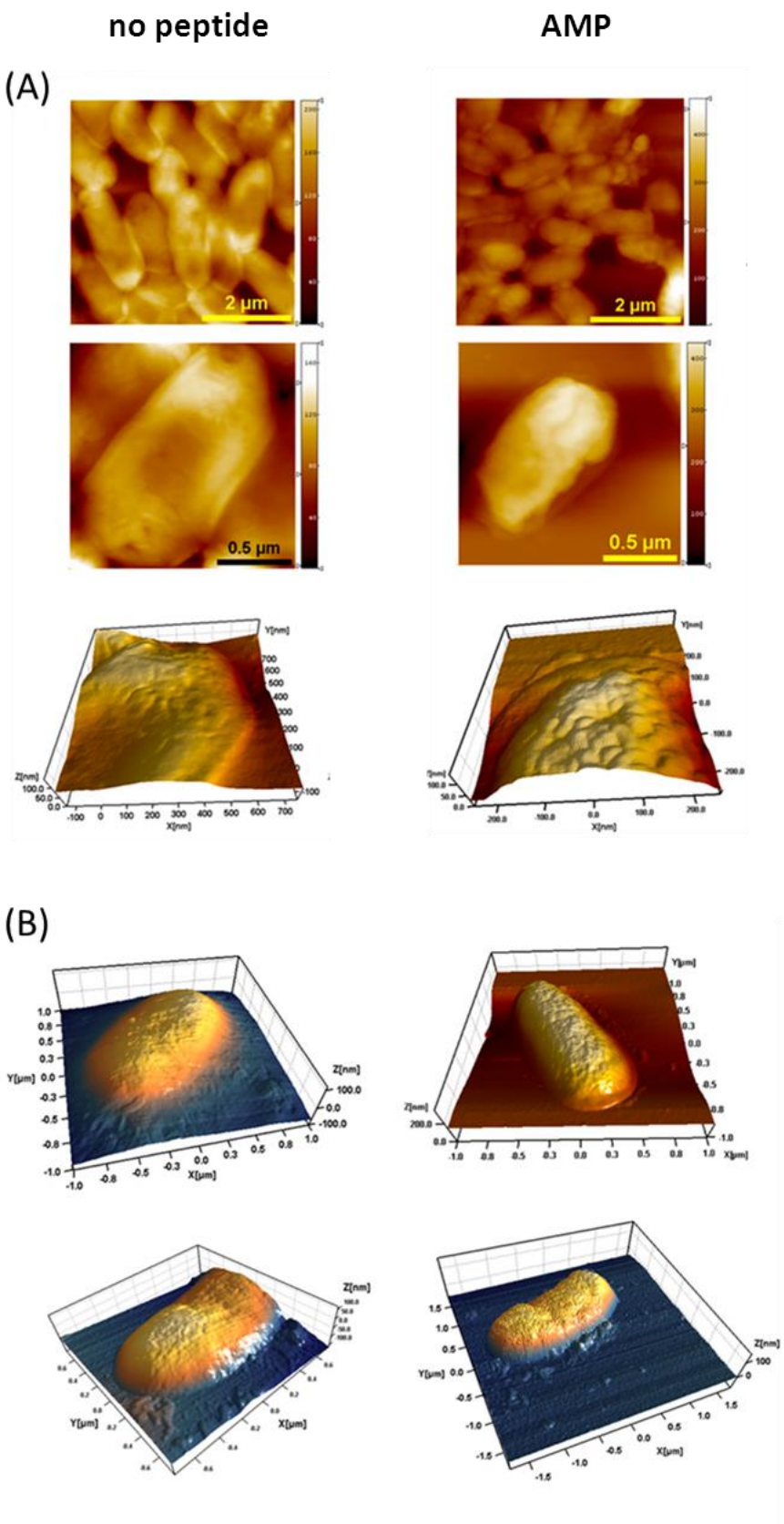

Figure 18. AFM images showing antimicrobial activity of AMP; (A) Topographic images of *E. coli* cells with and without AMP including high magnification 3D images of individual cells. (B) Low magnification 3D images of bacterial cells incubated with the AMP.

2.3.3 Nanoscale imaging

To allow the imaging of the AMP-membrane interaction by AFM and NanoSIMS, which are techniques used for surface analyses, the model system had to be first transferred onto a surface. Schematic drawing of the sample preparation protocol is shown in Figure 19. Lipids mimicking microbial membranes, of the same as used previously composition, were deposited on an oxidised silicon substrate to form supported lipid bilayers. The artificial membranes were then incubated with peptide solution and finally dehydrated by flash-freezing and freeze-drying to preserve changes and peptide in the bilayer.

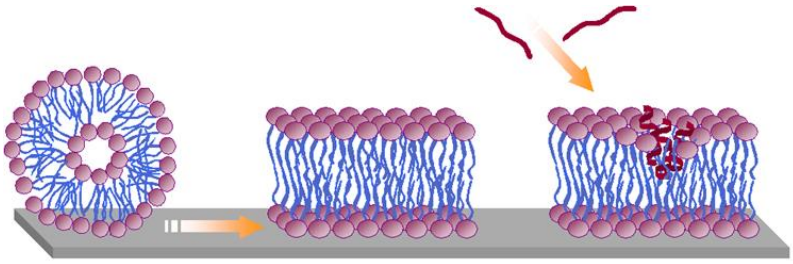

Figure 19. Schematic drawing of supported lipid bilayer creation on the substrate surface. Next, sample is incubated with AMP, flash-frozen and freeze-dried.

Supported lipid bilayer substrates were treated with AMP and then were imaged using AFM and NanoSIMS. Distinctive features suggesting pore formation were observed on the lipid bilayer surfaces. As shown in Figure 20, AFM imaging revealed asymmetric, circular patterns. Apart from such pores, filament-like features running across the sample surface were also evident, suggesting that peptide molecules may migrate across the lipid bilayer. Further image analyses indicated that the circular structures bare a shape of a crater. The diameters of the craters measured on the analysed sample area span from 100 nm to 350 nm. The depth of the craters was rather consistent and averaging 4 nm.

Further investigation on these circular patterns was carried by NanoSIMS. Obtained images exposed similar patterns, when the acquired spectra were scanned for a characteristic $^{12}C^{14}N^-$ signal (Figure 21 (A)). The analysis of untreated lipid bilayers, used as controls, revealed featureless surfaces and negligible signal from contamination on the sample (Figure 21 (B)).

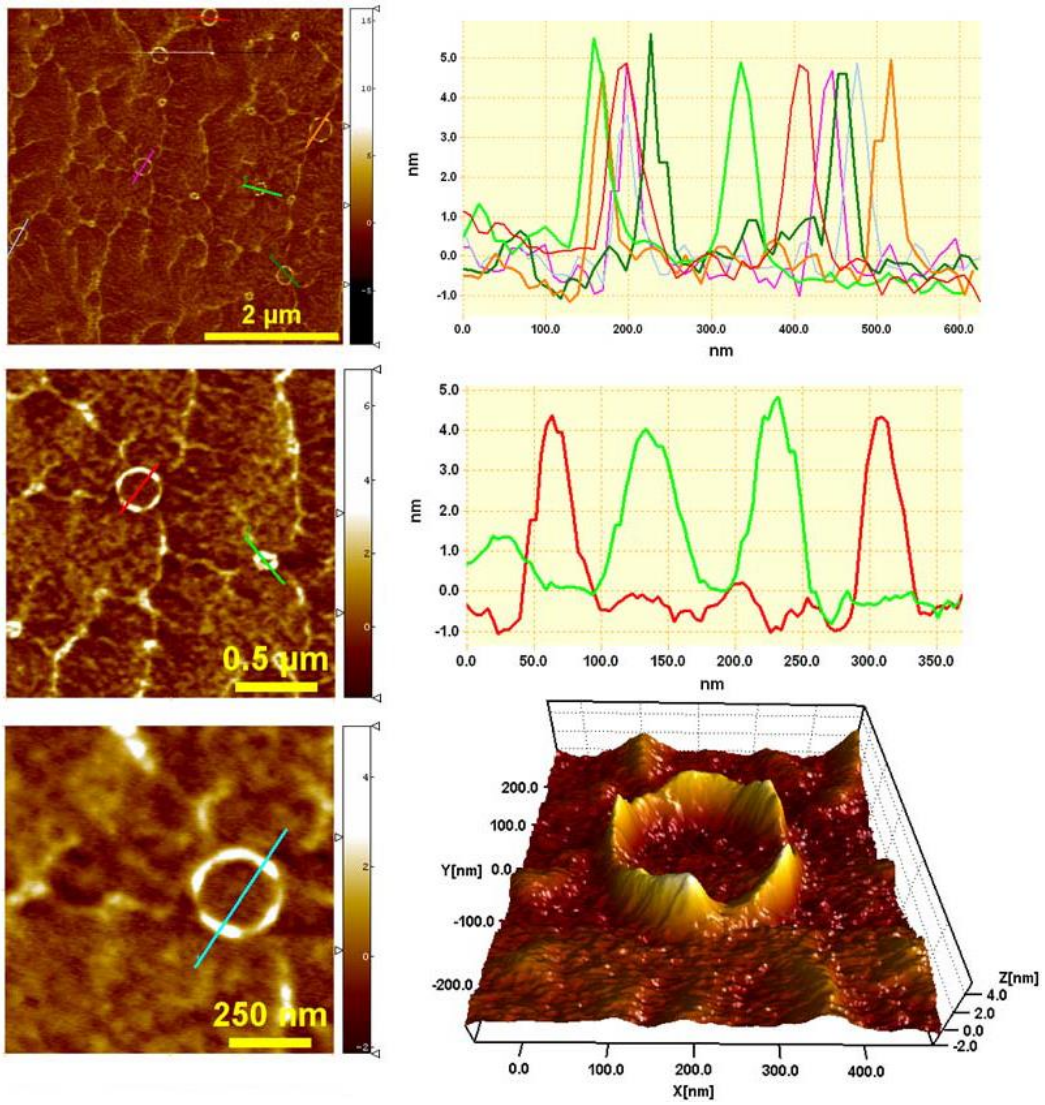

Figure 20. Topographic AFM images and cross sections of pores created in supported lipid bilayers treated with AMP.

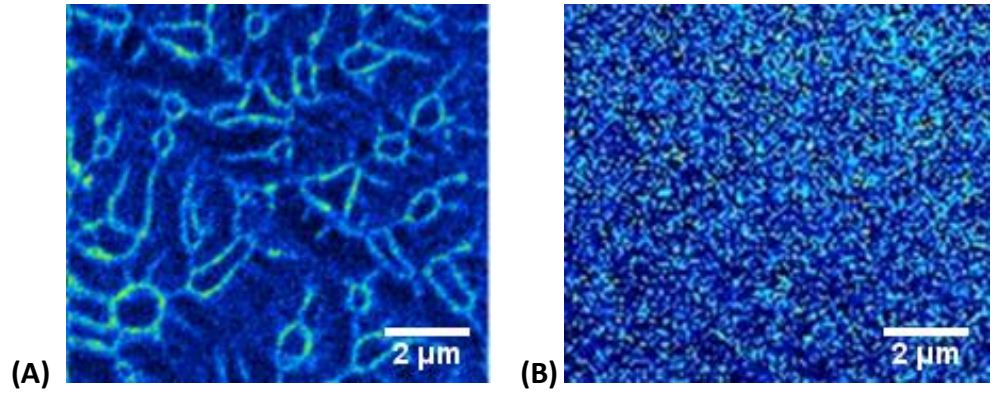

Figure 21. NanoSIMS HIS images showing the intensity of $^{12}C^{14}N^-$ ion signal obtained from (A) lipid bilayer treated with AMP, (B) control lipid bilayer.

Next, an isotopically labelled peptide was employed. Even though the action of the AMP was evident from the acquired images, the label was necessary to aid the definitive interpretation of the obtained results. Stable isotope labelling allows for precise location of the peptide molecules on the sample. It also confirms that the changes to the sample surface are caused by the interaction with AMP rather than by possible mechanical damage which could occur during sample preparation. In biological studies, the most common stable isotopes used to label molecules are: ^{2}H, ^{13}C, ^{15}N, and ^{18}O, which are all readily imaged by the NanoSIMS.[146-149]

An isotopically labelled AMP was obtained: ^{15}N-AMP, with ^{15}N isotopes at all alanine and leucine residues (sequence: KQKL*A*KL*KA*KL*QKL*KQKL*A*KL*–am). The interaction of the ^{15}N-AMP was firstly imaged by AFM, confirming the earlier observation of the formation of pores in the supported lipid bilayers (Figure 22). AFM again revealed pore-like structures of different diameters (average diameter 2.7± 1.3 μm) and filament-like features, and showed an average step height at the pore edges of 3 – 4 nm, consistent with the long axis of the peptide molecule, 3.2 nm. As negative controls, lipid bilayers treated with Non-AMP as well as bare silicon substrates treated with AMP were also imaged, showing no effect the peptides had on the analysed surfaces (Figure 23).

Next, on the ^{15}N-AMP treated samples NanoSIMS imaging was performed. The acquired images appeared to be in good agreement with those obtained by AFM. Secondary ion images of $^{12}C^{15}N^{-}$ and $^{12}C^{14}N^{-}$ signals coming from samples treated with ^{15}N-AMP provided, this time, direct evidence for the precise localisation of the peptide both on the pore edges and in the filament-like features (Figure 24). The conclusions were further supported by $^{12}C^{15}N^{-}/^{12}C^{14}N^{-}$ ratio and hue saturation intensity (HSI) images - the sum of several sequential images to enhance the statistical significance of the measured signals, where $^{12}C^{15}N^{-}/^{12}C^{14}N^{-}$ ratios were far above natural abundance values of 0.37% (Figure 25).

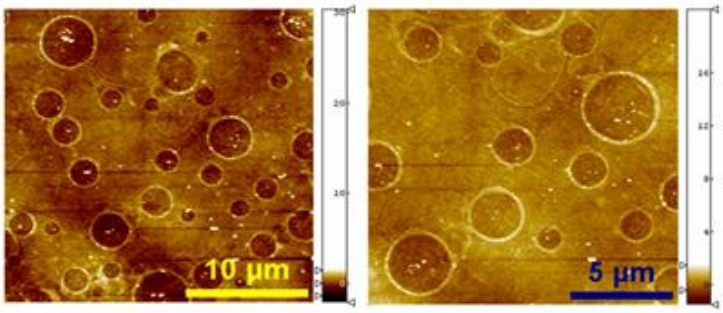

Figure 22. Representative AFM topographic images of the ^{15}N-AMP treated supported lipid bilayers. Copyright © 2013 National Academy of Sciences, USA.

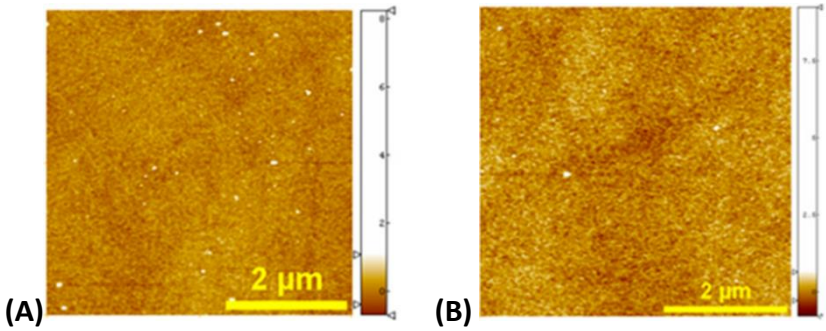

Figure 23. AFM images of control surfaces. (A) Supported lipid bilayers treated with the non-AMP. (B) Bare silicon wafer substrates treated with AMP.

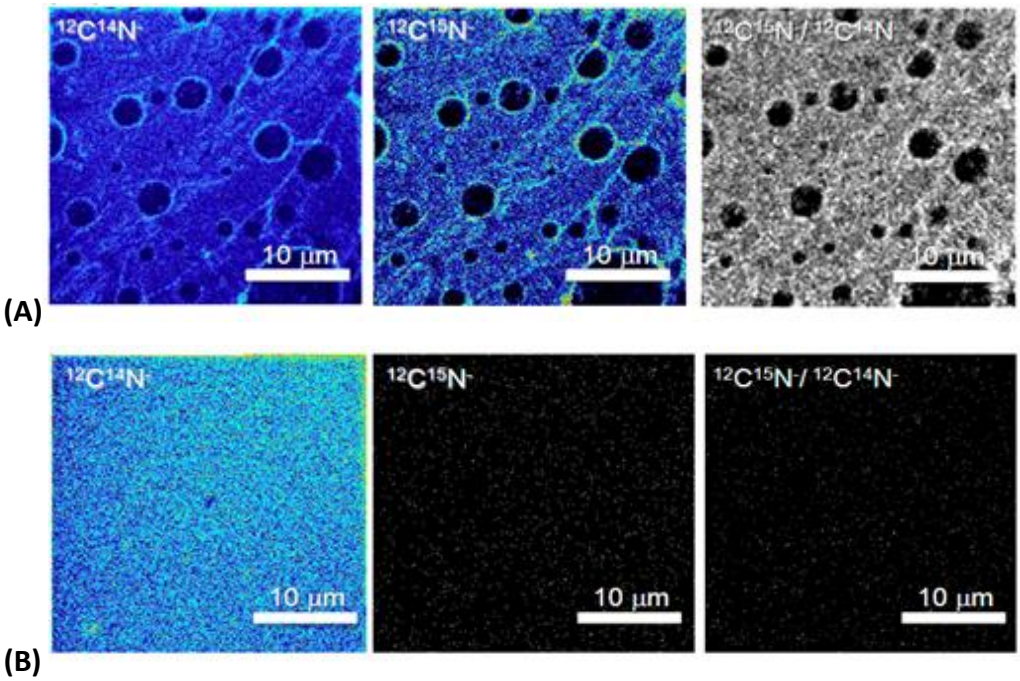

Figure 24. SIMS images of pores created by the AMP and control surfaces; (A) $^{12}C^{14}N^-$, $^{12}C^{15}N^-$, and $^{12}C^{15}N^-/^{12}C^{14}N^-$ signals from the supported lipid bilayers treated with ^{15}N-AMP, (B) corresponding signals from the supported lipid bilayers with no peptide treatment. Copyright © 2013 National Academy of Sciences, USA.

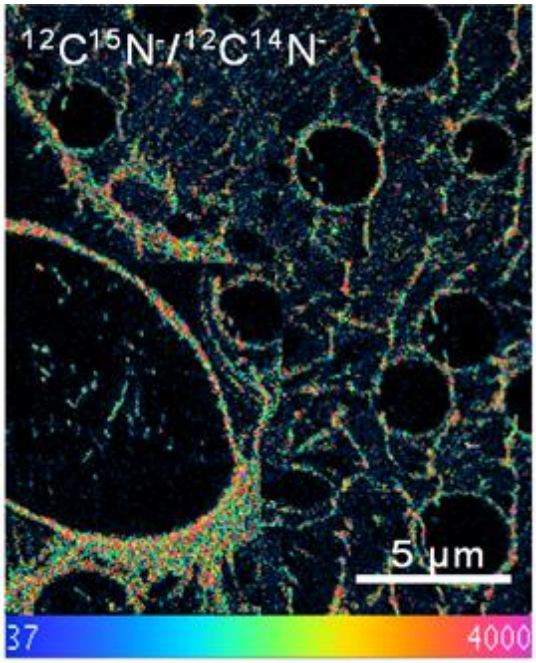

Figure 25. SIMS image of $^{12}C^{15}N^-/^{12}C^{14}N^-$ ratio expressed as HSI images. The rainbow scale changes from blue (natural abundance ratio of 0.37%) to red (40%, >100 times the natural ratio). Copyright © 2013 National Academy of Sciences, USA.

It was demonstrated that the undertaken approach of the combination of AFM and nanoSIMS imaging can be used to visualise the action of the peptides with lipid membranes. What was also noticed is that the poration caused by AMP is not limited to a particular pore size. The forming pores are expanding in the sizes spanning the nano-to-micrometer scale. The appearance of peptide-rich filament-like structures on the sample the surface, connecting individual pores, points to the probability of peptide migration across the bilayer surface.

To confirm that the poration mechanism in not transient, the dynamics of the peptide migration in the membrane has been next probed by performing real time AFM imaging in liquid. Low concentration AMP solution was introduced directly into a liquid cell containing supported lipid bilayer deposited on a mica substrate. The small pores started forming after the first 10 min of incubation and continued multiplying and growing in size over the time, resulting in total removal of the lipid bilayer from the substrate surface (Figure 26, Figure 27). These results indicate that pores can expand laterally at the nano-to-micrometer scale leading eventually to complete membrane disintegration.

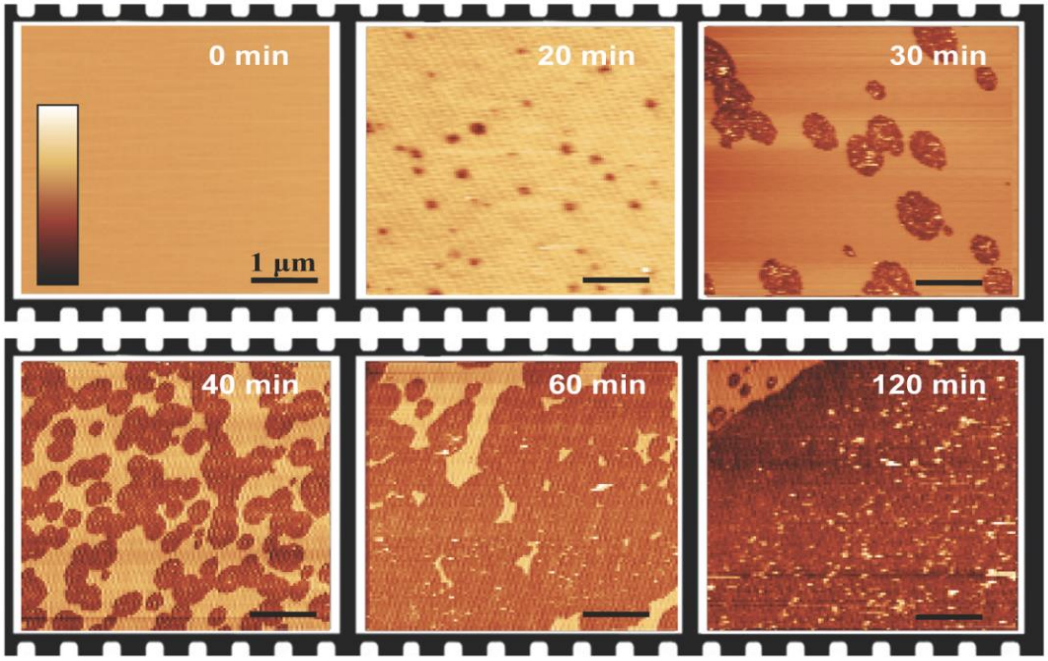

Figure 26. Topography images from real-time, in-liquid AFM imaging of supported lipid bilayer treated with AMP. Copyright © 2013 National Academy of Sciences, USA

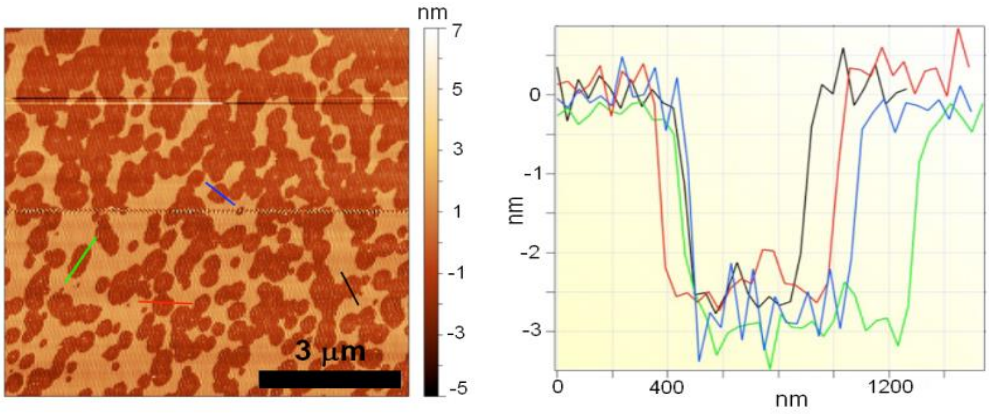

Figure 27. AFM topography image of the supported lipid bilayers after 40-min incubation with AMP. On the right presented are corresponding pore cross-sections along the highlighted on the AFM image lines. Copyright © 2013 National Academy of Sciences, USA.

2.4. Conclusions

De novo designed peptide with antimicrobial properties was investigated to probe selective cellular membrane targeting. The interactions of the AMP with lipid bilayers, mimicking microbial and mammalian cell membranes were analysed by molecular biophysics. The results confirmed that the AMP interacts differentially

with the model bilayers. The peptide does not expose destructive effects towards mammalian membranes and, at the same time, possesses effective antibacterial properties, as confirmed by microbiological studies.

The ultimate aim is to use engineered peptides as ligands in functionalised nanoparticle-based probes. Since antimicrobial peptides distort bacterial membranes, this research concentrated on the elucidation of the mechanism of these interactions.

The dominant molecular model for antimicrobial action has been based, to date, on the formation of stable or transient pores. The obtained by the project results proved otherwise. The interactions of the *de novo* designed archetypal AMP were imaged by the combination of AFM and stable isotope imaging by NanoSIMS. This enabled high-resolution visualisation of the topography of peptide-treated membranes, complemented by chemical imaging which revealed the precise localisation of peptide molecules in the membranes. The acquired images showed that pores formed by antimicrobial peptides in supported lipid bilayers are not necessarily limited to a particular diameter, nor they are transient, but can expand laterally at the nano-to-micrometer scale to the point of complete membrane breakdown. The latter was endorsed further by real-time AFM imaging in liquid.

The correlative AFM and NanoSIMS imaging allowed monitoring and analysis at the much-desired nanoscale. Bearing in mind the intended use of nanomaterials to create peptide-based nanoprobes this makes this combination highly beneficial. This research provides a strong base for the further use of peptide rational design for specific cell surface and trans-membrane targeting as well as the creation of nanoparticle conjugates with molecular peptide ligands.

CHAPTER 3

CELLULAR UPTAKE OF CELL PENETRATING PEPTIDES

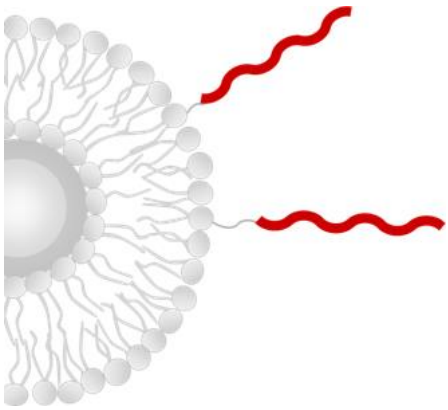

3.1. Summary

The previous chapter described the effect of antimicrobial peptides on bacterial cell membranes. This part focuses on the study of interactions of membrane-active peptides with mammalian cells. This chapter presents the implementation of a minimalistic approach, based on multidimensional chromatography followed by mass spectrometry, to quantify the cellular uptake of cell penetrating peptides (CPPs), bearing in mind the ultimate aim of using the peptides as model ligands to functionalise NPs for intracellular targeting and delivery. The work described here, resulted in the following publication: 'Probing label-free intracellular quantification of free peptide by MALDI-ToF mass spectrometry', P D Rakowska, B Lamarre, M G Ryadnov; *Methods*, 2014, 68 (2), 331-337[150], which can be found in the 'Publications from the project' section of this thesis.

3.2. Introduction

3.2.1 Cell penetrating peptides

Membrane-active peptides, studied in this project, are able to interact with both antimicrobial and mammalian cell membranes. However, the membrane type influences the particular effect of those interactions. The main difference between

bacterial and mammalian membranes lies in their lipid composition. Microbial membranes are built from anionic lipids, while mammalian cells contain predominantly zwitterionic species. As previously described, antimicrobial peptide actions are non-selective and aimed at the membrane disruption with cytolytic effect. The same peptides can expose, however, cell penetrating properties when in contact with mammalian cells. In this setting they turn, from antimicrobial, to cell penetrating peptides (CPPs).

The role of the CPPs is to deliver the cargo into cells. The carried material can be associated with the peptides either via covalent bonds or via non-covalent interactions. Most known, naturally occurring CPPs are not cell type specific, and their interaction with mammalian cell membranes as well as penetrating properties rely primarily on their positively charged, at physiological pH, amino acid sequences and electrostatic interactions with subtly anionic cell-surface molecules. Increasing number of reports suggest that the CPP intracellular delivery is governed by endocytosis, which is then followed by the endosomal escape and release of unmodified cargo.[32, 151, 152] Schematic representation of the process is presented by Figure 28.

CPPs hold great potential as gene or drug delivery mediators, for use in medicine and research. They facilitate cellular uptake of various molecular moieties i.e. small chemical molecules, fragments of nucleic acids or nanosize particles. By further manipulating their properties towards selectivity for particular cell compartments or components, classes of novel drugs and antibiotics or specific probes could be devised. One example could be peptides engineered as an efficient nucleic acid (NA) delivery system (Figure 28). These type of peptides should be able to (i) efficiently condense NA into compact particles, (ii) transfer the NA across cellular membranes in the process of endocytosis, (iii) induce endosomal peptide escape and (iv) target the NA cargo to the nucleus for gene expression.[153]

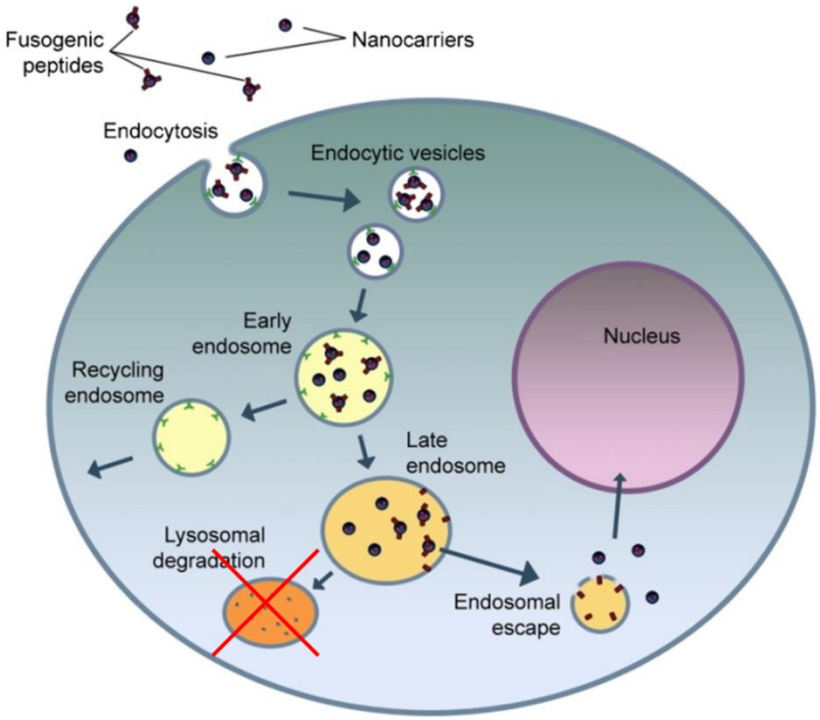

Figure 28. Conceptual illustration of intracellular transport pathways encountered by a model nuclear targeting delivery system incorporating fusogenic peptides as means of endosomal escape. Reprinted with modification from Huang, et al., Nano Today, 2011.[154] Copyright © 2011, with permission from Elsevier.

3.2.2 Quantitative approaches

The quantification of the cellular uptake of CPPs remains largely inconclusive. CPPs can efficiently traverse the plasma membrane and deliver various cargo materials but the functional efficiency of cargo often depends on the completeness of intracellular peptide uptake. Therefore, before CPPs can be used as robust and specific delivery agents or used to create functionalised molecular probes for intracellular targeting, it is important to firstly understand, characterise and quantify their uptake. Current quantification methods use fluorescent or radioactive reporter probes that are monitored by fluorescence microscopy and mass spectrometry.[151, 155] These appear to help quantify the CPPs uptake. However, controversies remain regarding discordant results in different studies and the need for artificial labelling, which continue questioning the general applicability of these methods.[156]

To progress with quantification necessitates the development of direct detection protocols. A notable example is quantification by MALDI TOF mass

spectrometry, briefly described in CHAPTER 1 of this thesis.[77] This protocol makes use of an internal standard labelled with a stable isotope. The standard and the detected analyte are both functionalised with biotin which ensures their capture by streptavidin-coated magnetic beads and subsequent pre-concentration and purification before mass spectrometry analysis. With typical variations of < 20% the protocol has no upper limits of detection which can also be adjusted by the amount of the internal standard added. A critical stage in these measurements is the addition of the standard into cells before cell lysis which is performed at elevated temperatures. Heating is meant to prevent peptide degradation by proteases that are released during cell lysis but become denatured upon heating. The following capture by streptavidin-coated magnetic beads should be equally efficient for the standard and analyte that are prone to the same type of side interactions, i.e. with nucleic acids.[77] However, elevated temperatures can cause aggregation that may hamper the capture and analysis of the internalised peptides, whereas the transfection efficiency of a tagged peptide may be different from that of its free form. These points are important to consider in the development of quantitative protocols to be sufficiently generic for intracellular drugs including those that are thermally labile or for which introducing a tag is not acceptable.[157]

Unless the total peptide recovered from cell lysates can be estimated it remains difficult to benchmark tag-based methods. Surprisingly however, little information is available with regards to the intracellular quantification of free intact peptide from cell lysates. This chapter introduces a strategy which intends to fill this gap. This chapter compares the transfection of a *de novo* design CPP with that of a naturally occurring cell penetrating peptide, TaT (HIV Trans-Activator of Transcription (Tat) protein). It probes free peptide concentrations, recovered from cell lysates using multidimensional liquid chromatography combined with isotope dilution MALDI mass spectrometry, without the use of labels, tags or specialist reagents (Figure 29). This method offers a minimalistic approach for intracellular quantification, which can be used as a correlative measure for fluorescence-based imaging methods.

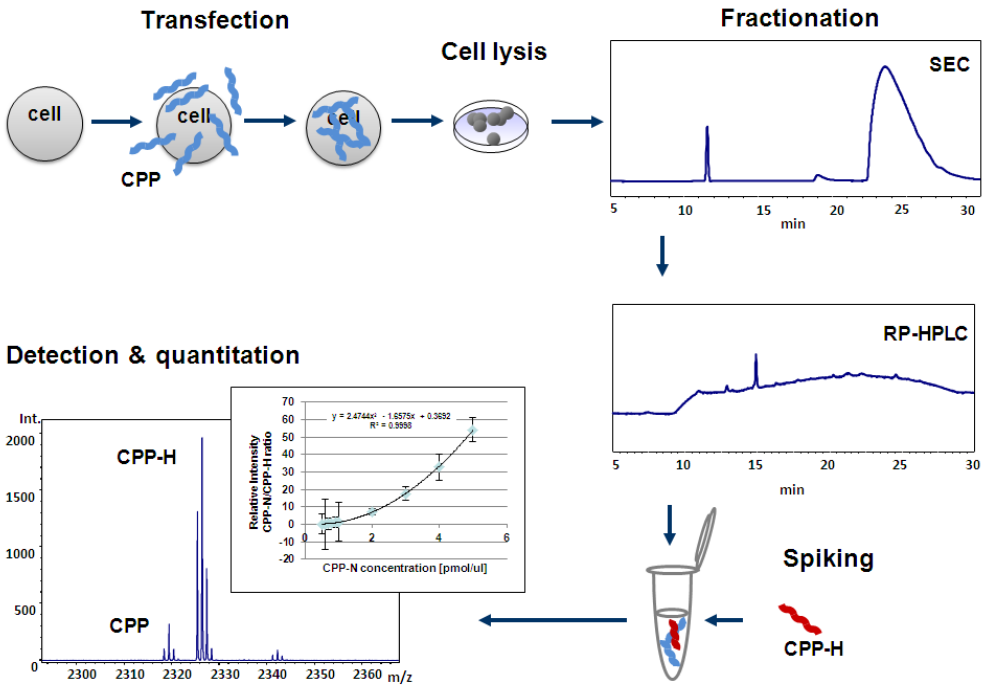

Figure 29. Schematic representation of the quantification method based on a LC-MS flow; Transfected with CPP cells are subjected to cell lyses. Cell lysate is fractionated by SEC, from where fractions are processed by RP-HPLC. To the fraction containing CPP isotopically labelled analogue of the peptide is added. The detection of the peptides is done by MALDI MS and concentration of the CPP is back-calculated based on the peptides' signal intensity ratios. Copyright © 2014, with permission from Elsevier.

3.3. Quantification of cellular uptake of CPPs

3.3.1 Model cell penetrating peptides

De novo designed peptide with cell penetrating properties: CPP (sequence: KIAKLKAKIQKLKQKIAKLK-am) was used in this study. In practice, the described in preceding chapter AMP could serve as a cell penetrating peptide model. However, to enhance the cell penetrating properties, cargo carrying ability and endosomal release, the sequence of previously used AMP was altered. The rational design of the peptide has been described by Lamarre *et al*. [32]

Similarly to the *de novo* AMP, the sequence design of the CPP was based on a repeated heptad pattern, which promotes the formation of amphipathic helices[135-137], allowing the hydrophobic and polar amino acid residues to segregate

into distinct regions upon the peptide folding during the interactions with cellular membranes (Figure 30). The designed AMP and CPP are nearly equally sized and of similar amino acid composition. However, CPP comprises a combination of hydrophobic isoleucine and leucine residues, as opposed to the AMP containing leucine only in its hydrophobic face. This limits the potential peptide aggregation to assembly of lower oligomers.[124, 125] Neutral face of the folded peptide does not contribute to membrane binding but promotes efficient condensation of nucleic acids. In addition, a lysine sub-face is incorporated within the neutral region of the helix to enable and balance out the efficient nucleic acid binding without compromising the interaction with the membrane (Figure 30).

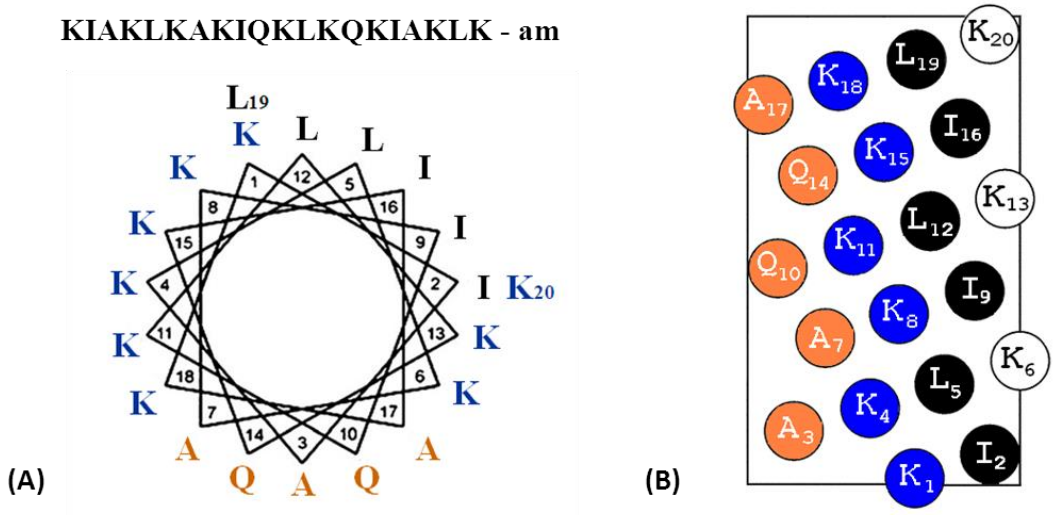

Figure 30. Representation of CPP folding; CPP sequence introduced as (A) an α-helical wheel and (B) an helical net plot, showing amino acid residues clustering into three regions: cationic (blue residues), hydrophobic (black residues) and neutral and polar (orange residues).

The properties of the CPP were evaluated by Lamarre *et al.*,[32] proving it to be an effective gene transporter. The preferential binding to anionic membranes (bacterial and acidified endosomal) was probed by CD and LD spectroscopy (Figure 31) and microbiology assays. The CPP undergoes differential membrane-induced folding, providing a strong antibacterial response. This renders it both endosomolytic and antibacterial. The cell-penetrating ability and NA-delivery properties were monitored by fluorescence microscopy using HDFa cells.[32] The peptide penetrates eukaryotic cells and promotes active DNA transport into mammalian cells by undergoing receptor-independent mammalian cell entry.

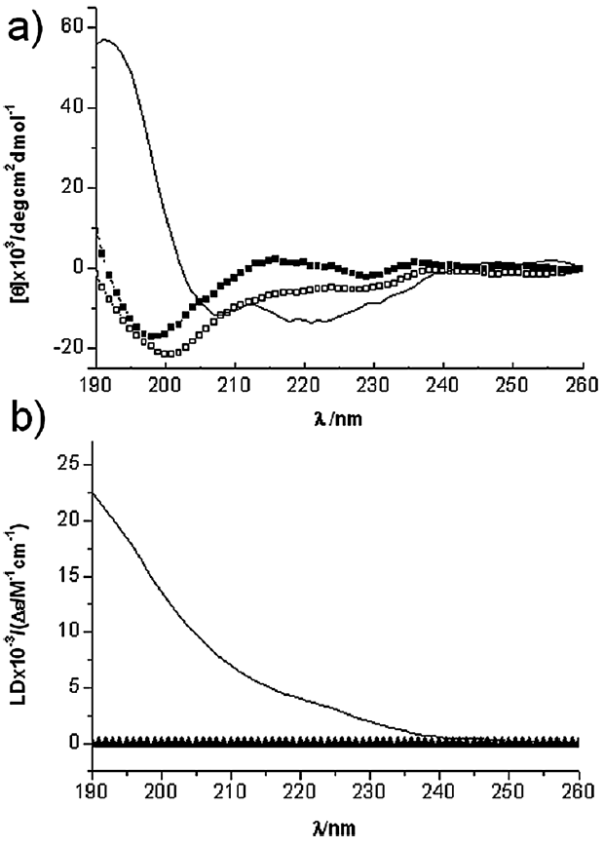

Figure 31. CPP folding probed by circular and linear dichroism; (a) CD spectra for GeT in 10 mM phosphate buffer (white squares) and with anionic (solid line) and zwitterionic (black squares) membranes: pH 7.4, 4 mM peptide. (b) LD spectra for GeT (solid line) and non-GeT (black triangles) with anionic membranes, 30 mM peptide. Adapted with permission from Lamarre et al.; *Chem Commun* 2011.[32] Copyright © 2011 the Royal Society of Chemistry.

Using the earlier established imaging methods, the antimicrobial activity of the CPP was also probed by the real-time AFM imaging. The analysis confirmed similar, to the previously probed AMP, mode of antimicrobial action (Figure 32). After several minutes of treatment of supported synthetic microbial membranes with the CPP, creation of small pores can be observed on the sample surface. The pores multiply and continue growing, leading eventually to the complete lipid bilayer disintegration.

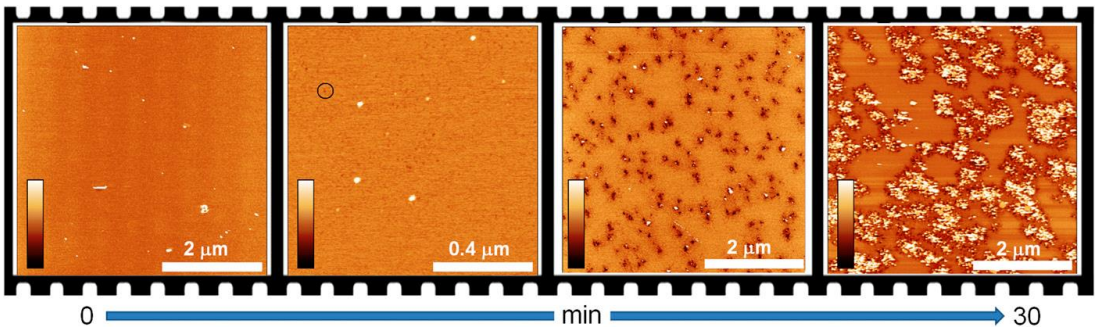

Figure 32. In-liquid AFM imaging of CPP-treated supported lipid bilayers. The circle highlights a pore. Colour scales (insets) from left to right: the first three are3 nm, the last one is 8 nm.

For comparison and as a positive control, naturally occurring peptide (TaT) was also employed in the study (sequence: YGRKKRRQRRR-am). The peptide is a transduction domain (TaT 47-57) of a HIV-Trans-Activator of Transcription (HIV-Tat) protein, which is well characterised and known to carry cell penetrating properties. However, unlike the designed CPP this peptide is not able to escape endosomes into the cytoplasm.[137, 158-161]

3.3.2 Transfection evaluation by confocal microscopy

To be able to compare and correlate the proposed quantification approach to the fluorescence-based imaging methods the uptake of CPP and TaT was firstly evaluated by confocal-fluorescence microscopy. Confocal microscopy is a powerful tool in imaging of cell samples in situ. It enables the fluorescence monitoring of fluorophore-labelled ligands in real time. Both peptides were labelled with a standard fluorophore (CPP-Flu and TaT-Flu), carboxyfluorescein (Figure 33), commonly used as a tracer agent for fluorescence based analysis.

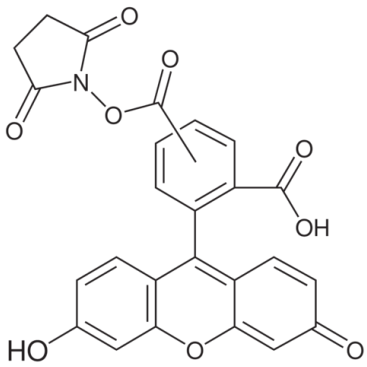

Figure 33. Chemical structure of carboxyfluorescein.

Human Dermal Fibroblasts (HDFa) were incubated with CPP-Flu and TaT-Flu. Visible fluorescence in cells was detected within the first hour of incubation at micromolar concentrations for both peptides. It was dominated by punctuate staining, pointing to their endocytic uptake (Figure 34). Longer incubations, up to 24 hours, revealed more apparent differences in the fluorescent patterns of the two peptides suggesting differential accumulation. The peptides do not accumulate in the nucleus, which implies that transfection was not nucleus-specific and did not lead to cytotoxicity. While CPP-Flu fluorescence tended to disperse in the cytoplasm, that of TaT-Flu continued being vesicularly localised (Figure 34 & Figure 35). These results are consistent with previous studies and with that CPP efficiently escapes into the cytoplasm by permeabilising endosomal membranes, whereas TaT remains entrapped in the endosomes.[32, 162] Incubations with free carboxyfluorescein used as a negative control gave no fluorescence.

Comparative analysis of transfection, as a function of fluorescence at a constant peptide concentration, was carried out. Incubation of the cells in 10 µM peptide solutions revealed that 10% of total cells were transfected within the first hour for both peptides. Increases to 70 and 90% of total transfected cells were observed within 3 hours for TaT-Flu and CPP-Flu, respectively (Figure 36). The 20% difference between CPP-Flu and TaT-Flu appeared to be consistent with the more dispersed fluorescence of CPP-Flu (Figure 34, Figure 35). Transfection of all cells was complete within the first 8 hours of incubation. 24-hour incubations, which were within the first cell doubling time, gave 15 and 30% decreases in fluorescence for CPP-Flu and TaT-Flu (Figure 36).

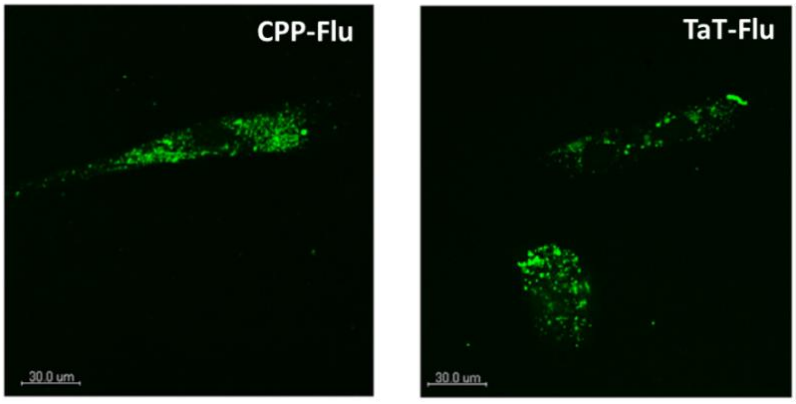

Figure 34. Confocal fluorescence micrographs of HDFa after 3-hour incubation with peptides. Copyright © 2014, with permission from Elsevier.

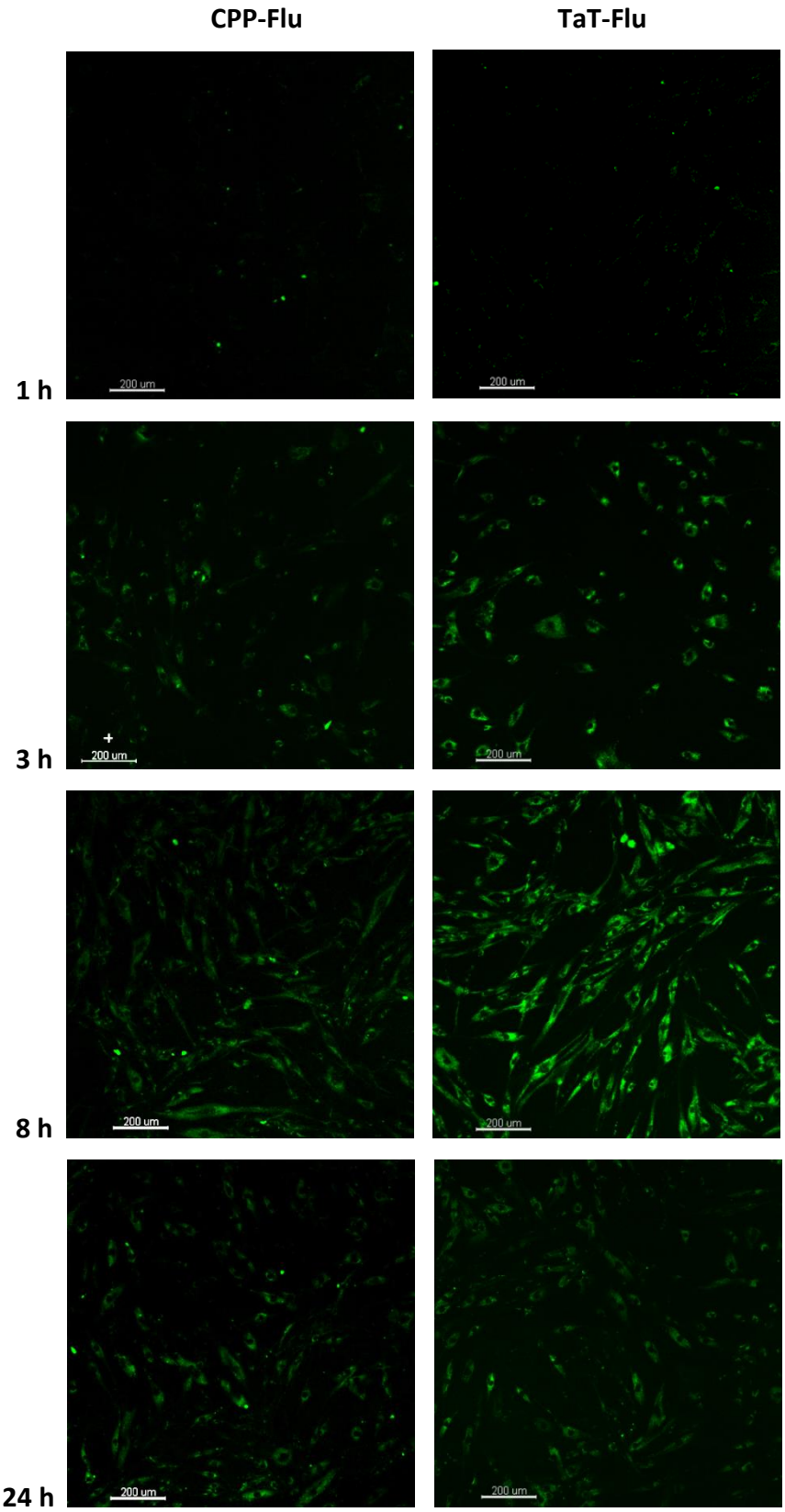

Figure 35. Transfection monitoring; confocal fluorescence micrographs of HDFa incubated with 10 μM CPP-Flu and TaT-Flu. The micrographs were taken at different time points of incubation.

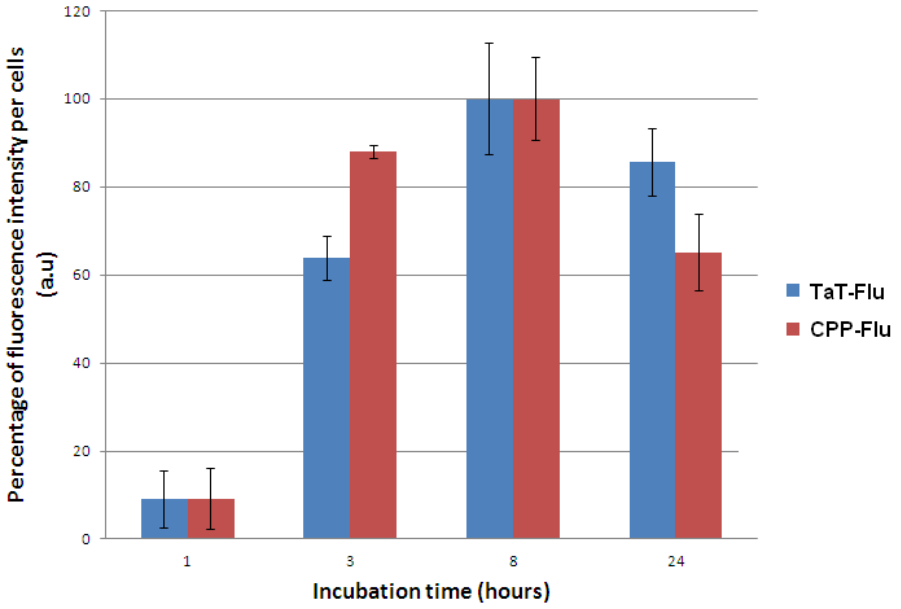

Figure 36. Transfection efficiency as a function of relative fluorescence intensity per cell; total fluorescence divided by the total number of cells. Copyright © 2014, with permission from Elsevier.

3.3.3 Quantification by isotope dilution LC-MALDI

Fluorescence studies showed that efficient peptide translocation is reached within the first 3 hours. Therefore, the same transfection conditions were used for free peptides to probe their quantification from transfected cell lysates. Two-dimensional chromatographic separation preceding mass spectrometry analysis was applied. SEC was chosen to allow for the pre-fractionation of lysate samples which was then followed by an off-line RP-HPLC purification of the concentrated and reconstituted SEC fractions (Figure 29).

Following incubation of Human Dermal Fibroblasts (10^5 cells in the culture) with CPP and TaT solutions, the cells were washed and subjected to cell lysis. Two protocols of cell lysis were considered: first with the use of Triton-X 100 solution and second with the use of Rapigest detergent, as described in the methodology section. The use of the Rapigest protocol seemed somewhat advantageous because it allows for the removal of DNA from cell lysates prior to further analyses and hence can improve the separation of compounds during the following SEC fractionation. However, as tested further by RP-HPLC and MALDI MS, CPP was not detectable in any of the collected fractions (Figure 37). Since this peptide is known

to bind DNA[32] it is believed it has been extracted from the sample together with the DNA. In contrast, Triton-X 100 proved highly efficient. This non-ionic surfactant enables complete disintegration and denaturation of cellular structures at very low concentrations.

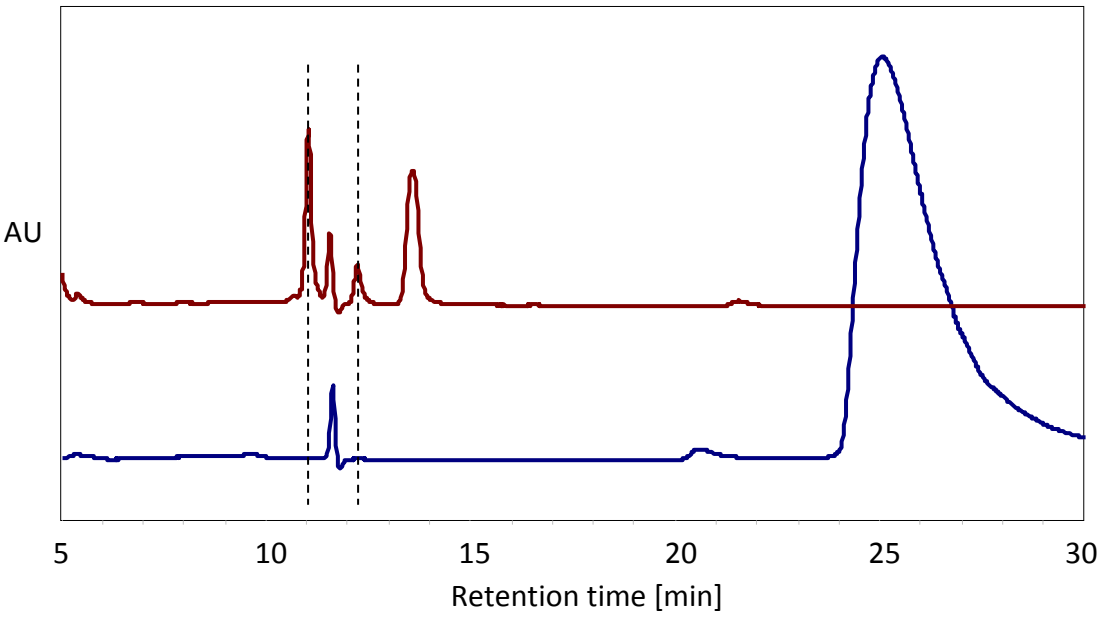

Figure 37. SEC chromatogram of the CPP-transfected HDFa lysates obtained from Triton X treatment (red trace) and from Rapigest treatment (blue trace). Marked is the retention time, during which the peptide was expected to elute and the fractions were collected for further analysis.

Indeed, SEC of processed Triton-X 100 lysates of non-transfected cells and the same lysates spiked with GeT or TaT at known concentrations revealed components with lower molecular sizes than the peptides. Figure 38 shows representative chromatograms obtained for CPP. Peptide peaks on the chromatograms obtained for pure peptide samples and peptide-spiked lysate samples had comparable intensity and area values suggesting that no stable complexation between the peptide and other components in the lysates occurred (Figure 38). SEC profiles for Triton-X 100 lysates of the transfected cells were nearly identical to those obtained for the peptide-spiked lysates (Figure 37 & Figure 38). The fractions at the same retention time showed a somewhat larger peptide content, which may be attributed to other lysate components eluting at the same time (data not shown).

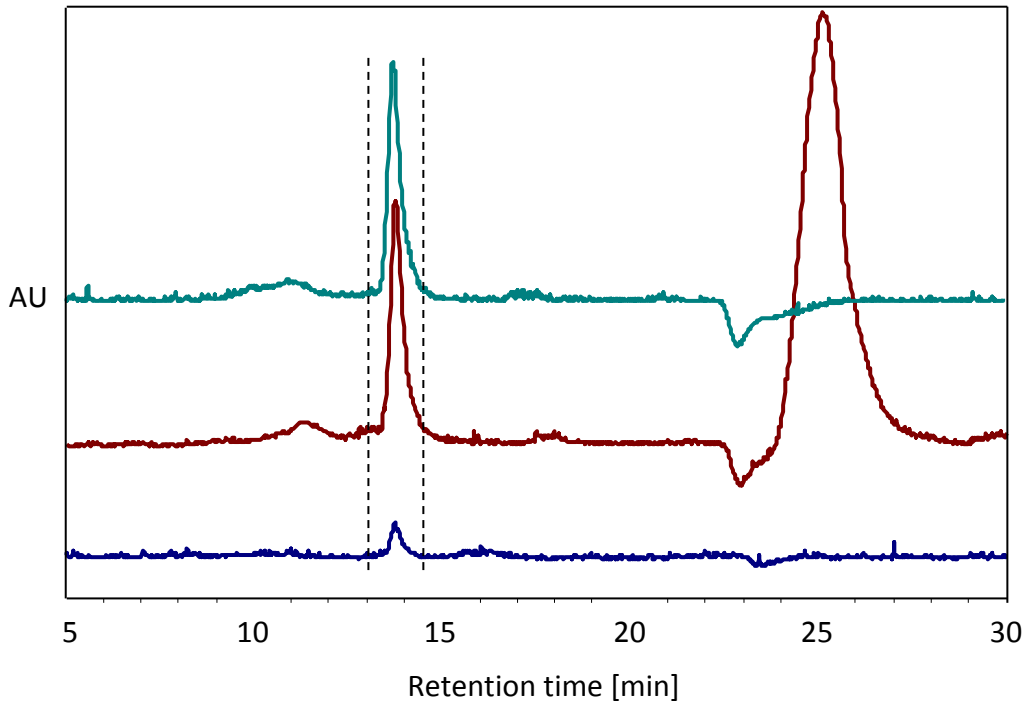

Figure 38. Separation of CPP by SEC; Chromatograms of 10 µg CPP (green trace), 1 µg CPP (blue trace) and spiked with CPP cell extract containing 10 µg of CPP (red trace). Marked is the retention time, during which the fractions were collected for further analyses. Copyright © 2014, with permission from Elsevier.

The collected during SEC analysis fractions containing CPP and TaT were concentrated and re-purified by analytical RP-HPLC. RP-HPLC traces of the reconstituted SEC fractions for CPP revealed clear peaks at retention time of 14.7 min corresponding to the elution time of pure CPP peptide (Figure 39). No trace of TaT peptide was observed during the RP-HPLC separation (Figure 40). This is, most likely, due to the lower value of extinction coefficient, at the 214 nm wavelength, in comparison to the extinction coefficient of CPP. Nevertheless, further MALDI MS analyses of the collected RP-HPLC fractions confirmed the presence of both the peptides in the collected fractions, confirmed at the same time the peptide identities (data not shown).

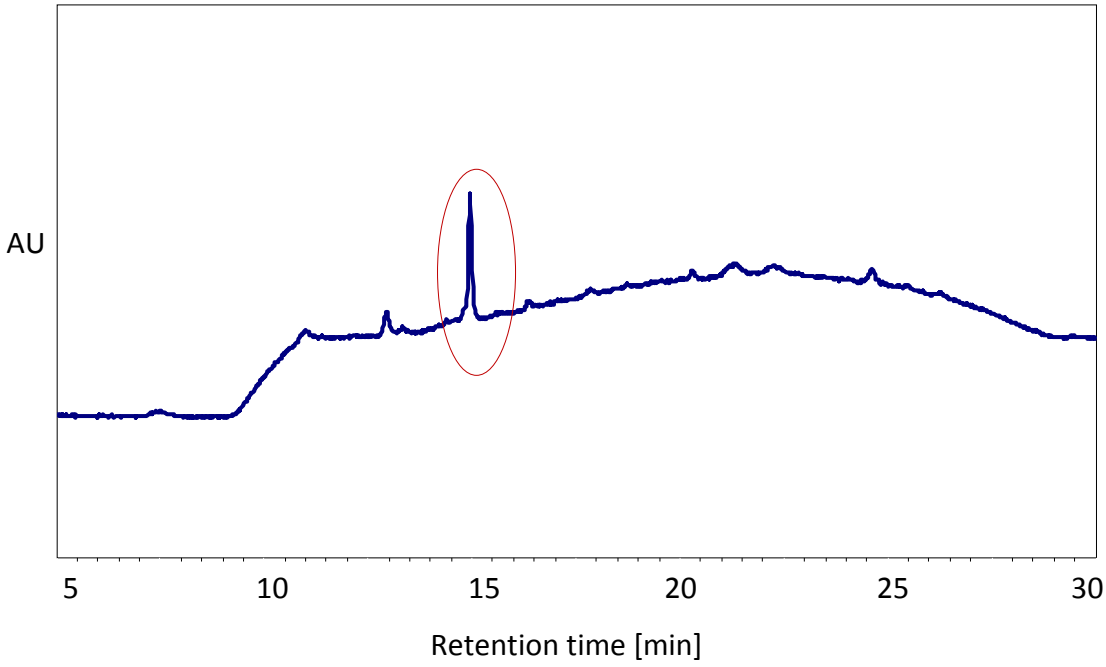

Figure 39. RP-HPLC analyses of SEC fraction containing CPP; Analysis of the Triton cell lysate from HDFa transfected with the CPP. The elution of CPP is marked by the red circle.

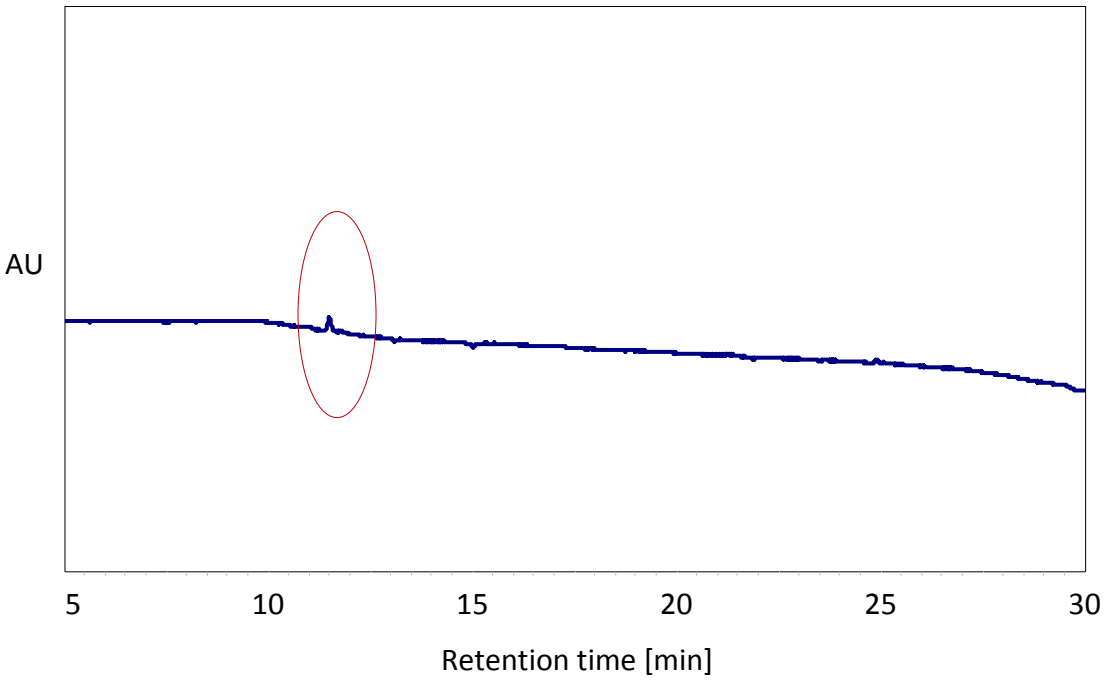

Figure 40. RP-HPLC of sample containing TaT. The chromatogram shows the analysis of SEC 11th minute-fraction from Triton cell lysate. Expected retention time of TaT marked.

To enable the quantification of peptides by MALDI mass spectrometry, isotopically labelled analogues of CPP and TaT were produced (CPP-H and TaT-H, respectively), where one of the amino acids in the peptides sequences: leucine at the position 19 (in CPP) and glutamine at the position 5 (in TaT) were ^{13}C / ^{15}N isotopically labelled (Figure 41).

KIAKLKAKIQKLKQKIAKL*K-am **YGRKKRRQ*RRR-am**

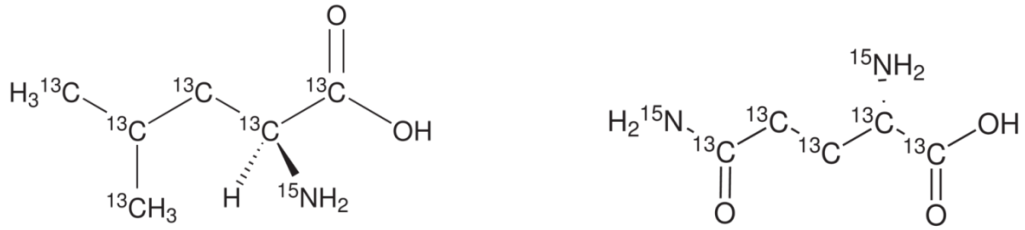

A) **B)**

Figure 41. Labelled sequence residues and chemical structures of: A) Leu 6C13N15 and B) Glu 5C132N15, used for labelling of CPP and TaT, respectively.

The RP-HPLC peptide fractions were spiked with an appropriate peptide analogue and the amounts of the internalised intact peptide were determined by MALDI MS using prior-built standard curves (see 5.2.3 'Isotope dilution standard curves'). The prepared curves plot the ratio of the intensity of the peptide ion to the heavy analogue ion intensity against the concentration of the peptide (Figure 42 & Figure 44). Representative MALDI MS spectra of the analysed samples, to which heavy peptide analogues were added, can be found in Figure 43 and Figure 45.

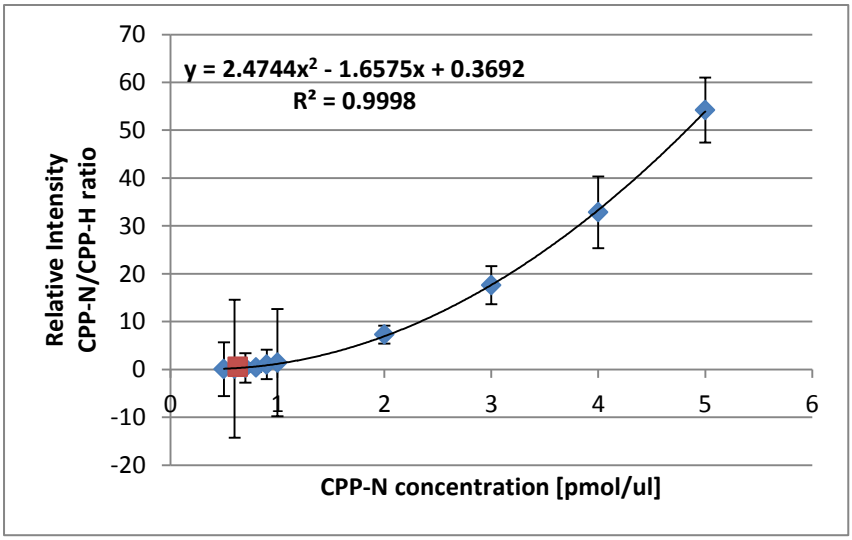

Figure 42. The quantification standard curve of CPP, with indicated in red, calculated average CPP concentration recovered from cell lysate. Error bars represent % standard deviation. Copyright © 2014, with permission from Elsevier.

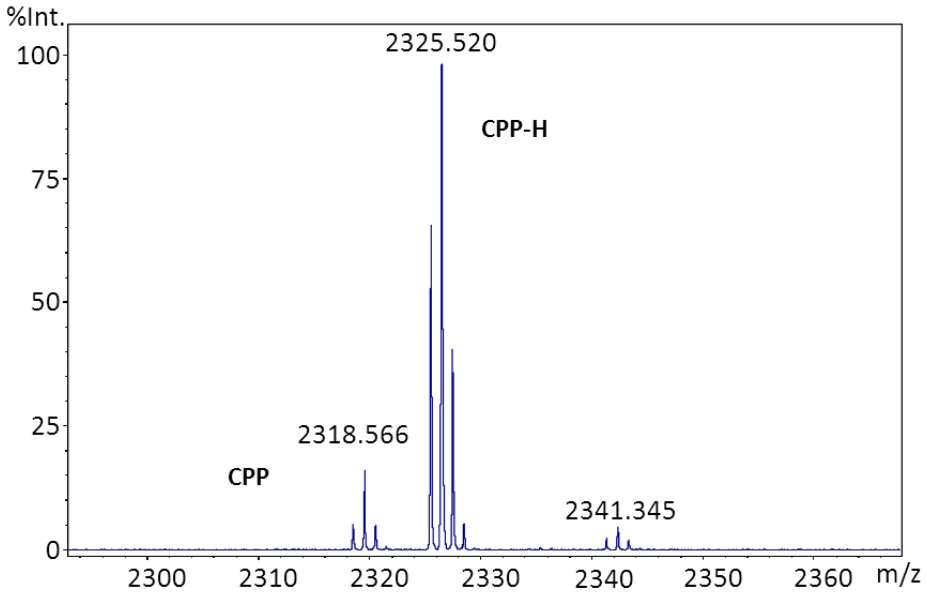

Figure 43. MALDI MS spectra showing the final detection of CPP (2318 Da) in the spiked with the CPP-H (2325 kDa) RP-HPLC fraction. Copyright © 2014, with permission from Elsevier.

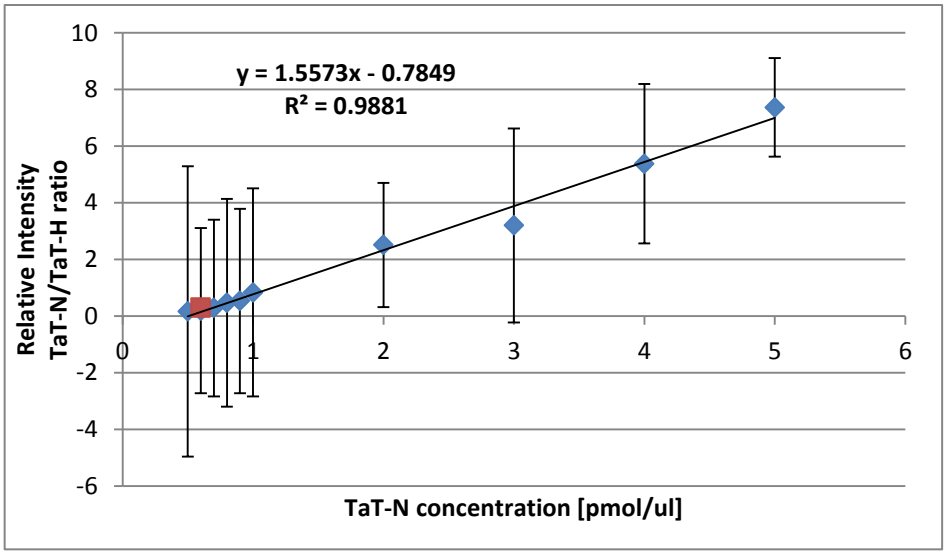

Figure 44. Standard curve for the quantification of TaT. Calculated average TaT concentration recovered from cell lysate is indicated in red. Error bars represent % standard deviation. Copyright © 2014, with permission from Elsevier.

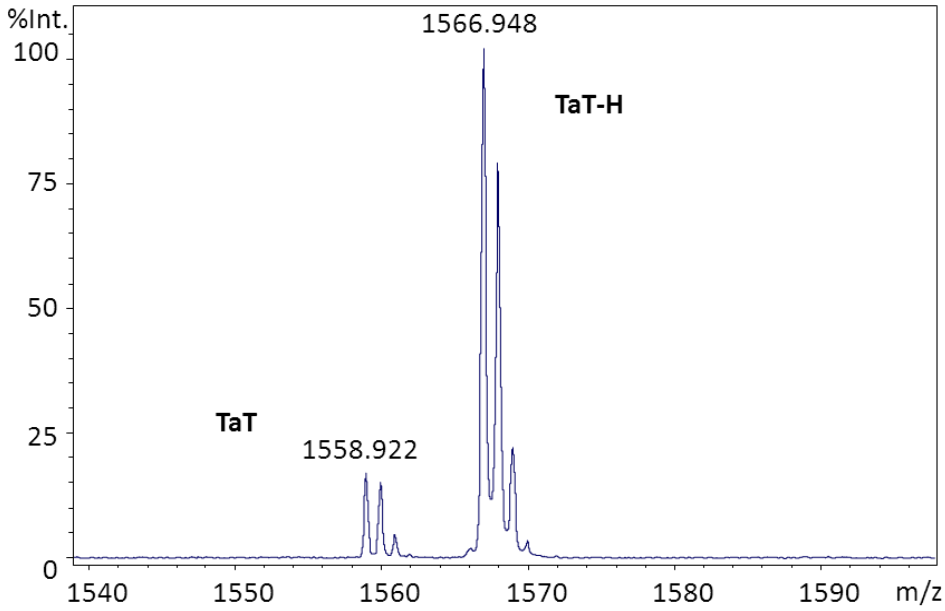

Figure 45. MALDI MS spectra for RP-HPLC TaT fraction (1558 Da) spiked with the TaT-H (1556 kDa). Copyright © 2014, with permission from Elsevier.

The amounts of the peptides in the RP-HPLC fractions were calculated. The returned values of 0.63 ± 0.08 pmol and 0.59 ± 0.08 pmol for CPP and TaT, respectively, were found to be at approximately 14 ± 1.7% (CPP) and 13.1 ± 1.7% (TaT) of the total peptide used for the quantification. Thus, 1.4 ± 0.17 μM peptide was recovered from 10^5 cells incubated with 10 μM peptide for 3 hours. The recovered

concentration corresponds to a total intracellular concentration of 3.7 ± 0.06 μM at the intracellular volume of 3.4 pL per cell.[163, 164] Quantifications using this protocol gave reproducible results with typical variations of <15%, which are within the reported 5-20% ranges.[77]

The obtained results allow also correlations with fluorescence data. In this case, the ~2 μM intracellular concentrations found for 3-hour incubations correspond to 70% and 90% of total fluorescent cells for TaT and CPP, respectively. The microscopy data, which relies entirely on fluorescence, suggests that CPP is more efficient, while mass spectrometry does not fully support this. Instead, it indicates that CPP is as efficient in penetrating human fibroblasts as TaT. Interestingly, however, the results are consistent with the broader distribution of fluorescence in the cytoplasm for CPP.

3.4. Conclusions

This part of the project concentrated on the study of interactions of membrane-active peptides with mammalian cells. Toward the aim of the development of peptide functionalised nanoprobes, model cell penetrating peptides were used to investigate targeted intracellular delivery and endosomal release. *De novo* engineered CPP and naturally occurring TaT, were used and compared in the study.

Human Dermal Fibroblasts, transfected with the model, fluorophore-labelled peptides were monitored by confocal fluorescence microscopy. Results showed different fluorescent patterns for the two peptides, suggesting their differential accumulation within the cells. While CPP tended to disperse in the cytoplasm, TaT continued being vesicularly localised. These results confirmed that the *de novo* design of CPP promotes peptide escape to into the cytoplasm by permeabilising endosomal membranes. TaT peptide remained entrapped in the endosomes.

Focus was given to the intracellular quantification of the two cell-penetrating peptides. Existing quantitative approaches rely on the use of radioactive and fluorescent labels or tags which allow colorimetric, fluorescent or spectrometric detection, but lack the ability to detect free peptide. Therefore, the aim of this study was to quantify free peptide concentrations recovered from cell lysates without the use of labels, tags or specialist reagents. The applied strategy was also compared to the results obtained by fluorescence analysis.

A multidimensional quantification approach was implemented and validated. The method consisted of combination of liquid chromatography and isotope dilution mass spectrometry. To allow accurate peptide analysis by matrix assisted laser desorption / ionisation mass spectrometry (MALDI MS) isotopically-labelled analogues of cell penetrating peptides were used as reference standards. The quantities of designed and naturally occurring peptides internalised in primary cells were measured. Determined peptide concentrations were similar to those reported for cell-penetrating peptides used to transfect other cell lines.[155] Similar values for a more basic (than TaT) CPP could be attributed to several factors including peptide complexation with lysate components, degradation and material loss during purification and processing. However, the same protocol was used for both peptides. CPP had broader distribution in the cytoplasm than TaT, which tended to remain in endosomes, and may also have higher affinities to phospholipid membrane components and nucleic acids.[32]

Several advantages of the applied method can be pointed out. Firstly, it is label- and tag-free – only free peptide is used, isolated and quantified. This is in contrast to other methods including those based on MALDI-ToF quantification that use biotin-tagged peptides and introduce labelled standards before lysis, which in itself can lead to additional uncertainties regarding the concentration of the standard.[77, 155] Secondly, it is performed at benign temperatures, which eliminates potential artefacts associated with peptide aggregation. Thirdly, it gives a realistic estimation of recoverable peptide concentrations using a minimalist approach that can be readily replicated by others without specialist materials. Nevertheless it can be also used as a correlative measure for fluorescence-based imaging methods.

The obtained results were reproducible and suggest that, under applied experimental conditions, the designed CPP is similarly efficient in terms of cell entry in comparison to the naturally occurring TaT. This observation is promising in terms of the rational design of efficient exogenous peptide biomarkers and peptidic delivery vectors.

CHAPTER 4

NANOPROBE DEVELOPMENT AND ITS ASSESSMENT IN BIOLOGICAL SAMPLES

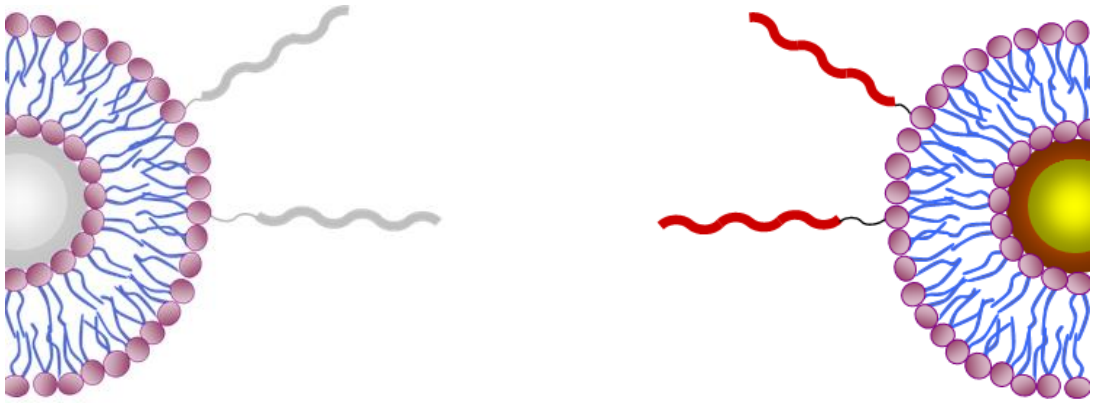

4.1. Summary

This chapter describes generic nanoprobe models. The models comprise metal nanoparticle with surfaces passivated by lipid bilayer and polyethylene glycol coatings, and functionalised with designed cell penetrating peptides. The ability of the created probes to interact with mammalian cells is investigated by transmission electron microscopy.

4.2. Introduction

There is a demand for more robust, sensitive and reliable tools to enable intracellular delivery as well as the detection of biomarkers present in cells. Platforms aiding in quantitative determination, targeted drug delivery and simultaneous imaging are of particular interest. The development of such technologies would improve not only early diagnosis of diseases but also their therapy and monitoring of progress.

Nanoparticles could underpin the development of very specific and sensitive platforms. They present a diverse class of nanoscale materials. As described in CHAPTER 1 of this thesis, their surfaces can be modified to create highly selective adsorbing species or to incorporate any desirable molecule. Nanoparticles can be functionalised with multimodal components, serving multiple purposes in various biological assays. Targeting moieties such as *de novo* designed peptides can be conjugated to the particle surface. Nanoparticles can also be utilised in drug delivery. Furthermore, the incorporation of multiple imaging modalities is also possible.

Cell penetrating peptides can assist targeted intracellular delivery of the nanoparticles, hence the variety of ligands that can also be to the particles conjugated. The unspecific mode of action of CPPs towards mammalian cells has already led to the design of various peptide-based delivery platforms, as exemplified in Figure 46. By the application of rational peptide design and by merging peptide marker with nanoparticle system into a single bio-functional platform one could enable a transfer targeted to specific tissues, cell types or cellular compartments.

One main obstacle, when working with metallic nanoparticles arises from the nanoparticle properties. Complex biological samples, such as cells, cellular extracts or serum, contain many different components, which can react with the nanoparticle surface. Therefore, before particles can be used for analysis in such systems their surfaces should be passivated to prevent non-specific interactions. For example, lipid bilayer coverage around nanoparticle can be utilised to increase the particle stability and prevent undesired physisorption. Polyethylene glycol (PEG) coating can provide bio-inert properties and prolong the nanoparticle life in biological systems such as cells or blood.[165, 166]

This chapter describes the functionalisation of metallic nanoparticles with surface-passivation coatings, to which designed model peptides of cell penetrating properties are next conjugated. The employment of nanoparticles in the study enables their direct imaging (without the need of additional tags or staining) by transmission electron microscopy. Therefore, the ability of the created probes to interact with mammalian cells is investigated by this technique. The platform forms a base for the fabrication of nanoprobes, which can be readily conjugated with peptidic moieties with desired properties and specific activities, resulting in specific

bio-molecular markers, intracellular cargo delivery or selective biomarker targeting and binding.

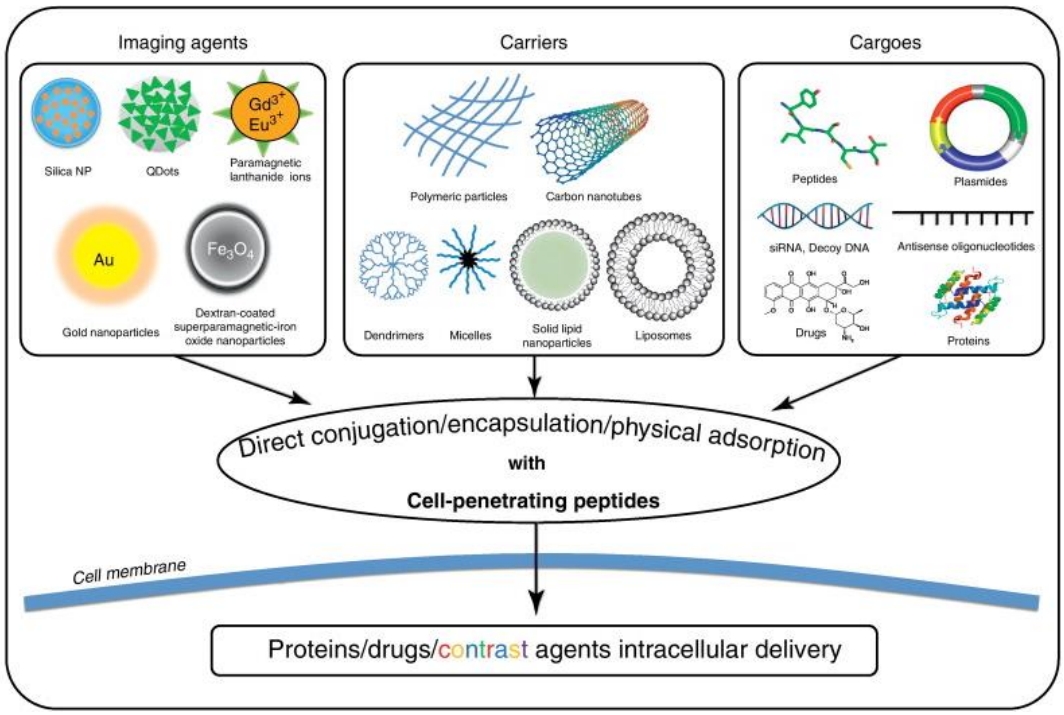

Figure 46. Applications of cell-penetrating peptides as molecular delivery vehicles for a variety of drugs, nucleic acids, proteins, therapeutics, and imaging agents. Adapted from E. Koren and V. P. Torchilin, *Trends in Molecular Medicine*, 2012.[167] Copyright © 2012, with permission from Elsevier.

4.3. LipoNP

To prevent unspecific binding of undesirable molecules to NP surfaces, an investigation of covering the particles with lipid bilayer was carried out. A method was developed, based on the conjugation of thiol-modified lipids onto the NP surface. This resulted, firstly, in a NP encapsulated in an inverted lipid micelle. Next, the second lipid was added to form lipid bilayer around the particle.

Head group modified thiol-lipid: 1,2-dipalmiotyl-*sn*-glycero-3-phosphotioethanol (DPPTE) (Figure 83) was coupled to silver nanoparticles (AgNPs) of sizes: 10 nm and 20 nm, using the high affinity of the thiol group to silver. The initial coupling of the thiol-lipid to silver was performed in two solutions: water and chloroform. The two solutions were probed to assess the best conditions for the reaction, bearing in mind planned further steps of nanoparticle coating and also, taking into

consideration the insolubility of DPPTE. Next, the experiments concentrated on adding the second lipid: DLPC (Figure 79) and creating a lipid bilayer around the AgNPs. The production of the construct (lipoNP) took place between two phases: aqueous-water and organic-chloroform (Figure 84). To exclude the question if DLPC reacts with AgNPs, additional experiment was conducted, where in place of the DPPTE, DLPC was employed.

Firstly, NPs encapsulated in inverted lipid micelles were evaluated. Two different preparations of the complex were carried out: (1) in chloroform and (2) in water.

When only chloroform was added to the initial AgNPs solution, the NPs remained in the aqueous phase. When the chloroform solution of DPPTE was mixed with the AgNP aqueous solution, the colour of the aqueous phase, yellow/brown, was immediately transferred to the organic phase, indicating that the AgNPs became soluble in chloroform via coupling with DPPTE (Figure 47, Figure 49 B). The complex in chloroform seemed to be stable. However, the separation by centrifugation of the DPPTE-conjugated 10 nm AgNPs appeared to be difficult, while being very efficient for the 20 nm ones.

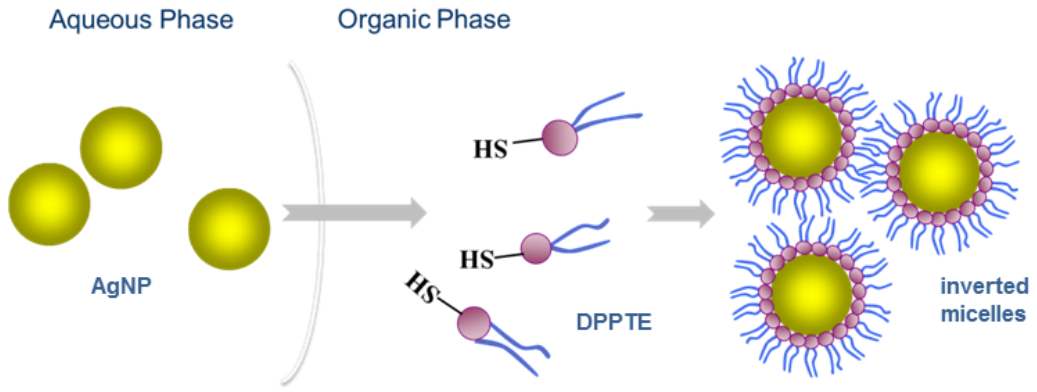

Figure 47. Scheme of inverted micelles creation. AgNPs, upon reaction between Ag and the sulfhydryl group of DPPTE, are being transferred from the aqueous solution to the organic phase, which contains excessive amount of the thiol-lipid. Finally, the AgNPs surface is completely covered with the lipid residues.

Preparation of the complex in water resulted differently. The milky suspension of DPPTE disappeared after mixing with AgNP and the solution gained transparency, suggesting the conjugation of the lipid onto the NP surface. Nevertheless, aggregation of the complex occurred, as judged by the solution colour change.

20 nm AuNPs aggregated more rapidly. MALDI MS and DLS measurements have confirmed the presence of lipid dimers and trimers as well as larger aggregates in the solutions (data not shown).

Further experiments concentrated on covering the micelles with the second lipid – DLPC; DLPC resuspended in water was added to the pellet of DPPTE-AgNPs conjugates (kept in few drops of chloroform). After vigorous shaking and sonicating of the mixture, the gain of the colour by the aqueous phase of the solution indicated the transfer of the DPPTE-AgNPs to the aqueous phase, as a result of the conjugates being covered by the layer of DLPC (Figure 48, Figure 49D). In a parallel experiment, DPPTE was replaced by DLPC and, as expected, it was not possible to transfer AgNPs from aqueous solution to the organic phase containing the lipid (Figure 49 B and C).

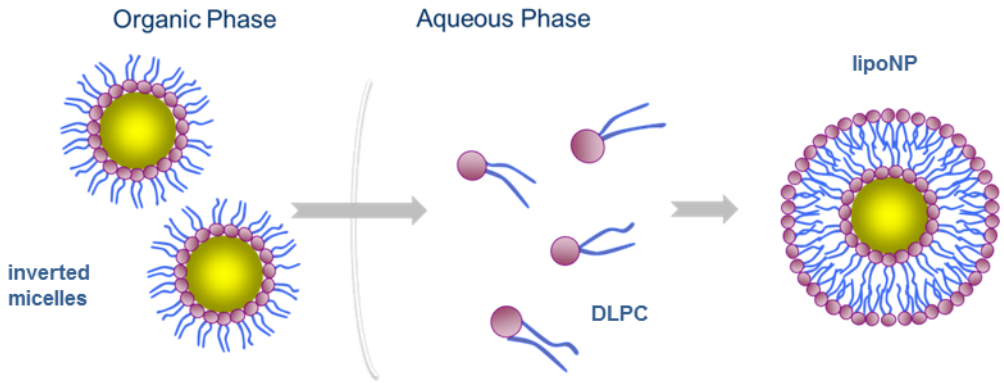

Figure 48. Drawing presenting the creation of the second lipid layer. AgNPs, covered with DPTTE in a form of inverted micelles, upon mixing with the aqueous solution containing DLPC are being transferred from chloroform to the aqueous phase. Finally, the AgNPs surface is covered with the lipid bilayer, giving LipoNP.

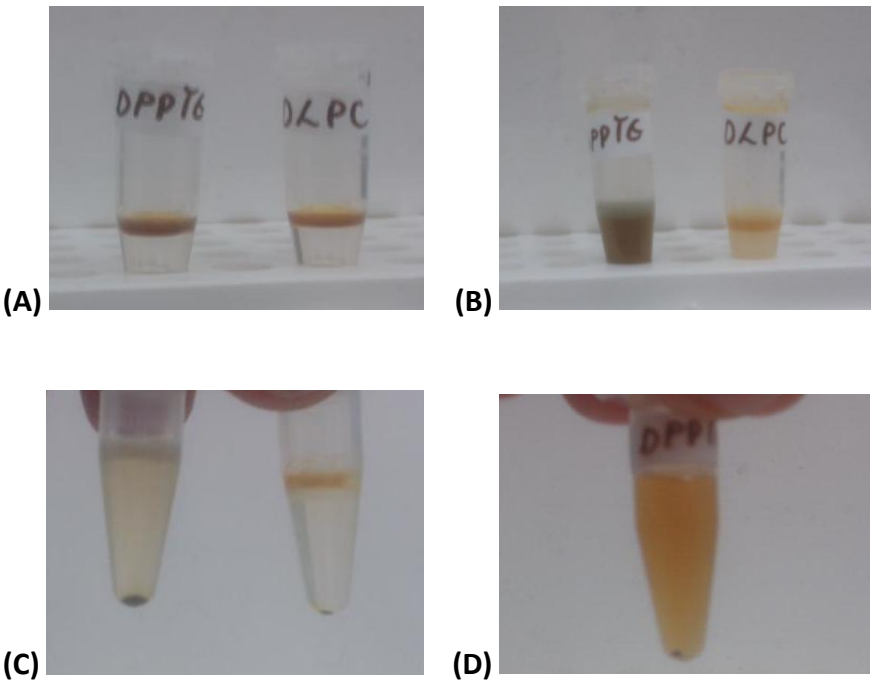

Figure 49. Production of AgNPs covered by lipid bilayer; (A) aqueous phase of AgNPs added to lipids dissolved in chloroform (right: DPPTE, left: DLPC); (B) colour change of the organic phase containing DPPTE due lipid-NP complexation; (C) after centrifugation DPPTE-AgNP form a pellet (left), while DLPC still remains in the aqueous phase (right); (D) DLPC solution added to the DPPTE-AgNP pellet – gain of colour indicates the bilayer formation.

Dynamic Light Scattering (DLS) measurements were used to assess the lipoNPs. DLS is a technique, which can be used to measure the size as well as the size distribution of particles held in suspension (see 5.1.6). The performed measurements suggested the necessity of construct extrusion. In the initial solution agglomerates of the LipoNPs were observed, as judged by the size distribution by intensity and volume (Figure 50). The agglomerates disassembled notably after passing, several times, through 50 nm pore size membrane (Figure 50).

Additionally, it was noted that LipoNPs construct proved stable in aqueous solutions and during repeated extensive centrifugation, which allows its efficient purification and recovery.

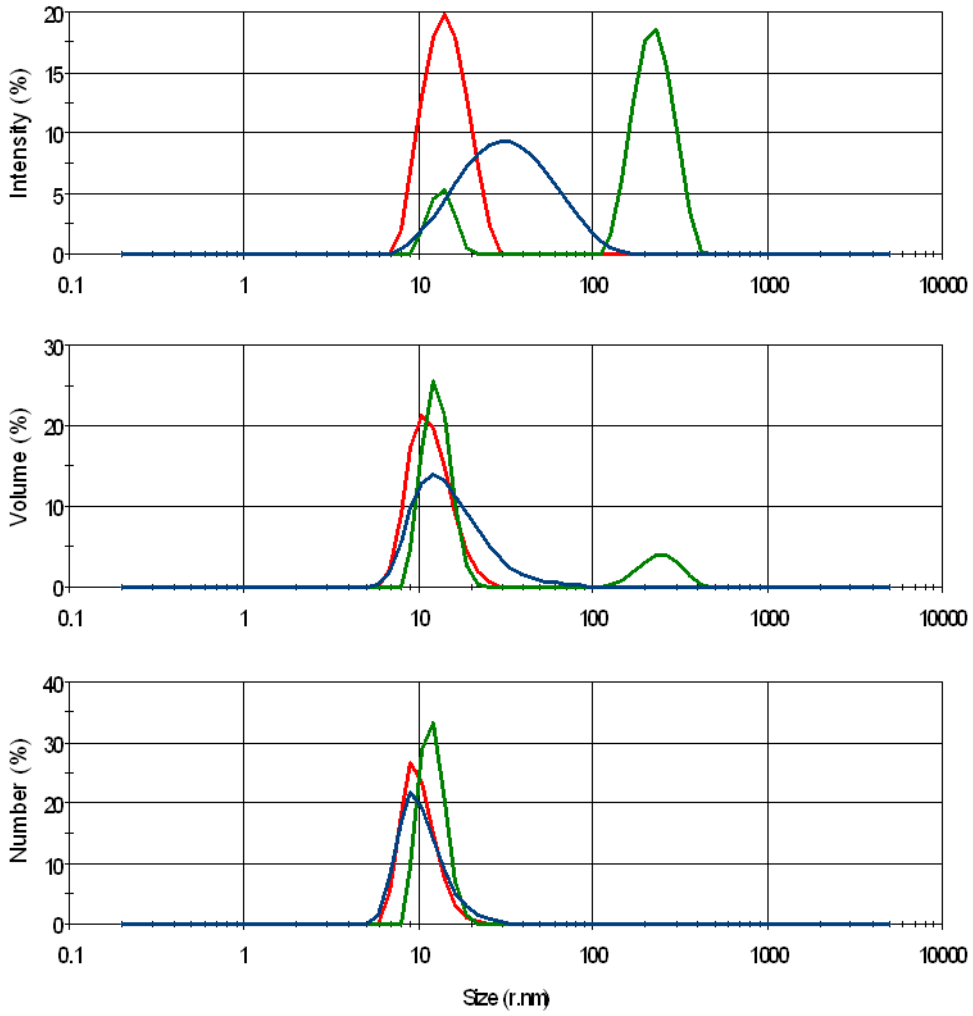

Figure 50. DLS measurements showing the difference between bare AgNPs 20 nm (red trace), lipo-AgNPs 20 nm without any treatment (green trace) and lipo-AgNPs 20 nm after extrusion through 50 nm pore size membrane (blue trace). The size distribution of particles in the samples is presented by intensity (top panel), volume (middle panel) and number (bottom panel).

Finally, the effectiveness of the nanoparticle surface passivation approach was probed. The lipoNPs complex was incubated with serum sample. In a parallel experiment bare AgNPs were employed as a control. After the incubation particles were recovered from the serum solution by centrifugation and, following several washing steps, introduced to MALDI MS analysis. The analysis revealed severe physisorption of serum compounds to the bare particles. Differently, in the case of the LipoNP construct, no unspecific binding was observed (Figure 51). This indicates the efficient passivation properties of the lipid bilayer.

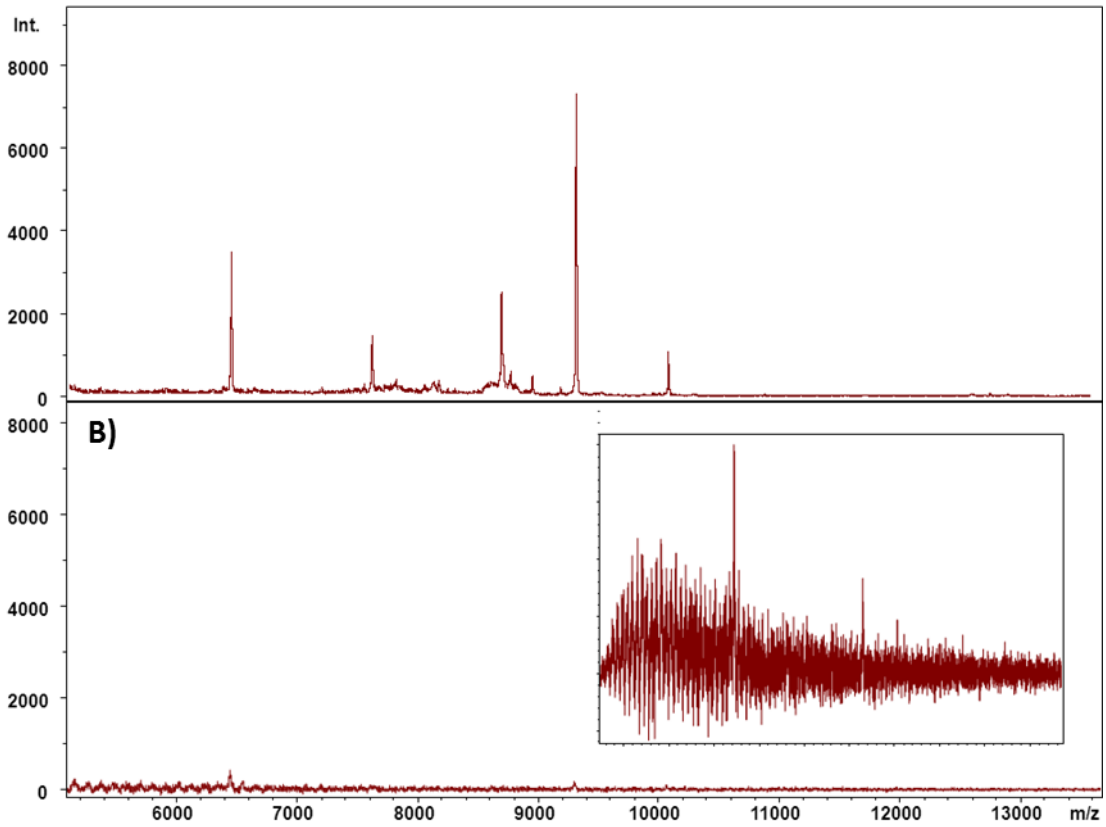

Figure 51. MADLI MS spectra of: A) bare AgNPs after incubation with serum B) lipoNPs after incubation with serum – the insert shows the spectrum normalised to the highest intensity ion.

4.4. Nanoprobe fabrication

The constructed LipoNPs proved to be stable and passive in terms of the surface non-specific binding. Therefore, the attempt was made to additionally functionalise the LipoNPs with the previously studied cell penetrating peptide (CPP), with the goal of developing a generic nanoprobe model. In parallel, an alternative approach to functionalise nanoparticles with CPP was also carried out, where polyethylene glycol (PEG) was used instead of the lipid bilayers.

The well-established cross-linker: 4-(N-maleimidomethyl)cyclohexane-1-carboxylic acid 3-sulfo-N-hydroxysuccinimide ester (SMCC) (Figure 52) was used as coupling moiety. SMCC is a heterobifunctional reagent, which incorporates an extended spacer with both sulfhydryl and amine reactivity. SMCC can form amide bonds with primary amines and can couple molecules containing free sulfhydryl group via thioether bond.[168]

To enable the attachment of CPP to LipoNPs via SMCC, the CPP was extended with one cysteine at the N-terminus (CKIAKLKAKIQKLKQKIAKLK-am). Also, the DLPC making up the outer layer on the LipoNPs was replaced by 1,2 dilauroyl-sn-glycero-3-phosphoethanolamine (DLPE) (Figure 85), which contains a primary amine group.

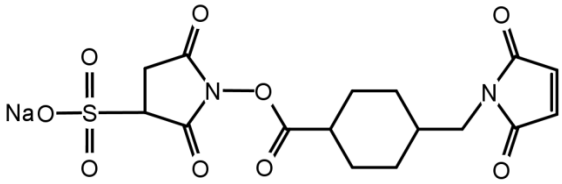

Figure 52. Chemical structure of SMCC.

Schematic representation of the LipoNP functionalisation process is shown in Figure 84. The protocol consists of four steps. Firstly, AgNPs are conjugated with thiol-modified lipid (DPTTE) as described previously. In parallel, the cross-linker is attached to DLPE, giving rise to DLPE-MCC. Next, the two are combined together resulting in NP covered with lipid bilayer and malemide reactive groups. Lastly, cysteine modified CPP is attached to the construct by reacting with the malemide groups.

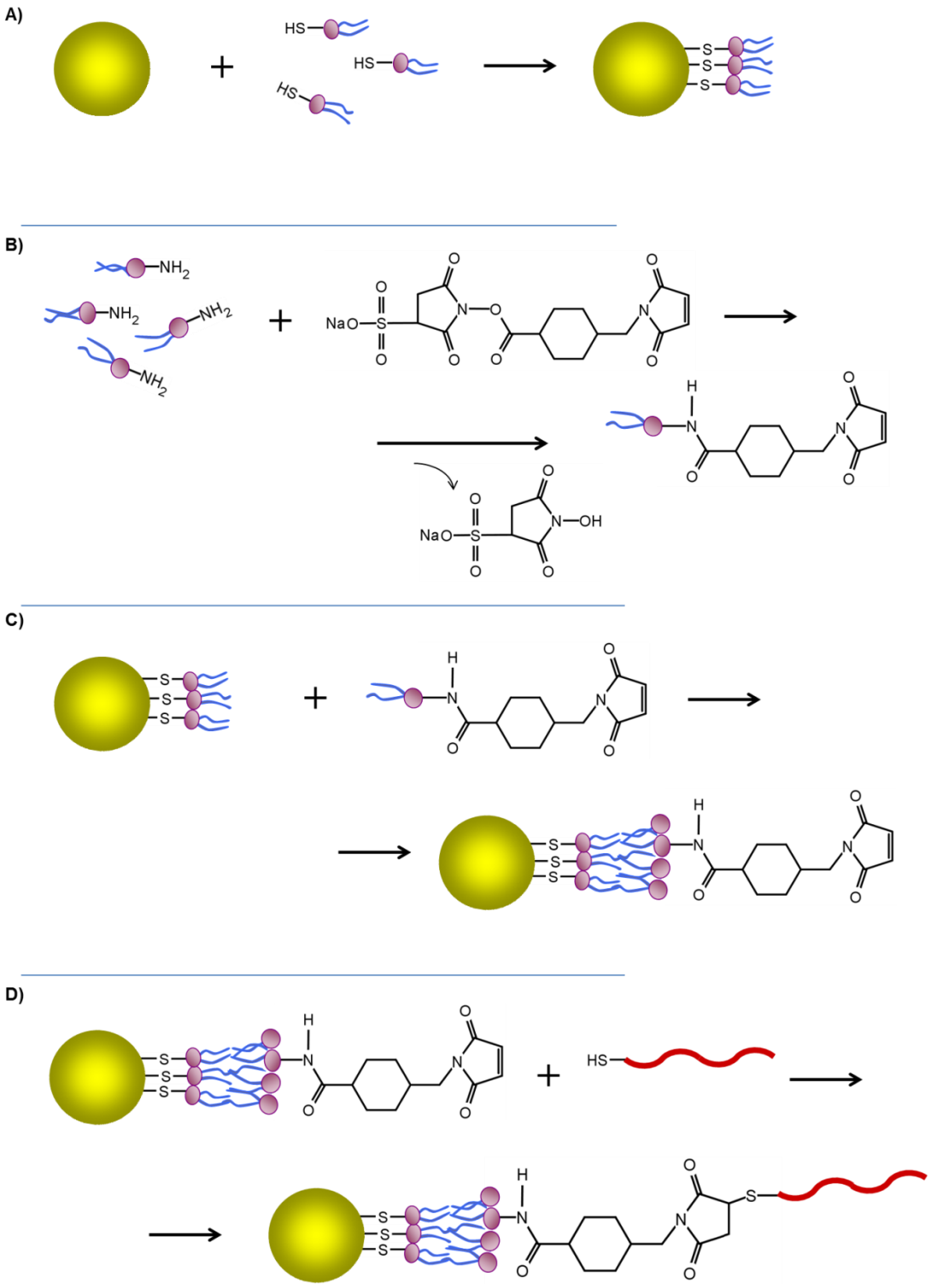

Figure 53. LipoNP-CPP fabrication: A) AgNPs are conjugated with DPTTE resulting in AgNP-DPTTE; B) in parallel SMCC is attached to DLPE; C) AgNP-DPTTE and DLPE-MCC are combined together into AgNP-DPTTE-DLPE-MCC; D) CPP-Cys is conjugated to AgNP-DPTTE-DLPE-MCC resulting in LipoNP-CPP.

Second approach involved the use of polyethylene glycol in place of the lipid bilayers. PEG is inexpensive, water soluble, coiled polymer of repeating ethylene ether units, commonly used to functionalise the surface of nanoparticles. The molecule is known to improve particle stability and passivate the NP surface from unspecific physisorption when applied to biological samples. It has been also reported that PEG coating, known also as PEGylation, can enhance the particle transport through biological barriers. [169-172]

Thiol-PEG-amine (2000 Da) (Figure 54) was obtained and applied to the AgNP functionalisation, what also allowed the use of SMCC cross-linking chemistry for the CPP attachment.

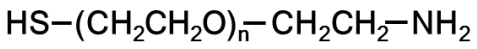

Figure 54. Thiol-PEG-amine.

The protocol of the probe fabrication with the use of PEG was developed. Schematic representation of the process is shown in Figure 55 below. This procedure consists of three steps; Firstly, AgNPs are covered with PEG molecules using thiol-silver chemistry. Next, the cross-linker is attached to the PEG by reacting with PEG's primary amines. This step is followed by the addition of CPP-Cys bonding to the construct by reacting with the malemide groups.

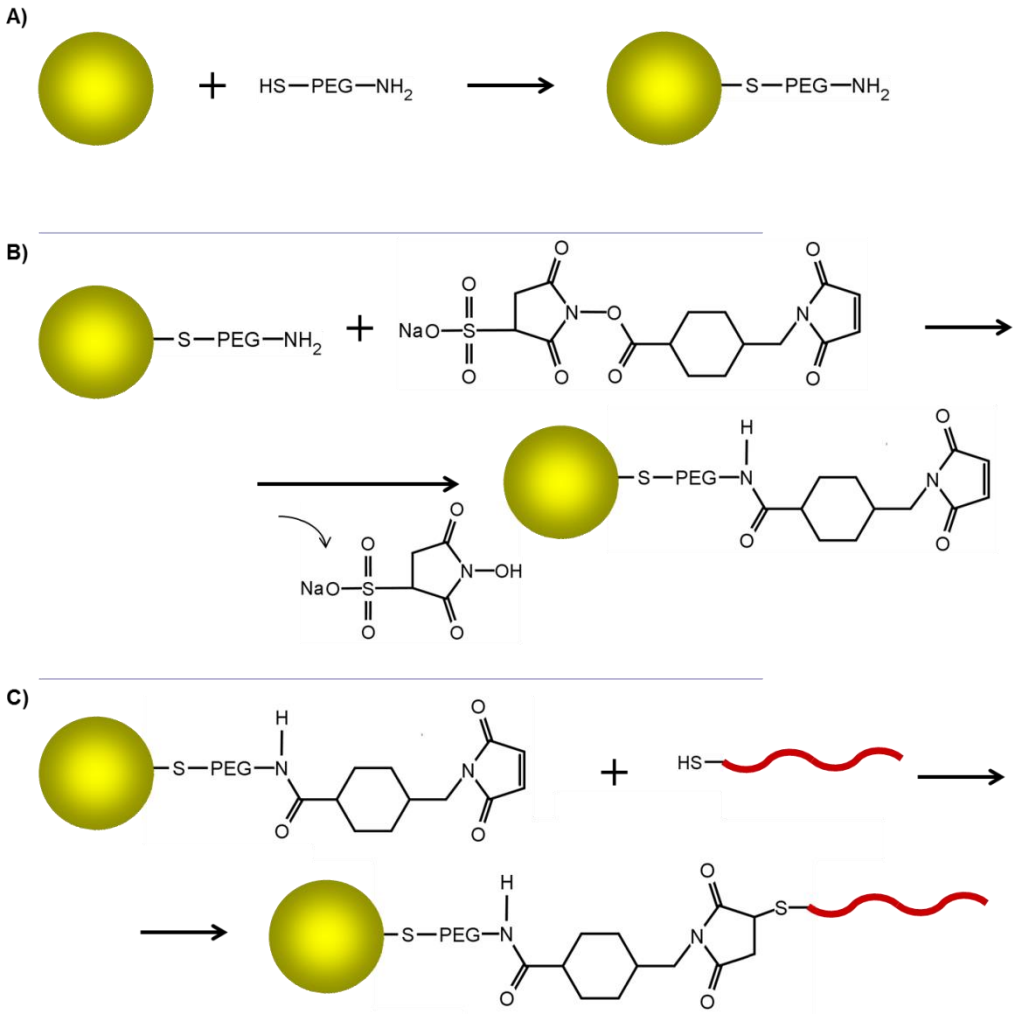

Figure 55. Fabrication of NP-PEG-CPP: A) AgNPs are covered by Thiol-PEG-Amine; B) MCC is attached to the free amine groups on the PEG coated particles; C) CPP-Cys is conjugated to AgNP-PEG-MCC resulting in NP-PEG-CPP.

4.5. Nanoprobe assessment

To prove that the functionalisation of the nanoparticles with CPP-Cys was successful, the fabricated probes were next analysed by MALDI MS, DLS measurements and TEM imaging.

The mass spectra of the Lipo-NP-CPP showed the presence of DLPE-CPP conjugates: *m/z* 3221 $[M+H]^+$ and *m/z* 3265 $[M+2Na]^+$. This was expected taking into account the non-covalent nature of DLPE-CPP complex attachment to the particle. During the 'in-vacuum' mass spectrometric experiment the complex easily detaches from the nanoprobes (Figure 56).

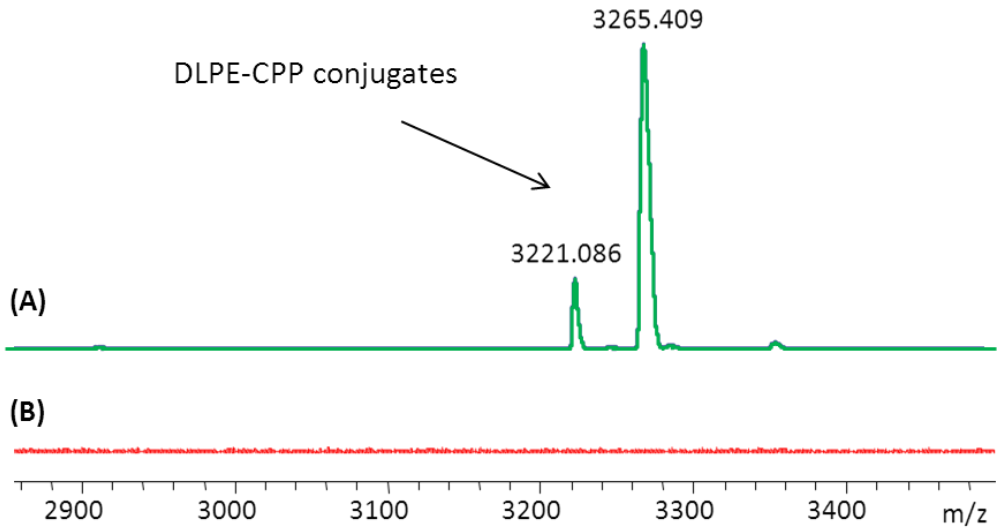

Figure 56. MALDI MS detection of DLPE-CPP complexes (*m/z* 3221 $[M+H]^+$ and *m/z* 3265 $[M+2Na]^+$) on the fabricated Lipo-NP-CPP probe (A). No ions of bare silver nanoparticles, analysed as negative control, were detected in the analysed mass range (B).

In order to confirm the presence of CPP in the NP-PEG-CPP construct, by MALDI MS, the pre-treatment of the probe was necessary. In this case all the links between different nanoprobe modules were of covalent nature. Hence, it proved difficult to fragment the construct into informative molecular ions. Ammonium thiocyanate, known to react with silver resulting in its precipitation, was added to the solution of NP-PEG-CPP. After 1 hour incubation the solution with dissolved silver particles and released PEG-CPP conjugates were analysed. Analysis of MALDI mass spectra revealed the presence of the PEG-CPP complexes: *m/z* 4805.8 $[M+H]^+$ (Figure 57).

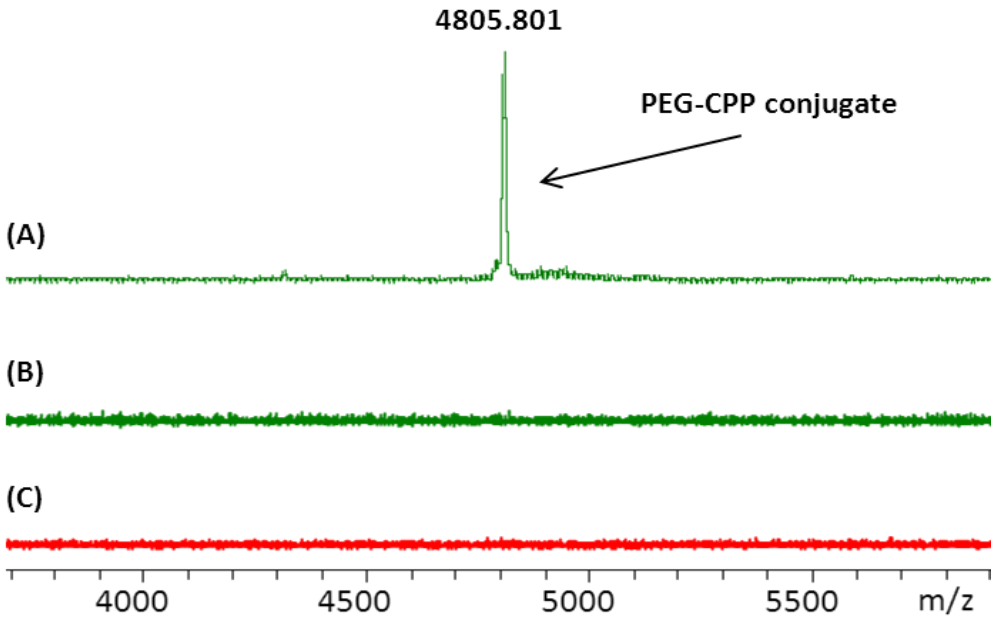

Figure 57. MALDI mass spectra of the detected PEG-CPP complexes (*m/z* 4805.8 $[M+H]^+$) from the fabricated and dissolved in ammonium thiocyanate NP-PEG--CPP probe (A). For comparison, spectra of intact NP-PEG-CPP probe (B) and bare AgNPs, where no ions were detected in the analysed mass range (C).

The functionalised nanoprobes were then analysed by DLS. For comparison, bare 20nm AgNPs were also employed. As previously, the LipoNP-CPP were extruded through 50 nm pore size membrane prior to the DLS analysis. No particular change in the particle diameter was observed when LipoNP-CPP were measured. In addition, a presence of high molecular weight components was observed in the solution (Figure 58).

The notable change in the diameter was observed for the NP-PEG-CPP complex. A fraction of aggregates within the sample was also observed, while calculating the size distribution by intensity. However, as indicated by volume and concentration records, monodisperse nanoprobes constituted the main population of particles in the sample (Figure 59).

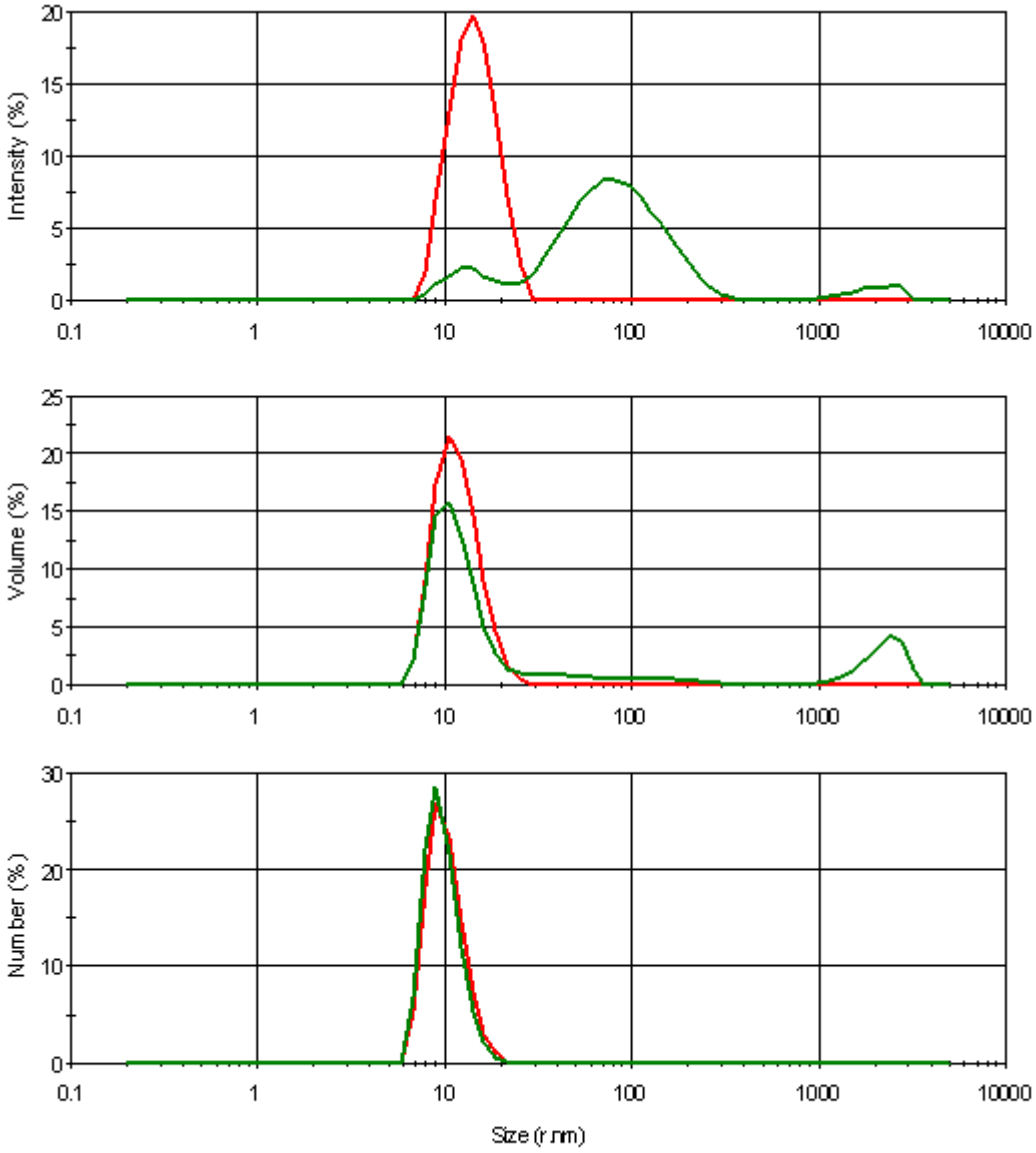

Figure 58. DLS measurements showing the difference between bare AgNPs 20 nm (red trace) and lipo-NP-CPP (green trace). Particle size distributions are presented by intensity (top panel), volume (middle panel) and number (bottom panel).

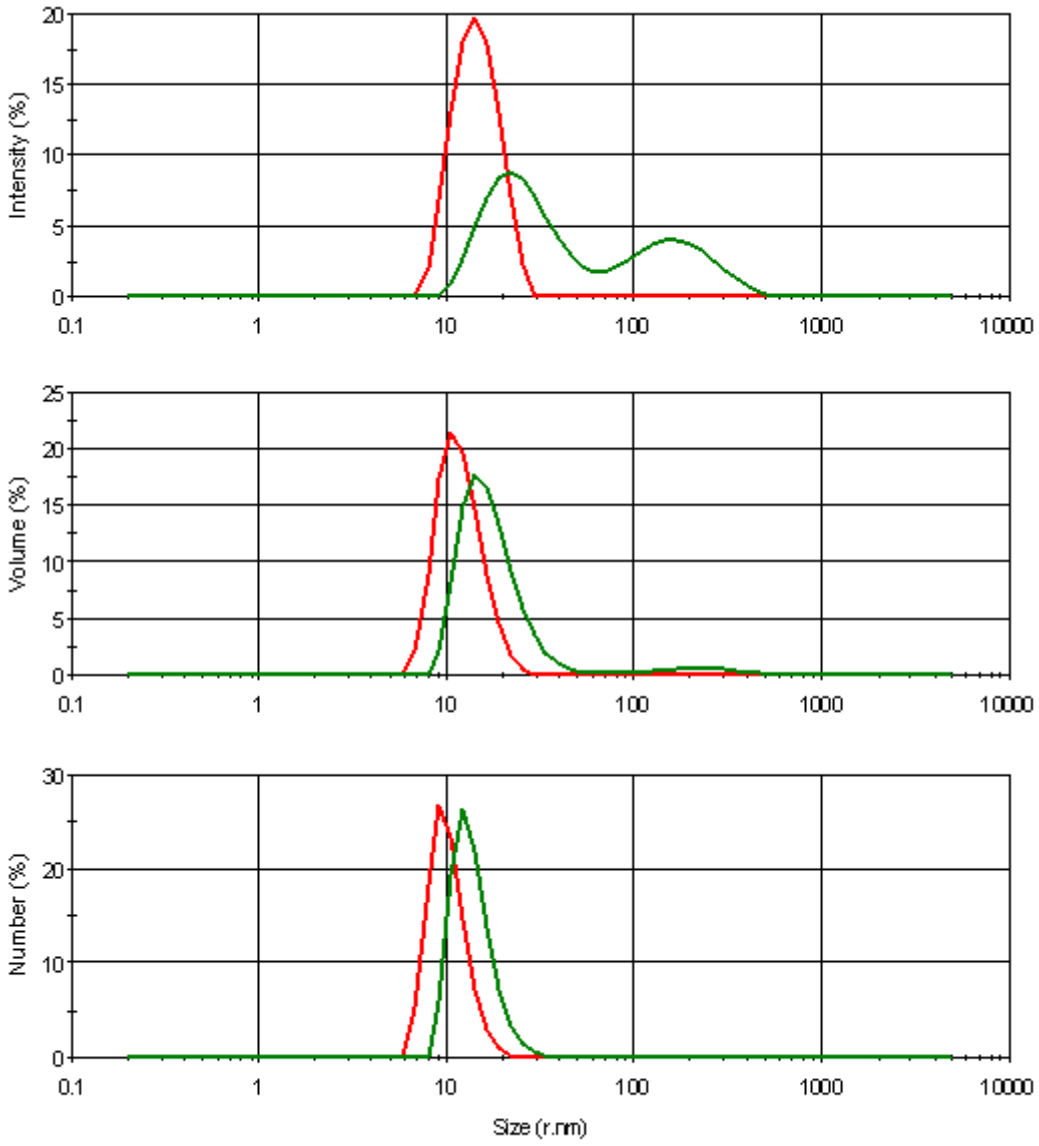

Figure 59. DLS measurements showing the difference between bare AgNPs 20 nm (red trace) and NP-PEG-CPP particles (green trace). Top panel presents particle size distribution by intensity, middle by volume and bottom panel by number.

Further assessment of the LipoNP-CPP and NP-PEG-CPP constructs was carried out by transmission electron microscopy (TEM). The method provides information of sample shape and morphology and enables imaging at high, sub-nanometer resolution (see 5.1.7).[173, 174] For comparison, bare particles as well as particles with only CPP-Cys attached (NP-CPP) were also imaged.

Examination by TEM showed the lack of aggregation of the constructed NP-PEG-CPP (Figure 60, Figure 61 & Figure 62). However, no visual difference could be observed between the NP-PEG-CPP and NP-CPP and NP-PEG-CPP particles.

In contrast, LipoNP-CPP samples revealed fibrillar structures decorated with nanoparticles (Figure 63). This explained the results obtained by the prior DLS measurement. Most likely, the fibres are a result of the interaction and co-folding of DLPE-MCC-CPP assemblies. AgNPs with conjugated DPTTE in a form of inverted micelles, from where the outer lipid layer was detached, are drawn to the fibres. The reports of similar peptide-lipid assemblies have been found in the literature.[175] It is believed that similar structures are created, not accidently, but as a result of different processes that are happening at molecular level. Nevertheless, this phenomenon eliminated the further use of the LipoNP-CPP for the studies of mammalian cell transfection as the fibre assembly causes nanoprobe decomposition. However, the nanoprobe construct as well as the fibres are being investigated and its antimicrobial properties are being evaluated.

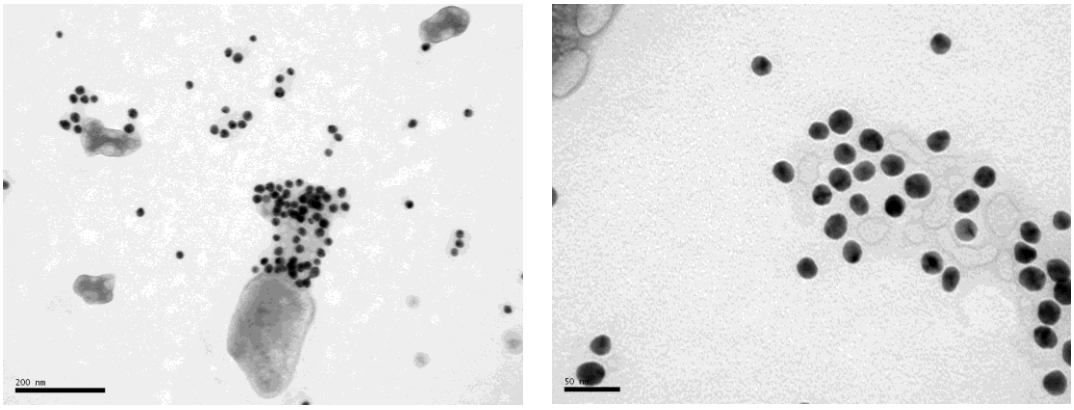

Figure 60. TEM images of bare 20 nm AgNPs.

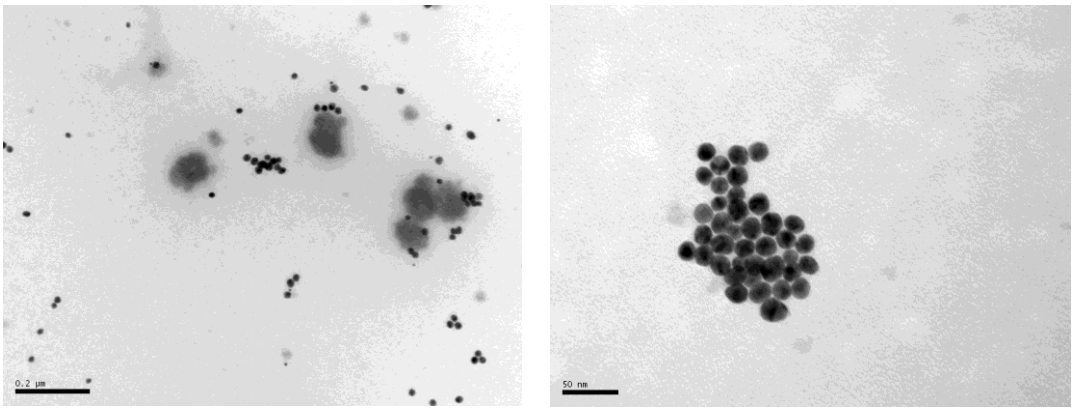

Figure 61. TEM images of AgNP-CPP conjugates.

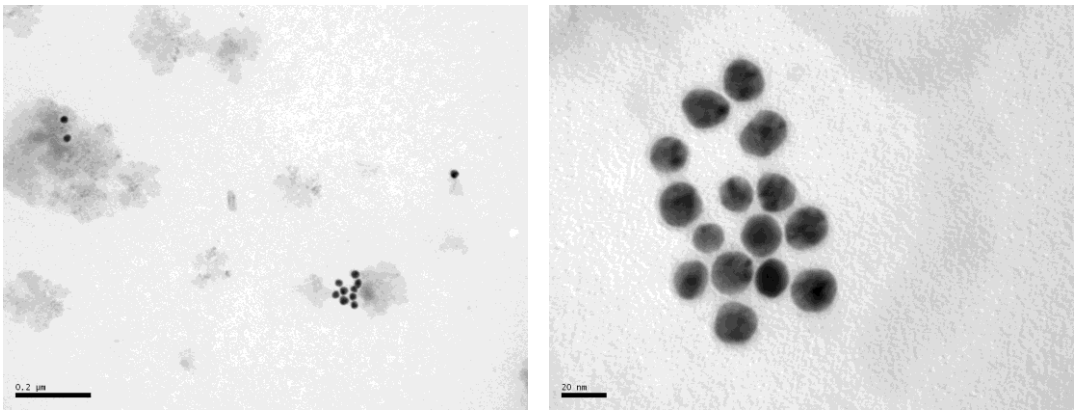

Figure 62. Images of NP-PEG-CPP.

(A)

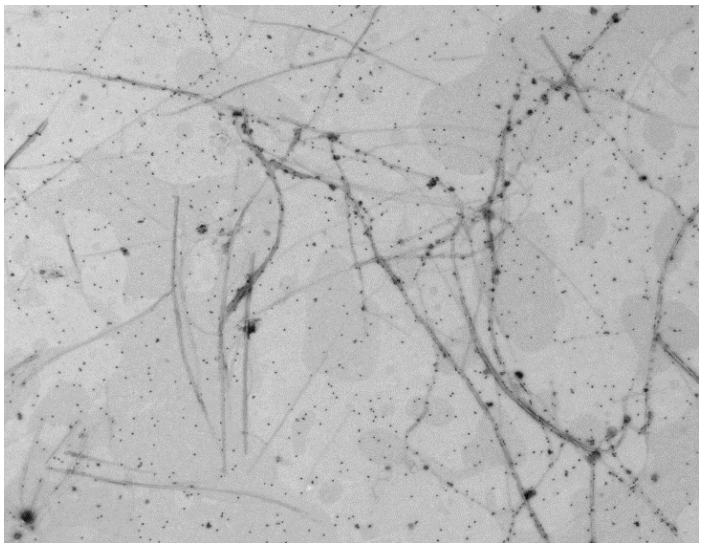

(B)

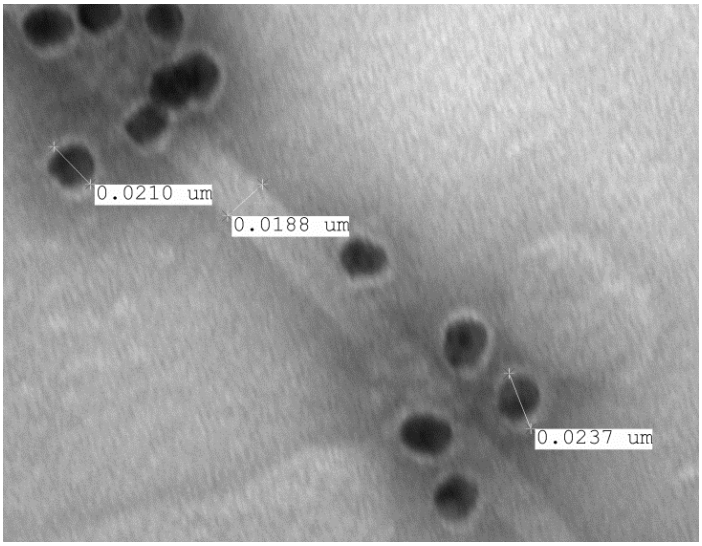

Figure 63. LipoNP-CPP imaged by TEM, revealing fibre like structures (A)) and magnification showing nanoparticles attached to the fibres (B)).

4.6. Nanoprobe use in biological samples

Following the successful nanoparticle functionalisation, cell transfection with the NP-PEG-CPP was next carried out.

In three parallel experiments, human dermal fibroblasts (HDFa) were incubated with bare AgNPs, NP-CPP and NP-PEG-CPP. All three types of the particles were used at the same AgNP concentration of 5 μg/mL for 3 and 6 hours. Bare particles as well as NP-CPP served as a comparison. Precipitation of large fraction of particles was observed after adding bare AgNPs to the incubation medium. Nothing similar was noticed in the case of the two remaining types of nanoprobes. After washing off the cells from the non-internalised particles, cells were fixed by treatment with gluteraldehyde, embedded in resin and, following resin block slicing, imaged by TEM. The imaging revealed that all, the bare AgNPs as well as the functionalised NP-CPP and NP-PEG-CPP were taken up by the cellular cytoplasm. The representative images can be found in Figure 64 to Figure 69. From the obtained images it was not possible to state the amount of internalised particles. Also, as judged by visual observation, the different incubation times did not result in any difference in the NPs uptake.

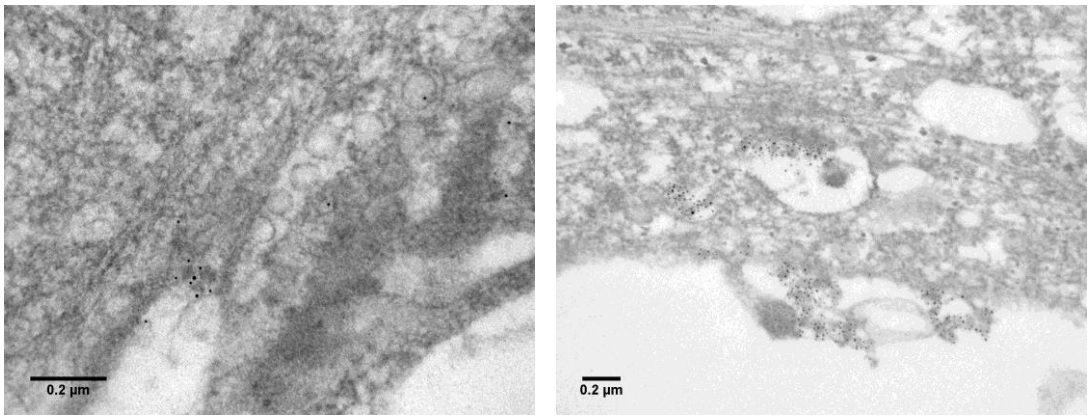

Figure 64. Representative TEM images of HDFa cells transfected with bare AgNPs after 3 h incubation.

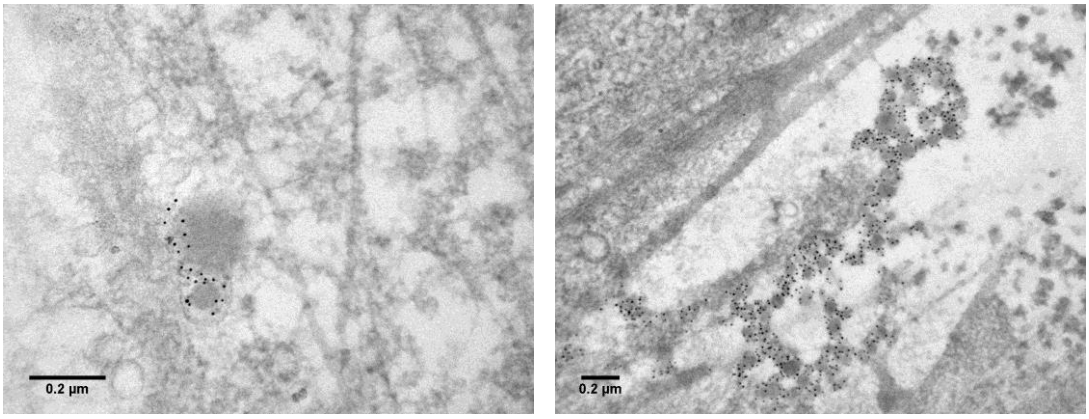

Figure 65. Images of HDFa cells transfected with bare AgNPs after 6 h incubation.

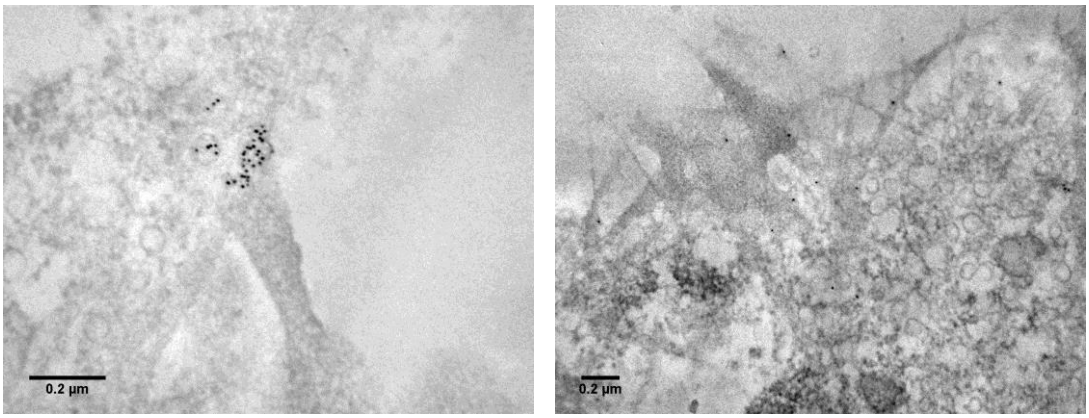

Figure 66. HDFa cells after 3 h incubation with NP-CPP.

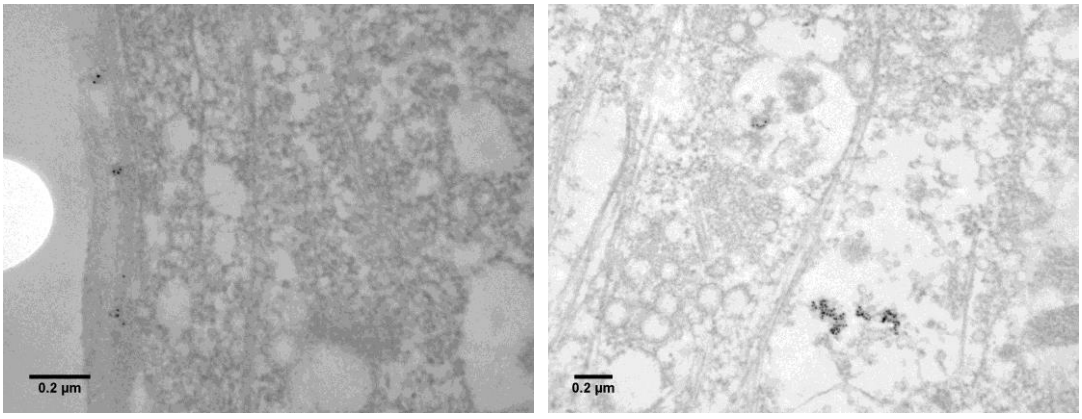

Figure 67. TEM of HDFa cells incubated with NP-CPP for 6 h.

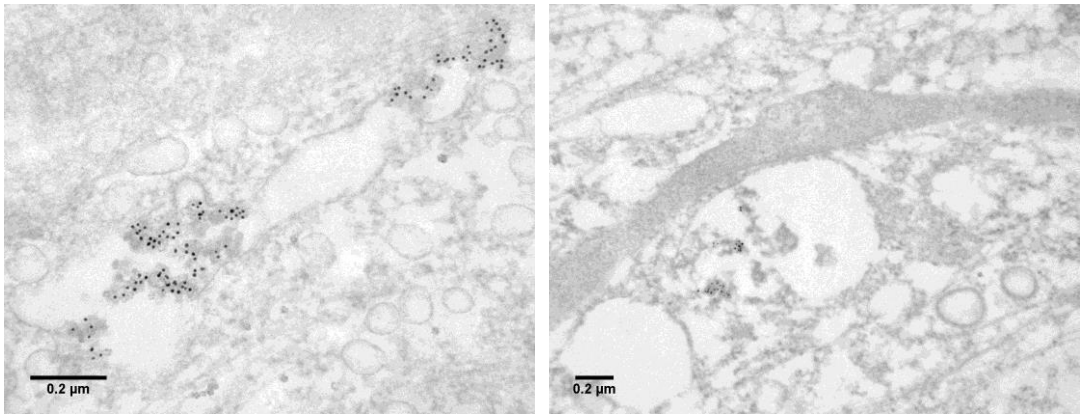

Figure 68. Representative TEM images of HDFa cells transfected with NP-PEG-CPP after 3 h incubation.

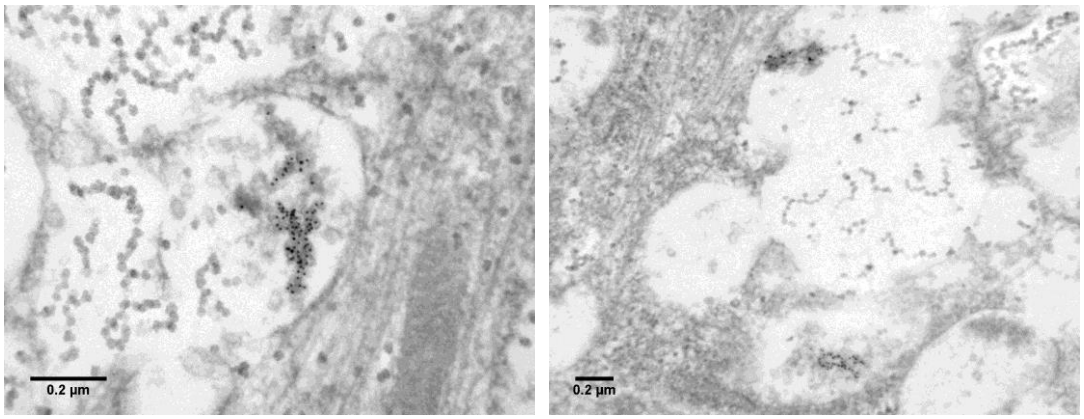

Figure 69. TEM images of HDFa cells transfected with NP-PEG-CPP after 6 h incubation. Beads-on-string structures are clearly visible.

Despite the lack of visible differences in terms of transfection efficiency between different particles, distinct structures, described for the purpose of this chapter as 'beads-on-string', were evident in the cells treated with NP-PEG-CPP (Figure 69, Figure 70). Similar structures could be observed in cell samples treated with gold nanoparticles, where osmium and lead staining was used (based on personal communication with Mark Turmaine, (UCL). The structures may present a fixation artefact. However, it is suspected that they are related to a protein or peptide material attached to the nanoparticles. There is also question arising from the fact, that those features were only observed when cells were incubated with PEG-coated probes and for longer time. Is this the functionalisation of the nanoprobes causing the cell to produce the 'beads-on-string', such as PEG-CPP assemblies, or is there a possibility of the probe interaction with specific molecules

within the cell? More studies are needed to investigate the findings and provide more information regarding content associated with the structures.

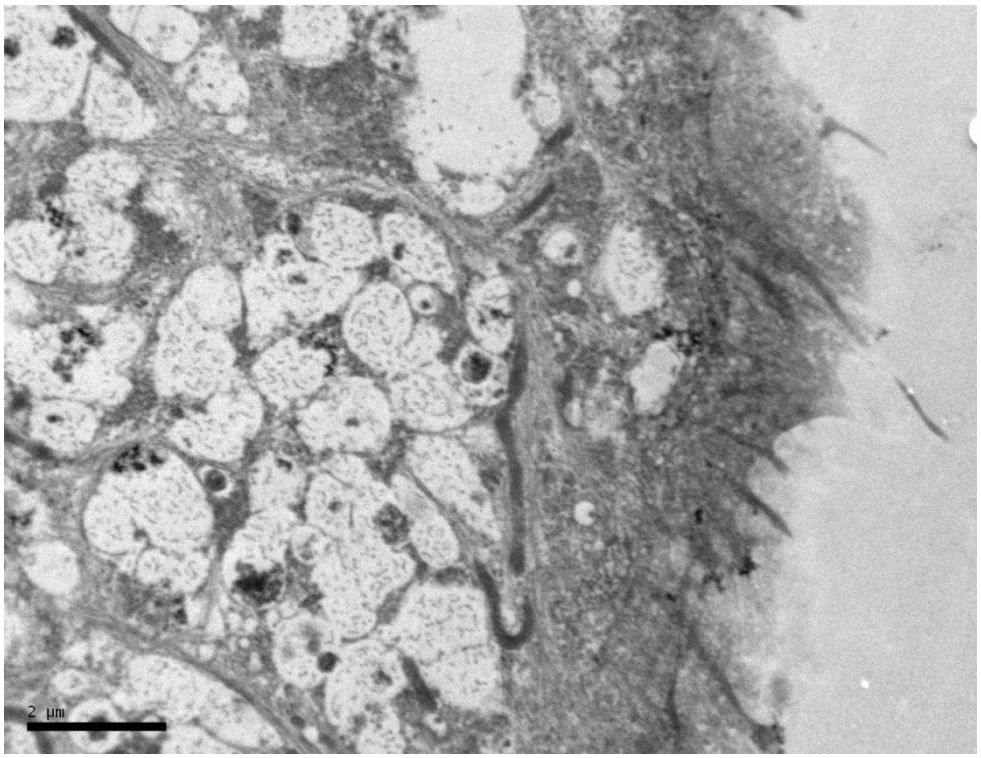

(A)

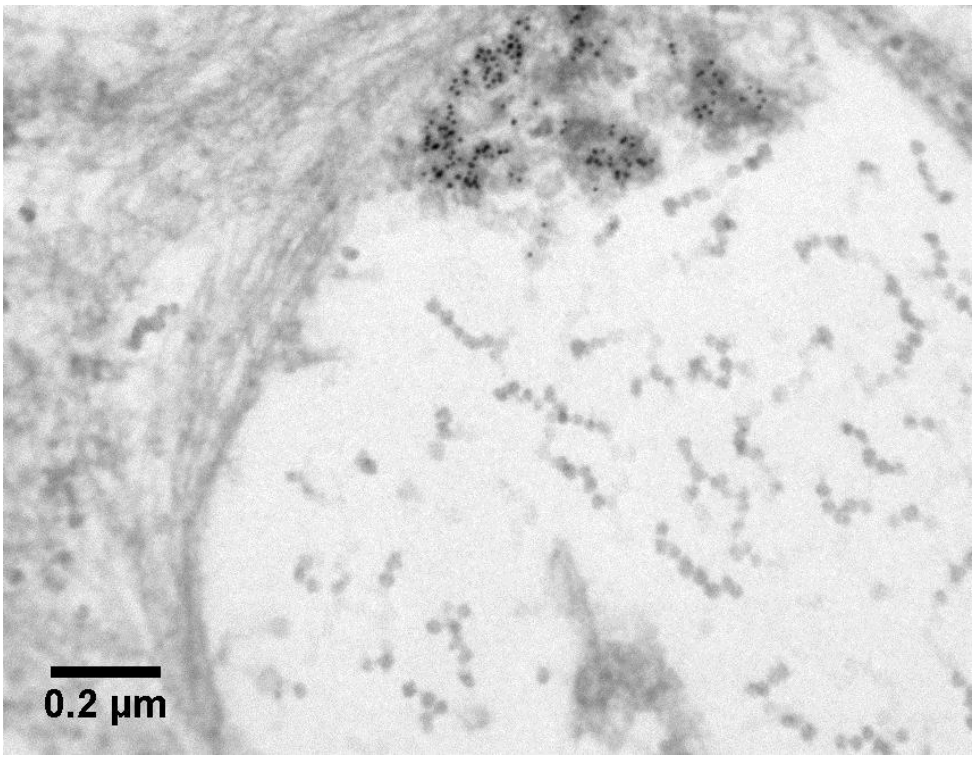

(B)

Figure 70. TEM images of "beads-on-string' like structures; lower (A) and higher (B) magnification. Those features were only observed in cells transfected with NP-PEG-CPP after 6 h incubation.

4.7. Conclusions

In this chapter, generic, functionalised peptide nanoprobes were described. Silver nanoparticles served as a base for creation of modalities for intracellular delivery.

Initially, metallic nanoparticles were coated to enable their surface-passivation. Covering the particles by lipid bilayer prevented non-specific surface physisorption of biomolecules from a complex serum sample. Also, such prepared particles proved easy to handle and stable under vigorous treatments.

Next, two protocols for the functionalisation of silver nanoparticles with a model cell penetrating peptide were developed. They included lipid bilayer and polyethylene glycol coatings, to which the CPP was cross-linked. The ability of the created probes to interact with the cells was investigated by transmission electron microscopy.

Examining of the created probes and their behaviour with the mammalian cells led to several conclusions:

Firstly, images of LipoNP-CPP exposed the presence of fibre-like structures in the samples, which are most likely a result of the co-folding of DLPE-MCC-CPP molecules. This observation excluded the further use of the LipoNP-CPP for the studies in cell transfection experiments;

Secondly, the transfection efficiency to HDFa cells of NP-PEG-CPP probes has been examined and compared to the uptake of bare AgNPs and peptide only-coated particles. Although no visible differences from the applications of the different particles have been observed, the NP-PEG-CPP proved well suited to the transfection purpose. Same time, distinct structures were discovered in the cells treated with NP-PEG-CPP. The nature of the structures is not known and requires further investigation.

The use of metallic particles as the base for the intended nanoprobes enabled their clear visualisation in cell compartments. The particles are imaged by TEM without the need for any additional dyes of fluorescent ligands. It would not be possible if only cell penetrating peptides alone were employed to the intracellular delivery studies.

At last, the employed nanoparticle surface coating appeared beneficial in comparison to the use of bare nanoparticles. Once created, the nanoprobes are

stable and insusceptible to aggregation and precipitation in high-salt solutions, such as cell culture media.

In summary, the attempt to functionalise nanoparticles with function-carrying model peptides was successful. In this study as a model system, a cell penetrating peptide was used, which directed the probes to the cell cytoplasm. The created platform forms a base for the fabrication of nanoprobes. In the future applications, nanoparticles can be readily conjugated with other peptidic moieties, targeting different organelles and with desired properties and specific activities, resulting in specific bio-molecular markers, intracellular cargo delivery or selective biomarker targeting and binding.

CONCLUSIONS AND OUTLOOK

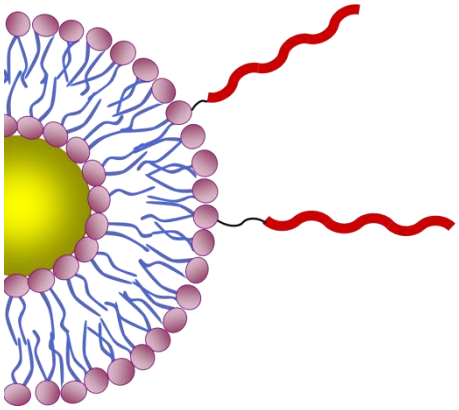

Peptides can serve as excellent biomarkers and can be also used as templates in chemical biology for the design of peptide-mediated probes. Advancements in nanotechnology provide opportunities to establish novel, sensitive, and selective methods for a wide range of bioanalytical platforms. This project investigated a specialist intra- and extracellular targeting, enabled by rationally designed membrane-active, as a base for the development peptide-based tools, for applications in cell biology, in a form of nanoscale probes.

De novo designed cell penetrating and antimicrobial peptides were assessed as candidates for a nanoprobe functionalisation to allow specific cell surface and trans-membrane targeting. The interactions of the peptides with model bacterial and mammalian cell membranes were assessed using molecular biophysics and microbiology assays. The results confirmed that the peptides differentially interact with the two kinds. The peptides possess effective antibacterial properties while not exposing destructive effects towards mammalian membranes.

The elucidation of the mechanism of the antimicrobial action was carried by new comparative approach, where atomic force microscopy analyses were combined with stable isotope imaging by Nano-Secondary Ion Mass Spectrometry. This provided high-resolution visualisation of the topography of peptide-treated membranes complemented by chemical imaging, revealing the precise localisation of peptide molecules in the membranes. The results allowed reviewing

the prevailing molecular model for antimicrobial mechanisms. It was shown that the formed pores are not limited to a particular diameter, nor they are transient, but can expand laterally at the nano-to-micrometer scale to the point of complete membrane disintegration. Real-time AFM imaging in liquid further confirmed the findings.

Model cell penetrating peptides were used to investigate targeted intracellular delivery and endosomal release. Confocal fluorescence microscopy revealed different fluorescent patterns for two studied peptides: *de novo* engineered CPP and naturally occurring TaT. Differential accumulation of the peptides in Human Dermal Fibroblasts (HDFa) was observed. CPP dispersed in the cytoplasm, while TaT remained entrapped within endosomes. These results confirmed that the *de novo* design of CPP promotes peptide escape to into the cytoplasm by permeabilising endosomal membranes.

In parallel, peptidomic processing approach was implemented and validated for the quantification of cellular uptake of the two cell penetrating peptides. The method presents tag-free approach and employs combination of liquid chromatography and isotope dilution MALDI mass spectrometry. The quantities of designed and naturally occurring peptides, internalised in HDFa were measured, compared against each other and correlated to the observations provided by fluorescence confocal microscopy. The applied methodology proved to be simple and reproducible and possessing several advantages over commonly used tag-based methods. The obtained results suggest that under applied experimental conditions, the engineered CPP is similarly efficient, in terms of cell penetration, as the endogenic TaT. This aids the concept of rational design and the use of synthetic biology for the development of novel tools.

The last part of the research focused on the development of a generic nanoprobe with the use of metallic nanoparticles and cell penetration peptides. Preliminary results pointed to the need of the particle surface passivation against the undesirable, non-specific binding of molecules from biological samples. For these reasons, the protocol for the coating of silver nanoparticles with lipid bilayer was established and the coated particles were assessed, proving their stability, ease of recovery as well as their passiveness towards surface non-specific physisorption.

Two protocols for the functionalisation of nanoparticles were established. In the first approach, CPP was attached to the particle via modification to lipid bilayer, in which the particle was enclosed. The second method comprised the covering of the particles with PEG coating, followed by the conjugation of the peptide. The created nanoprobes were examined by transmission electron microscopy. Images of LipoNP-CPP reviled the presence of fibre-like structures in the samples, which are most likely a result of the co-folding of DLPE-MCC-CPP molecules. This observation excluded the further use of the LipoNP-CPP. However, the construct is now investigated under separate project run in Bioengineering Group at NPL, where its assembly process and antimicrobial properties are being evaluated. The proficiency of the second designed probe, NP-PEG-CPP was tested with living cells and compared to the effect that bare AgNPs and particles coated with the peptide only have on the cells. Despite the fact that no visible differences from the applications of the particle variants were observed, some distinct structures, which can be described as 'beads-on-string', were noticed in the cells treated with NP-PEG-CPP. No reported evidence of similar phenomena has been found and presently their origin can only be speculated. The nature of the structures is not known and requires further investigation by carefully designed studies, taking into account many factors such as nanoprobe functionalisation and its interaction with biomolecules within the cells, the cell response to the treatment with the probe or thorough examination of sample preparation process for TEM imaging and its effect on the probed material. Still, the attempt to functionalise nanoparticles with function-carrying ligands was effective.

Research described in this thesis is complex and challenging. It resulted in several publications, reprints of which can be found in the following section. This research does not finish here and already several of its parts are investigated under follow-on projects. This research provides a base for the further use of rational peptide design for specific cell surface and trans-membrane targeting and intracellular delivery, and the fabrication of peptide-based tools in a form of multi-functionalised nanoprobes of desired properties and activities.

CHAPTER 5

METHODOLOGY

This chapter provides a brief overview of the main techniques employed in the course of the study, their short description and examples of relevant applications. Further, all methods used and detail protocols implemented to the described experiments are given.

5.1. Techniques

5.1.1 CD

Circular dichroism (CD) is a spectroscopic technique that measures the difference in absorbance of right-hand and left-hand circularly polarised light by optically active samples. CD can be expressed by the following equation: $CD = Absorption_{(right)} - Absorption_{(left)}$. Light absorbances in the ultraviolet (UV), visible and infrared (IR) wavelength regions are routinely used in chemical and biochemical research to probe secondary structure and conformational changes of molecules in solution. Therefore, CD has become a standard method in the characterisation of biopolymers such as peptides, proteins and nucleic acids.

Far-UV CD is applied for the structural characterisation of peptides allowing estimating the degree of peptide conformational order and secondary structure content (e.g. α-helix). To the key points for visual assessment of secondary structure, based on CD spectrum, belong the following facts: a) α-helix results in negative bands at 222 nm and 208 nm and a positive band at 193 nm; b) β-sheet gives negative bands at 218 nm and positive bands at 195 nm and c) the lack of any ordered secondary structure will not present any peaks above 210 nm. Exemplar CD spectra associated with various types of secondary structures can be found in Figure 71. [140]

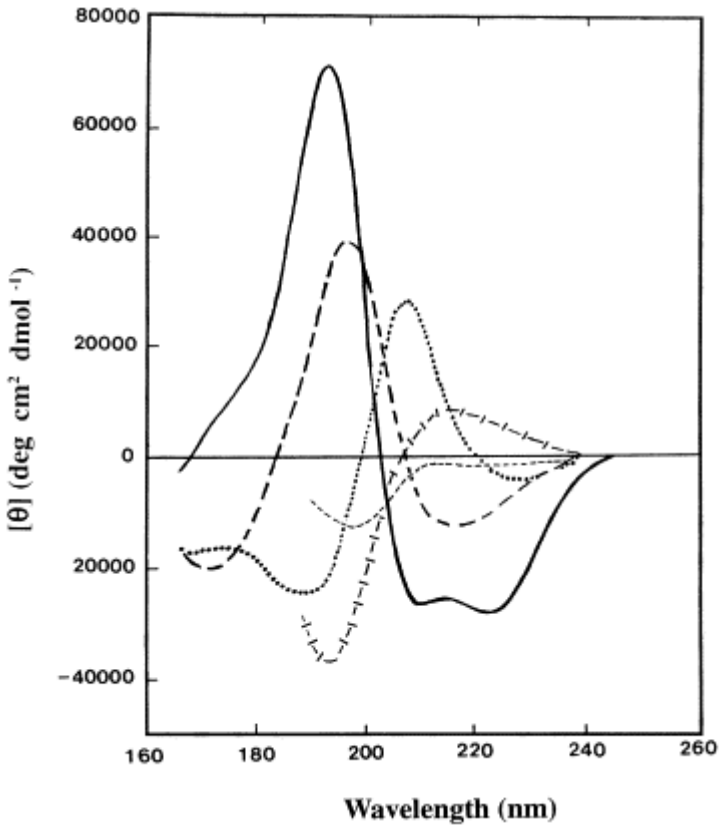

Figure 71. Far UV CD spectra associated with various types of secondary structure. Solid line, α-helix; long dashed line, anti-parallel β-sheet; dotted line, type I β-turn; cross dashed line, extended 31-helix or poly (Pro) II helix; short dashed line, irregular structure. Reprinted from Kelly, et al., *Biochim Biophys Acta*, 2005.[140] Copyright © 2005, with permission from Elsevier.

5.1.2 LD

Linear dichroism (LD) is related to the CD technique as both methods are based on the difference between the absorbances of differently polarised light beams. However, LD measurements are based on the differential absorption of linearly polarised light and are informative only when performed on systems that are or intrinsically oriented or can be oriented during the experiment. The difference in absorption of light linearly polarised parallel and perpendicular to the orientation axis is measured. Therefore, LD can be expressed by the following equation: $LD = Absorption_{(parallel)} - Absorption_{(perpendicular)}$. LD measurements are illustrated by Figure 72.

LD is an extremely attractive technique, which allows working in solution phase, providing information about conformation and orientation of sub-units of biomaterials and orientations of the whole biomaterial with respect to

an orientation axis. It can be used to study various samples such as: DNA, DNA-ligand complexes, carbon nanotubes, peptide and protein fibers. It can give insight into interactions between membrane proteins and peptides with liposomes. When the secondary structure of the probed molecule, such as peptide, is known (*e.g.* α-helical or β-sheet), it allows its orientation to be approximately determined. Figure 73 shows expected LD signals for an α-helix and a β-sheet species lying flat on the surface or being inserted in a membrane.

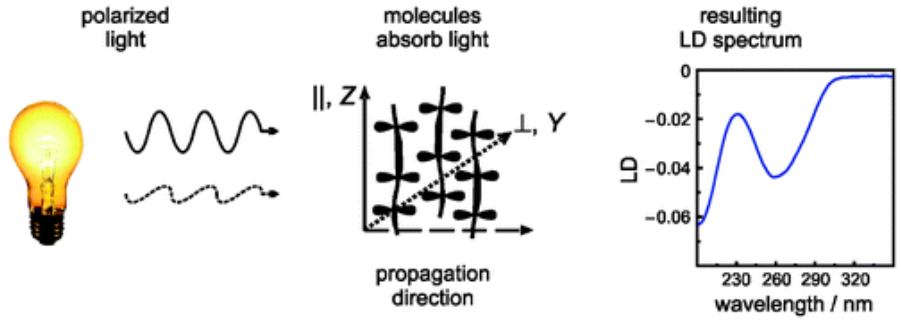

Figure 72. Schematic illustration of an LD experiment. Reprinted from Bulheller, et al., *Phys Chem Chem Phys,* 2007[176] with permission of the PCCP Owner Societies.

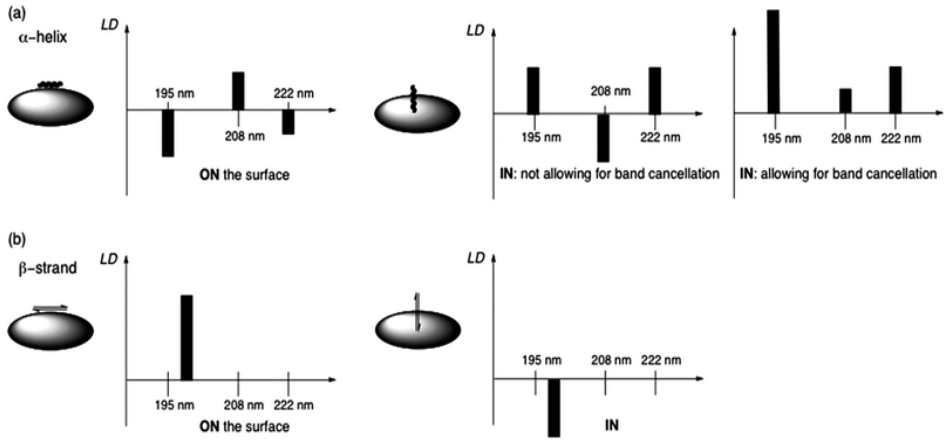

Figure 73. Scheme of expected LD signals; (a) an α-helix on or in a membrane, and (b) a β-sheet lying flat on the surface of or in a membrane. Reprinted from Hicks, et al., *Chem Soc Rev*, 2010[143] with permission from the Royal Society of Chemistry.

5.1.3 AFM

Atomic force microscopy (AFM) is a powerful surface analytical technique, which works by scanning a sample with a sharp, usually silicon tip, mounted at the end of a flexible cantilever. The AFM can image in a number of ways of which two most popular are: contact mode or an oscillating mode where the tip taps the surface. The forces between the tip and the sample during scanning cause the cantilever to deflect. Typically, the deflection is monitored using a laser beam and photodiode (Figure 74).

AFM allows generating high-resolution topographic surface images, with a spatial resolution down to 1-20 nm, depending on the sharpness of the used tip. It can be used to probe samples in air, in liquid or in vacuum. Apart from the topography, AMF can also provide some information on nanoscale chemical, mechanical, electrical and magnetic properties of the probed surface. AFM is commonly used in biology to study nucleic acids, proteins and peptides, tissues and living cells. The possibility to perform such measurements in situ is, next to the high-resolution the main advantage of this technique.

An example of AFM application is given below, represented by images obtained from the observations of the effects poly(amido amine) dendrimers have on supported 1,2-dimyristoyl-sn-glycero-3-phosphocholine (DMPC) bilayers (Figure 74).[177]

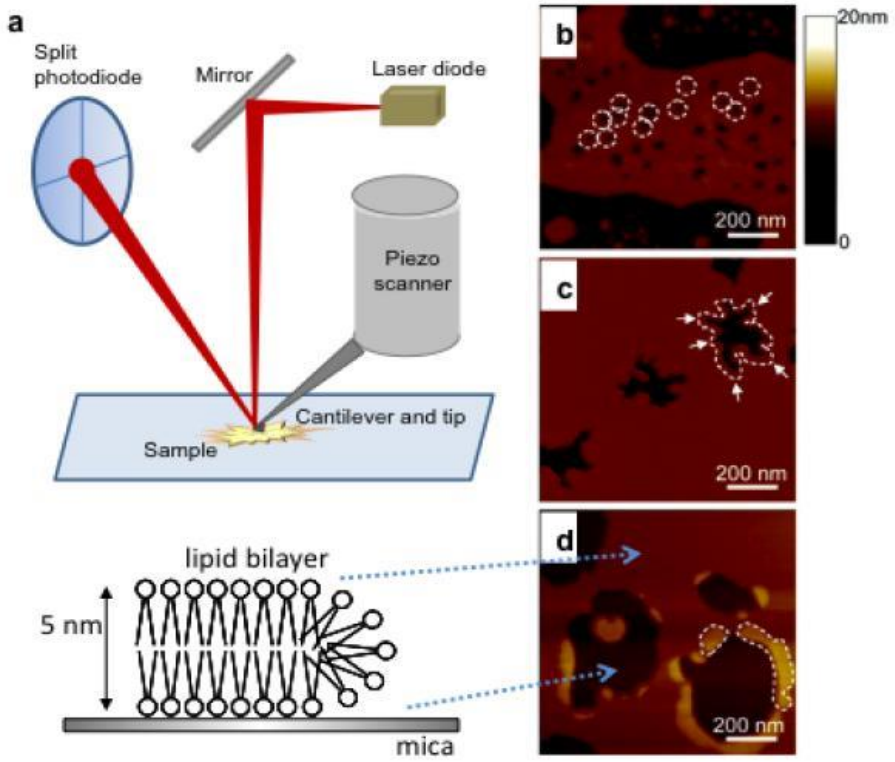

Figure 74. Diagram of an AFM: (a) AFM images surfaces or measures forces by scanning a tiny tip mounted at the end of the cantilever on a sample, which is controlled by a piezoelectric scanner. Interactions between samples and the tip are recorded by laser that is reflected to a split photodetector; (b)-(d) Example of AFM imaging of supported DMPC lipid bilayer after interaction with poly(amido amine) dendrimers. White lines highlight some of the areas where dendrimers have affected the bilayer (the dendrimer themselves cannot be seen on the images). (b) dendrimers cause the formation of small holes, 15–40 nm in diameter, in the previously intact parts of the bilayer; (c) dendinmers remove lipid molecules primarily from edges of existing bilayer defects; (d) Neutral in charge dendimers do not remove lipid molecules from the surface. Instead they adsorb to edges of existing bilayer defects. Reprinted with permission from Jin, et. al, *Microsc Res Tech*, 2010.[177] Copyright © 2010 Wiley-Liss, Inc.

5.1.4 NanoSIMS

Secondary ion mass spectrometry (SIMS) is a highly sensitive analytical technique for investigations of sample surface chemistry, being able to detect elements present in parts per billion ranges.

In SIMS, the surface is bombarded by charged primary ion beam in vacuum what effects in sputtering (desorption) of the top few atomic layers, and ejection of atoms, ions and clusters (Figure 75). The resulting secondary ions are collected and mass analysed. The great information content of this technique leads to

unambiguous identification of molecules by their mass and to visualisation of the distribution of the molecules in the sample. Images are obtained by scanning the primary ion beam across the sample and collecting a spectrum at each spot. SIMS, and in particular NanoSIMS, which gives the most precise molecular content of the surface in question, with spatial resolution down to 50 nm, allows to identify isotopic composition of the probed sample, which can be translated into chemical details.

The capability of detail analysis and powerful sensitivity of this method in biological research can be exemplified by the application of NanoSIMS to the detection and visualisation of trace amounts of selenium in wheat grains (Figure 76).[178]

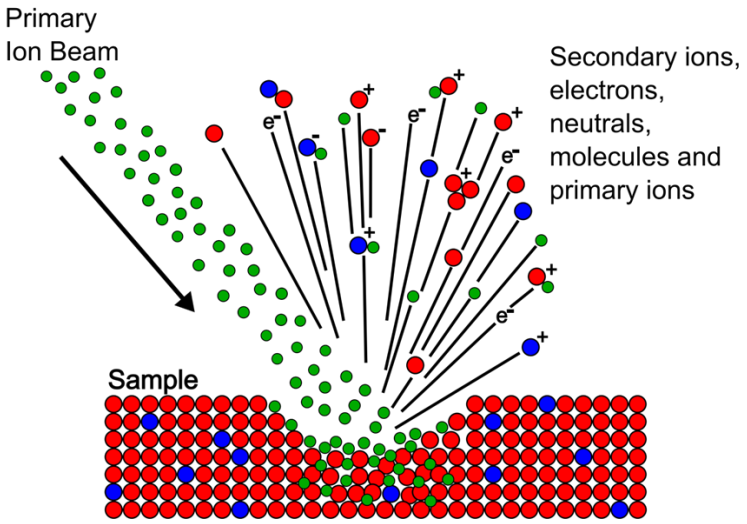

Figure 75. Cartoon presenting sputtering process in SIMS experiment. Image adapted from http://www.eaglabs.com/training/tutorials/sims_theory_tutorial/index.php.

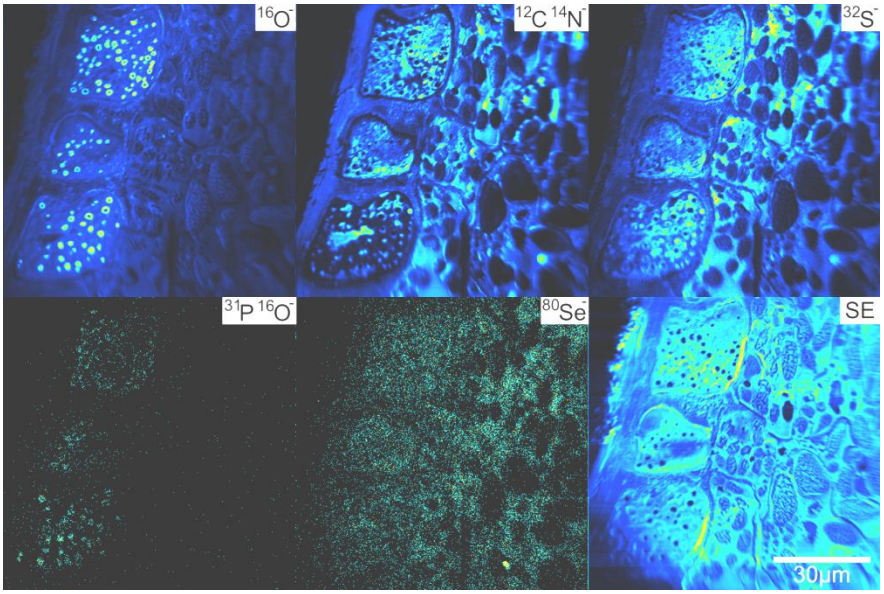

Figure 76. Example of NanoSIMS imaging; NanoSIMS ion maps of the outer part of the wheat grain showing the distribution of $^{16}O^-$, $^{12}C^{14}N^-$, $^{32}S^-$, $^{31}P^{16}O^-$, $^{80}Se^-$ and secondary electron (SE) signals. Reprinted with permission from K. L. Moore *et al.*, *New Phytol.*, (185), 2010.[178] Copyright © 2009 The Authors & Journal compilation New Phytologist.

5.1.5 MALDI MS

MALDI is a soft ionisation technique used in mass spectrometry allowing the analysis and of a wide range of organic and inorganic molecules. In MALDI MS a matrix compound, usually a small organic acid, is applied to the sample surface, where co-crystallisation of the sample with the matrix takes place. Ionisation of analytes occurs when the dried matrix is irradiated with a focused laser beam. The energy from the laser is absorbed by the matrix, resulting in a rapid desorption of the molecules from the radiated spot. A mass spectrum of the ions is then recorded.

MALDI MS has become an invaluable tool in life sciences, allowing accurate and sensitive analyses of various samples including: proteins and peptides, lipids, drugs and metabolites, carbohydrates, nucleic acids, synthetic polymers and large organic compounds. A great advantage of mass spectrometry is that multiple analytes can be monitored simultaneously from a single sample, without prior knowledge of their identities. Also in principle, there is no requirement for the use of target-specific reagents such as chemical tags, antibodies or large dye labels. Therefore, the insights into biological processes are provided with little or no disturbance of the native content of molecules in the samples.

5.1.6 DLS

Dynamic light scattering (DLS), also referred to as photon correlation spectroscopy, is a robust technique, which can be used to measure the size as well as the size distribution of particles held in suspension. The measurements are based on the time-dependent fluctuation in the light scattering intensity caused by Brownian motion (random, constant change in the distance) of molecules in the solution. When the laser beam, travelling through the sample to the detector, meets the particles in the sample, scattering of the light beam occurs. Larger particles will cause more scattering then the smaller ones. However the smaller molecules will result in greater change in scattering over a given time period as they will move quicker. Analysis of the fluctuation of the light intensity, hitting the detector, yields the information on the size of the particles. The changes of the scattered light are converted into electrical pulses, which are next fed into a digital correlator. Autocorrelation function is generated, from which appropriate data analyses are performed. The measurements are dependent on the concentration of molecules in the sample, the size of the particle core as well as the size of surface structures, and the type of ions in the suspension medium. In monodisperse systems, containing one particle population, the mean diameter of the particles can be effectively determined. Polydisperese systems would show multiple particle populations.

DLS can be utilised to characterisation of various particles including peptides, proteins, micelles, polymers, carbohydrates, etc. In particular, it has become an invaluable tool for sizing nanoparticles. The example of the use of DLS to the characterisation of engineered gold nanoparticles (GNPs) has been given by Pandey and co-workers[179], who constructed antibody-conjugated nanobioprobe for the detection of typhoid fever. The DLS measurements show clear change in the particle size as the result of modification to the particle surface.

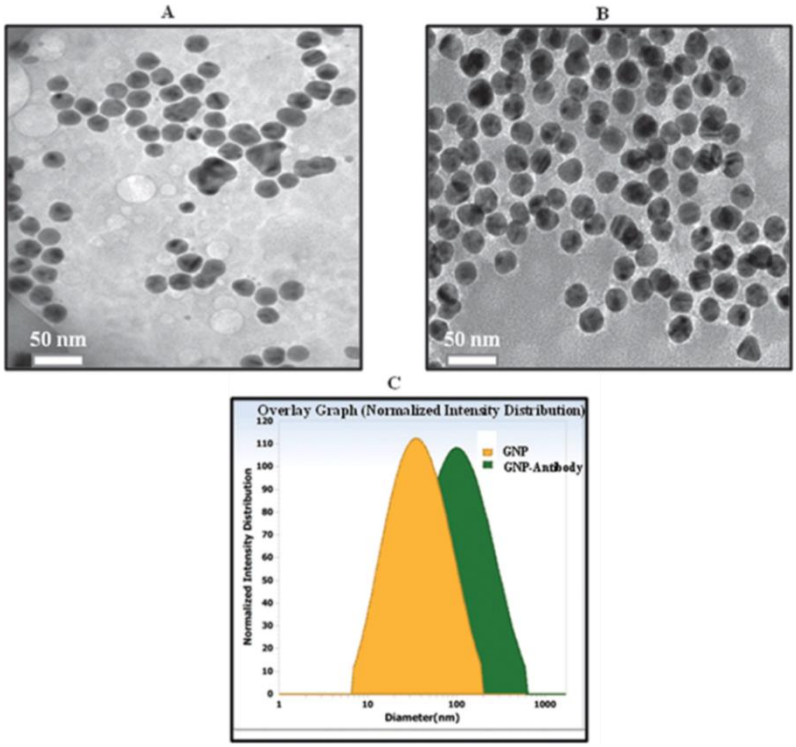

Figure 77. TEM images of colloidal gold particles (A) and GNPs–antibody conjugates (B). DLS (dynamic light scattering) data of GNPs and GNPs–antibody conjugate (C). Adapted with modifications from Pandey, et al., *Mol Biosys*, 2012[179] with permission from the Royal Society of Chemistry.

5.1.7 TEM

Transmission electron microscopy (TEM) uses a beam of electrons to create an image of the probed sample. It has much greater resolving power and is capable of considerably higher magnifications than a light microscope, what allows imaging smaller objects in finer detail, down to nanometer scale. The imaging method involves illumination a sample, in high vacuum, with high voltage electron beam and next detecting, the electrons transmitted through the sample. TEM enables obtaining two-dimensional, black and white “images”.

The preparation of a biological sample, such as cells or tissue to be viewed in an electron microscope, usually requires several stages, some of which are quite complicated and critical. It is mainly due to the analyses being held in high-vacuum. There are many approaches involved in the process, which will depend on the type of the sample, origin of the sample as well as the size of the specimens of interest. Firstly, sample has to be preserved, which can be done by, for example, cryofixation in liquid nitrogen or chemical fixation such as treatment with glutaraldehyde, used

to crosslink protein molecules and osmium tetroxide to preserve lipids. Also dehydration of the sample is required and the water is usually replaced with organic solvents like ethanol or acetone. Often embedding of the sample in a resin, such as LR White is carried out, which then is polymerised into a hardened block for subsequent sectioning. To give contrast between different structures, staining with heavy metals, e.g. uranium and lead, can be also employed. Finally, to prevent charging of the specimen that can result from the irridation by electron beam, sputter coating of the sample with electrically-conducting material, such as platinum, gold or chromium is applied.

TEM has proven to be an invaluable tool for analysis of various organic and inorganic structures. It allows, with a great detail, probing cell architecture. By visualisation and localisation of cell structures it enables their identification and brings insight into related to them functions. Therefore, TEM gained significant popularity in the fields of cell and tissue biology and became very useful in biomedical research. Since successful imaging of nanomaterials, including nanoparticles, can be too carried out, TEM imaging is also extremely attractive in the area of bio-nano research and applications. An example of the TEM imaging is given in Figure 78, which pictures internalisation by and distribution within of engineered nanoparticles particles by human glioma cells. [180]

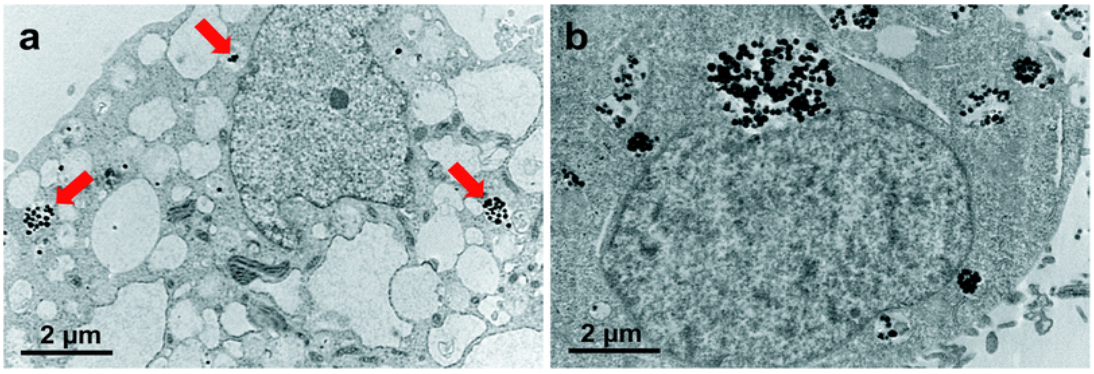

Figure 78. TEM images showing internalisation of mesoporous silica protected gold nanoclusters by 42-MG-BA human glioma cells. (a) Arrows indicate the intracellular distribution of nanoparticles in endosomes, which show variable size and particle number. (b) Large aggregates of nanoparticles could be related with some deficient dispersion in cell culture medium. Although nanoparticles localised frequently close to the nucleus they do not appear to enter. Reprinted from Botella, et al., *Dalton T*, 2012[180] with permission of the Royal Society of Chemistry.

5.2. Materials and methods

5.2.1 Materials and reagents

LC-MS grade water, α- cyano-4-hydroxy-cinnamic acid (ACCA), 2,5-dihydroxybenzoic acid (DHB), sinapinic acid (SA), succinimidyl 4-[N-maleimidomethyl]cyclohexane-1-carboxylate (SMCC) and sulfosuccinimidyl 4-(N-maleimidomethyl)cyclohexane-1-carboxylate (sulfo-SMCC) and serum were purchased from Sigma; Silver nanoparticles (AgNPs) 10 nm and 20 nm (1 mg/ml stock) in the form of BioPure silver, were obtained from nanoComposix, USA. Lipids: 1,2-dipalmiotyl-sn-glycero-3-phosphotioethanol (DPPTE) and 1,2-dilauroyl-*sn*-glycero-3-phosphocholine (DLPC), 1,2-dilauroyl-sn-glycero-3-phosphoethanolamine (DLPE) and 1,2-dilauroyl-sn-glycero-3-phospho- (1'-rac-glycerol) (DLPG) were obtained from Avanti, USA; and thiol-PEG-amine from NanoCS, USA. Peptide Calibration Standard as well as Protein II Standard Mix from Bruker; Human Dermal Fibroblasts (HDFa) (ATCC number PCS-201-012,), were taken from in-house stock (Bioengineering, NPL, UK); Cell culture media OptiMem Reduced Serum Medium and M106 were obtained from Gibco. Other used reagents used were from 'in-house' stock (Bioengineering, NPL, UK) and included: phosphate buffer, phosphate buffered saline (PBS), citrate buffer, glutaraldehyde, chloroform, acetonitrile, methanol, diisopropylethylamine (DIPEA); tris(2-carboxyethyl)phosphine (TCEP).

5.2.2 Peptides

The following peptides: AMP (sequence: KQKLAKLKAKLQKLKQKLAKL -am), non-AMP control (sequence QIAALEQEIAALEQEIAALQ-am) and CPP (sequence: KIAKLKAKIQKLKQKIAKLK-am) were de novo designed by Dr Maxim Ryadnov (Bioengineering, NPL, UK).

All peptides: AMP, non-AMP control, CPP, CPP-H (containing Leu 6C131N15 at residue 19), CPP-Cys (sequence: CKIAKLKAKIQKLKQKIAKLK-am), TaT (sequence: YGRKKRRQRRR-am) were chemically synthesised using a solid-phase peptide synthesis[181], either by Dr Angelo Bella or Dr Lloyd Ryan (Bioengineering, NPL, UK) ^{15}N-AMP, (labelled at all alanine and leucine residues) and TaT-H were purchased from AnaSpec, USA. AMP-F (containing Trifluoroethylglycine (TfeGly) at position 4)

was synthesised and provided in kind by Dr Ulla Gerling and Prof. Beate Koksch (Institut für Chemie und Biochemie, Freie Universität Berlin, Germany).

Peptides produced 'in house' were purified by semi preparative reversed-phase high performance liquid chromatography (RP-HPLC) on Jasco preparative liquid chromatography system. Purities of all peptides were checked by analytical RP-HPLC (analytical Jasco system) and MALDI-ToF mass-spectrometry (Autoflex III, Bruker).

Peptide concentration determination: Peptide concentrations were determined by converting UV absorbance measured at 214 nm, on Lambda 850 Spectrometer, using 1 cm path length quartz cuvette. The concentration was estimated based on the composition of amino acids, using calculated extinction coefficients[182]: ε_{214} [$M^{-1}cm^{-1}$]: 19621 (AMP, AMP-H and ^{15}N-AMP), 18556 (CPP and CPP-H), 18879 (non-AMP), 19704 (CPP-Cys) and 15462 (TaT).

5.2.3 Methodology

Preparation of liposomes: Liposomes of the following composition were used: 75% DLPC (Figure 79) and 25% 1,2-dilauroyl-sn-glycero-3-phospho- (1'-rac-glycerol) (DLPG) (Figure 80) (w:w). Firstly, the lipids were weighted up and dissolved of a solution consisting of $CHCl_3$ and CH_3OH (3:1 (v:v) respectively). The lipid solution was blow-dried under air stream and exposed, overnight, to vacuum. After, the dehydrated lipids were reconstituted in LC-MS grade water and ultrasonicated. To create small unilamellar vesicles (SUV), the obtained solution was extruded fifteen times through 50 nm-pore membrane (Waters).

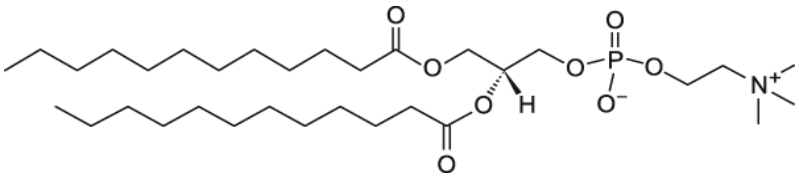

Figure 79. Chemical structure of DLPC.

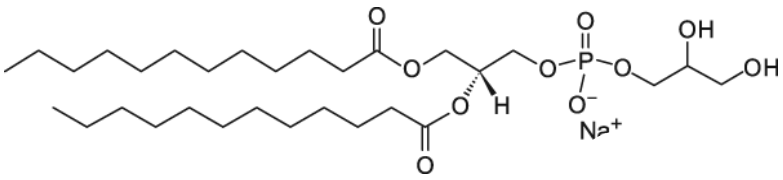

Figure 80. Chemical structure of DLPG.

Circular dichroism spectroscopy (CD): All CD spectra were recorded on a JASCO J-810 spectropolarimeter. The measurements were taken in ellipticities in mdeg and converted to molar ellipticities ([θ], deg cm^2 $dmol^{-1}$) by normalising for the concentration of peptide bonds. Aqueous peptide solutions (300 µL, 20 µM) were prepared in filtered (0.22 µm) 10 mM phosphate buffer, pH 7.4. CD spectra recorded in the presence of synthetic membranes are for lipid:peptide molar ratio of 100:1.

Linear dichroism spectroscopy (LD): The analyses were performed with assistance of Dr Jascindra Ravi (Bioengineering, NPL, UK). Solution-phase flow linear dichroism spectroscopy was performed on a Jasco-810 spectropolarimeter using a photo elastic modulator 1/2 wave plate, and a micro-volume quartz couvette flow cell with ~0.25 mm annular gap and quartz capillaries (Kromatec Ltd, UK). Molecular alignment was achieved through the constant flow of the sample solution between two coaxial cylinders – a stationary quartz rod and a rotating cylindrical capillary. LD spectra were acquired with laminar flow obtained by maintaining the rotation speed at 3000 rpm and processed by subtracting non-rotating baseline spectra. LD spectra recorded in the presence of synthetic membranes, DLPC and DLPC:DLPG (3:1), were prepared at a lipid:peptide molar ratio of 100:1 (2 mM total lipid, 20 µM peptide).

Stain-Dead Antimicrobial Assay. E. coli culture (1 mL) was centrifuged to give a cell pellet, which was washed twice with PBS (pH 7.4) before being reconstituted in PBS to give OD600nm = 0.008. One millilitre of the solution was dispensed in a two-well glass chamber (LabTek) with diluted (1/500) propidium iodide (PI) (1 mg/mL; Invitrogen). The chambers with surface-settled bacteria (60 min) were mounted on a confocal microscope (Olympus) equipped with an incubation chamber at 37 °C. PI fluorescence emission was monitored at 625 nm for 60 min (3 frames/min) using an appropriate filter after the addition of peptide (1 mL). Recorded movies (XYZ) were analysed using Fidji software to plot the number of fluorescent (stain-dead) cells as a function of time. Confocal microscopy analyses were performed by Mr Baptiste Lamarre (Bioengineering, NPL, UK).

Sample preparation for imaging: Oxidised silicon substrates (University Wafer, USA) were soaked in the previously described SUV solution and gently shaken for about 2 hours to enable the deposition of the lipid bilayer on the surface. The excess of vesicles was removed by plunging the substrates, covered with the bilayer, into fresh water and gently shaking for several minutes (repeated 2 times). The created supported lipid bilayer was then treated with the peptide solution. Following 30-min incubation and washing off the excess of the peptide, the samples were flash-frozen in liquid nitrogen and freeze-dried. This process allowed the removal of undesired water, and also 'fixed' the changed bilayer composition. Three types of samples were analysed: a) silicon substrate, b) silicon substrate covered with lipid bilayer; and c) lipid bilayer on the silicon substrate treated with peptides. Bacterial cells were imaged directly following peptide treatment and washing.

AFM imaging: The imaging was performed by Dr Santanu Ray (Surface & Nanoanalysis, NPL, UK). Topographic, amplitude and phase AFM images were recorded using tapping mode AFM on a MFP-3D Asylum AFM instrument (for imaging bacteria) and Cypher Instrument (Asylum Research, UK) for imaging supported lipid bilayers. All AFM images were flattened with a first order line-wise correction fit. AFM tips used were super-sharp silicon probes (Nanosensors, Switzerland, resonant frequency ~330 kHz, tip radius of curvature <5 nm, force constant 42 N/m). Images were processed using proprietary SPIP software, version 5.1.3.

NanoSIMS imaging: The NanoSIMS analyses were performed by Mr Haibo Jiang and Prof. Chris Grovenor (Materials Dept., University of Oxford, UK). SIMS images of chemical and isotopic distributions were acquired on a CAMECA (Gennevilliers) NanoSIMS 50 with lateral resolution down to 50 nm. The instrument uses a 16 keV primary $^{133}Cs^{+}$ beam to bombard the sample surface and collects five selected secondary negative ions using a Mauttach-Herzog mass analyzer with electrostatic sector and asymmetric magnet configuration. $^{12}C^{14}N^{-}$ and $^{12}C^{15}N^{-}$ secondary ions were collected. Three of the following signals were also recorded simultaneously to give information on sample morphology; ^{12}C-, $^{13}C^{-}$, $^{16}O^{-}$ and $^{31}P^{-}$. The ratio images ($^{12}C^{15}N^{-}/^{12}C^{14}N^{-}$) (30 by 30 µm, 256 by 256 pixels) were collected with a large primary aperture to match the pixel size in the images with the incident ion beam

diameter (~120 nm). A smaller primary aperture was used to achieve higher lateral resolution images (10 by 10 µm). The data was collected without preliminary $^{133}Cs^{+}$ implantation to avoid sputtering away the thin samples[23]. The images were calculated and processed using OpenMIMS software (MIMS, Harvard University, www.nrims.harvard.edu/), were multiplied by a scale factor 10,000, and processed by a median filter with one pixel radius. Ratios of the control samples were calculated as: ratio = $^{12}C^{15}N^{-}$ / ($^{12}C^{14}N^{-}$+$^{12}C^{15}N^{-}$) x 100%.

Preparation of supported lipid bilayers for AFM in water: Performed by Ms Alice Pyne (LCN, UCL, UK). Supported lipid bilayers were formed on mica as described previously[183] from a solution of 1.5 mg/mL DLPC:DLPG (3:1) in 150 mM NaCl, 20 mM HEPES pH 7.4 buffer with 20 mM MgCl2 and 20mM CaCl2. After absorption, the solution was then washed three 4 times with buffer, to remove the unfused vesicles from solution. Peptides were introduced in to the 100 µL fluid cell (JPK, Germany) at final concentration of 0.5 µM.

Liquid AFM imaging: The imaging was performed by Ms Alice Pyne and Dr Bart Hoogenboom (LCN, UCL, UK). Topographic images of supported lipid bilayers in liquid were recorded on a JPK Nanowizard I AFM, mounted on an Olympus IX71 inverted optical microscope, and operated in contact mode. The AFM probes used for all experiments in liquid were MSNL Silicon Nitride probes with spring constants of 0.005-0.03 N/m (Bruker AFM probes, CA, USA). Images were processed using Gwyddion (http://gwyddion.net/) for plane fitting and cross-section measurements.
Confocal fluorescence microscopy analyses were performed by Mr Baptiste Lamarre (Bioengineering, NPL, UK) using Olympus IX81 confocal microscope at 488 nm and using an x60 objective with appropriate filter. Images were processed using Imaris v5.1 and Image J software.

Cell transfection for quantification: Human Dermal Fibroblasts (HDFa) (ATCC number PCS-201-012,), from stock stored in in liquid nitrogen (NPL), were thawed and next seeded in 25cm2 flasks with 10 mL of complete M106 media (Gibco) and antibiotics (gentamicin and amphotericin B). Cells incubated at 37°C, 5% CO2 until at least 80% coffluency achieved. Next, media were removed and replaced with 10 mL of 10 µM peptide (CPP or TaT) in OptiMem Reduced Serum Medium (Gibco).

After 3 h of incubation at 37°C, 5% CO2, the solution with the excess (non-internalised) peptide was removed. To detach form the surface and to destroy any possible remaining on cell membranes peptide residues the cells were subjected to 7 min treatment by Trypsin. After spinning down the cells for 5 min at 150 rpm supernatant was discarded and cell pellet re-suspended in 1 mL of PBS pH7.4. 20 μL of the solution was next mixed with equal amount Trypan Blue (Fluka) and cells were counted using hematocytometer (Bright-Line) and optical microscope (Leica). The number of cells from at 5 squares were average, based on what the total amount of cells in the remaining solution was calculated.

Cell transfection for fluorescence studies: Human dermal fibroblasts were seeded in 4-well plates (10^4 cells per well) and were grown in serum-supplemented M106 for 2 days under the controlled environmental conditions. Cells were washed in a serum-reduced Opti-Mem medium and were transfected with 10 μM peptide (0.2 mL per well). Fluorescence was visualised at different time points (1, 3, 8 and 24 hours) by an Olympus IX81 confocal microscope at 488 nm using x10 and x20 objectives with an appropriate filter. Life cell imaging was performed under the controlled environmental conditions. Images were processed using Imaris v5.1 and ImageJ software. Transfection efficiency was calculated by dividing total fluorescence by the total number of cells. The highest value for each peptide (8-hour incubations) was taken as 100% after the subtraction of background fluorescence. Statistical analysis was performed by OriginPro 8.5 using ANOVA followed by a Fisher post-test for three independent experiments done in triplicate. The analyses were performed by Mr Baptiste Lamarre (Bioengineering, NPL, UK).

Cell lysis in Triton X: The counted cells suspension was divided in to two. Half of the solution was next spun-down (5min at 150 rpm) and re-suspended in lysis solution: 0.1 % Triton X and 0.075 % TFA. Next the solution was subjected to four times freezing and thawing cycles and further incubation for few hours at room temperature, with several sonication and mixing steps in the meantime. Finally, the debris pellet was spun down and the supernatant containing cell lysate collected, freeze – dried and re-constituted in LC-MS grade water to volume of 500 μL. For the control, human dermal fibroblasts, which do not contain the CPP, were also lysated.

Cell lysis in Rapigest: Half of the solution of counted cells was spun-down (5min at 150 rpm) and to the 100 uL of 50 mM NH4HCO3 buffer containing: 0.5 % (w/v) Rapigest Extraction Buffer (Waters), Protease Inhibitor Cocktail (Roche) and 2 µg / mL DNAse II (Sigma) was added. Three cycles of vigorous mixing and sonicating were applied and after 30 min DNA in the form of slimy threads was removed from the sample. Then two freeze-thaw cycles in liquid nitrogen were performed and the debris was removed by ultracentrifugation for 10 min at 14000 rpm. Clear supernatant was collected and diluted to volume of 500 µL. For the control, human dermal fibroblasts, which do not contain the CPP, were also lysated.

Size Exclusion Chromatography (SEC): SEC was performed on Jasco analytical LC system equipped in multi-wavelength detector MD-2010 Plus; The column used was BioSep-SEC-s200, 300 x 7.8 mm (Phenomenex); The following run conditions were set: mobile phase: PBS, pH 7.4; Isocratic flow rate at 1 ml/min; Room temperature; Detection: UV absorbance at 214 nm. Sample amounts: 50 µg of pure solutions of CPP, CPP-H, TaT, TaT-H and molecular weight standards, 100 µL of cell lysates. The column performance was evaluated by injecting several molecular weight standards: BSA (66 kDa), Ferritin (450 kDa), Lysozyme (14 kDa), Ovalbumin (45 kDa) and Conalbumin (76 kDa). Next, the pure solutions of CPP, CPP-H, TaT and TaT-H were injected onto the column and their elution time was estimated. Fractions collected, freeze dried and reconstituted in 200 µL of LC-MS grade H_2O.

Reversed-phase HPLC (RP-HPLC): *For MALDI MS quantification:* RP-HPLC was performed on Jasco analytical liquid chromatography system; The column used was Vydac 218TP C18 5µ, 250 x 4.6 mm (Grace); The following run conditions were set: Mobile phase A: 5% Acetonitrile (ACN) in 0,1% Trifluoroacetic acid (TFA), Mobile phase B: 95% ACN in 0.1% TFA; Gradient: 95% A for 10 min, B → 80% in 40 min, 80% B for 5 min, B → 5% in 5 min, 95% A for 5 min, Flow rate at 1 ml/min; Room temperature; Detection: UV absorbance at 214 nm, Sample amounts: 50 µg of pure solutions of CPP, CPP-H, TaT and TaT-H and 100 µL of reconstituted SEC fractions. Fractions corresponding to the CPP elution time were collected for further analysis by MALDI MS.

MALDI MS of peptides was performed on Autoflex III (Bruker) Smart Beam, equipped with a nitrogen laser (337 nm, 200 Hz maximum firing rate), in positive polarity mode. The target plate used was AnchorChip 800 µm (Bruker) and the MALDI MS matrix was α- cyano-4-hydroxy-cinnamic acid (ACCA) (Sigma). The reflector detection mode was used to analyse CPP, CPP-H and respective to them samples. Linear detection mode was used to analyse TaT and TaT-H samples. The instrument was calibrated using Peptide Standard Mix (Bruker).

Isotope dilution standard curves: Stock solutions of known concentrations of CPP and CPP-H were prepared. The concentration of the peptides was determined using UV absorbance at 214 nm. A set of solutions was prepared from the peptides' stock solutions, with the amount of CPP ranging from: 0.5 pmol/µL to 5 pmol/µL and the CPP-H at the final concentrations at 1 pmol/µL. All the samples were next mixed with ACCA matrix in 1:1 ratio and deposited onto MALDI target plate in duplicates. To achieve good quality signal, for each sample spectra from at least 2000 laser shots and different positions on the sample spot were summed. Standard curves was built, which plots the ratio of the intensity of the CPP ion to the CPP-H ion intensity against the concentration of the CPP (Figure 81). The same procedure was employed to build up the standard curve for the quantification of TaT peptide (Figure 82).

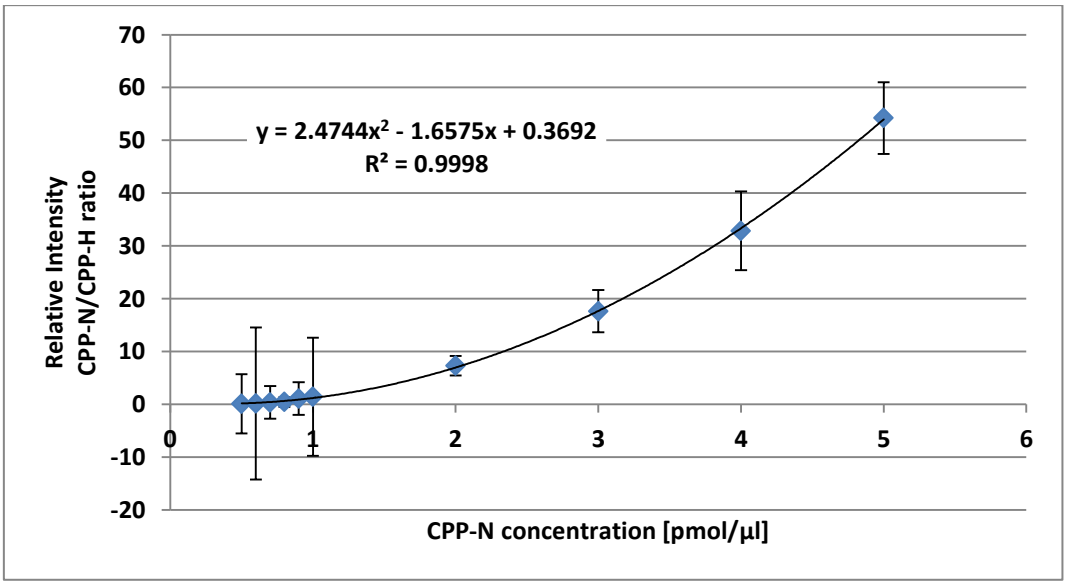

Figure 81. Standard curve showing the relation between the ratio of CPP and CPP-H ion intensities against concentration of CPP. The CPP-H was kept at the concentration of 1 pmol/µL while the concentration of CPP varied from 0.5 pmol/µL to 5 pmol/µL.

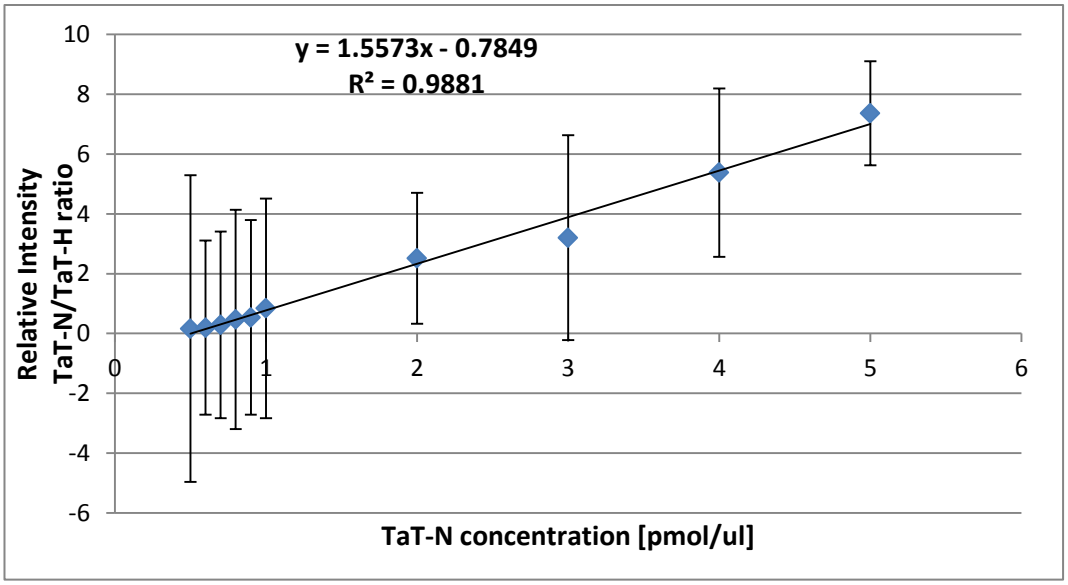

Figure 82. Standard curve of the relation between the ratio of TaT and TaT-H ion intensities against concentration of TaT. The TaT-H was kept at the concentration of 1 pmol/µL while the concentration of TaT varied from 0.5 to 5 pmol/µL.

Preparation of lipoNPs: 6 mg of DPPTE (Figure 83) was dissolved in 2 ml chloroform. To 340 µL of this solution 60 µL 20 nm AgNPs was added. The sample was next sonicated for 30 min with occasional vigorous mixing. Next the sample was spun down (30 min at 10k rpm) and the supernatant removed. To remove DPTTE excess the NP pellet was three times with chloroform. 6 mg of DLPC was suspended in 2 ml of water. 500 µL of this solution was next added to the tube with the AgNP-DPPTE pellet and the sample was next sonicated for 1 h with occasional vigorous mixing. The remaining drop of chloroform was next extracted from the bottom of the tube and the sample was spun down (30 min at 10k rpm) and washed 3 times with water to remove excess DLPC vesicles. Schematic representation of the process is shown in Figure 84 below. To make sure that the created construct does not contain agglomerates, the lipo-AgNPs were extruded through a membrane of 50 nm pore size.

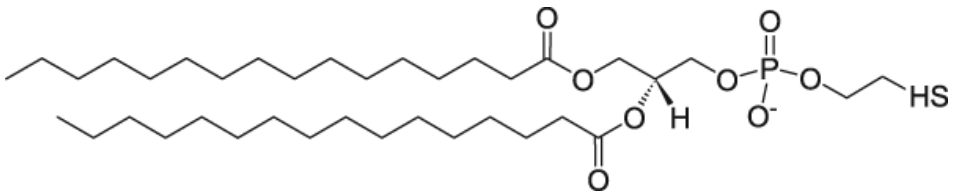

Figure 83. Chemical structure of DPPTE.

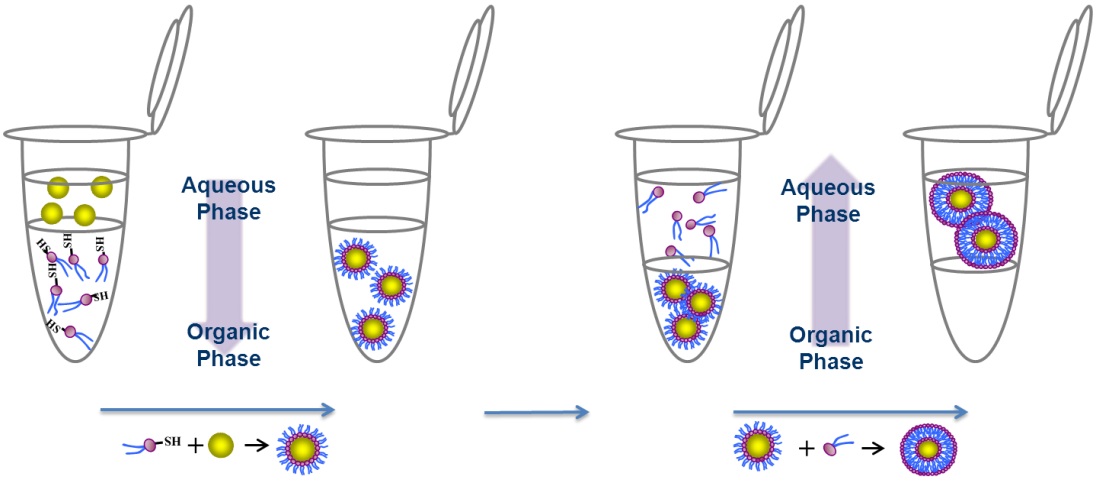

Figure 84. Schematic representation of lipo-AgNPs preparation: A) AgNPs, kept in aqueous solution, upon mixing with DPPTE dissolved in chloroform, move to the organic phase; B) AgNPs covered by DPTTE are separated by centrifugation and washed several times with chloroform to remove excess lipid; C) Ag-NPs – DPPTE conjugates, kept in chloroform, upon mixing with DLPC suspended in aqueous solution, move to the aqueous phase; D) The AgNPs, covered with lipid bilayer, are separated by centrifugation and washed several times to remove excess lipid.

Incubation of lipoNPs with serum: 10 µL of concentrated AgNPs and lipo-NP solutions were incubated with 500 µL of serum for 2 h at room temperature. The nanoparticles as well as the lipo-NPs were next separated from the serum by ultracentrifugation (30 min at 10k rpm) and subsequent washing with water (repeated four times).

MADLI MS analyses of nanoparticles: The reflector detection mode was used; the samples were placed on the AnchorChip 800 µm target plate together with the MALDI matrix: DHB for the probing of lipo-AgNPs. SA matrix was used and linear detection mode for the analysis in higher molecular weight range to probe serum-incubated samples. The instrument was calibrated using Peptide Standard Mix or Protein II Standard Mix.

DLS measurements were performed on a Zetasizer Nano (Malvern Instruments, UK) and carried out in a low volume disposable cuvette at 25°C. Hydrodynamic radii were obtained through the fitting of autocorrelation data using the manufacture's software, Dispersion Technology Software (DTS version 5.10).

Preparation of LipoNP-CPP*:* 6 mg of DPPTE was dissolved in 2 ml chloroform. To 340 μL of this solution 60 μL 20 nm AgNPs was added. The sample was next sonicated for 30 min with occasional vigorous mixing. Next the sample was spun down (30 min at 10k rpm) and the supernatant removed. To remove DPTTE excess the NP pellet was washed three times with chloroform. 25 mg of DLPE (Figure 85) was solubilised in 1 mL of $CHCl_3$/CH_3OH 9:1 (v:v). To this solution 7.5 μL of DIPEA and 14 mg of SMCC were added. Using indicator paper pH of the solution was checked (optimal pH 7.4) and the reaction solution was incubated with gentle shaking at room temperature. After 2 hours, to obtain dry crude of the DLPE-MCC conjugate the solution was dried under nitrogen flow. DLPE-MCC conjugate was next resuspended in 500 μL of $CHCl_3$/CH_3OH 9:1 (v:v) 100 μL of this solution was next added to the tube with the AgNP-DPPTE pellet, followed by addition of 500 μL H_2O, and the sample was next sonicated for 30 min with occasional vigorous mixing. The sample was spun down (30 min at 10k rpm) and the aqueous phase, containing AgNP-DPTTE-DLPE-MCC construct was removed from the tube and placed in a fresh tube. To the remaining DPPTE-NPs pellet another 100 μL of DLPE-MCC solution and 500 μL of H20 were added and the sonication and spinning process repeated. The obtained additional AgNP-DPTTE-DLPE-MCC construct was separated and pooled with the previously collected one. The sample was mixed vigorously and spun down (30 min at 10k rpm). After discarding the supernatant, 500 μL of fresh water was added and the sample was sonicated for 15 minutes until the solution gained clarity. The spinning down of the sample was repeated and after water removal the concentration of the silver particles in the remaining solution was determined (as described further). 500 μL of CPP-Cys solution in 10 mM phospahe buffer and 1 mM T-CEP was added to the remaining AgNP-DPTTE-DLPE-MCC pellet in 1.1:1 molar ratio and the reaction was allowed for 3 hours at room temperature and with gentle stirring. The created LipoNP-CPP molecules were next washed three times by spinning down and supernatant replacement with fresh water. To make sure that the created construct does not contain agglomerates, LipoNP-CPP were next extruded through a membrane of 50 nm pore size. The prepared particles were next kept refrigerated.

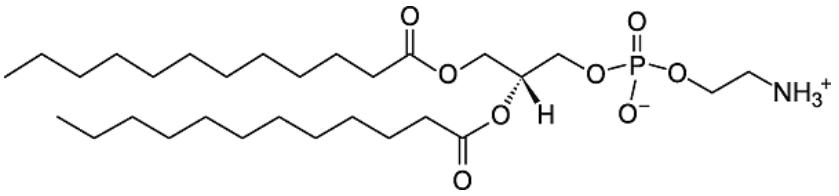

Figure 85. Structure of DLPE.

Preparation of NP-PEG-CPP: Conjugation of HS-PEG-NH_2 to AgNPs was carried out, based to the protocol described elsewhere[184]. In summary, 60 µL of 20 nm AgNPs were diluted in 440 H_2O. 4.7 mg of HS-PEG-NH_2 was dissolved in 500 µL of water, sonicated for 15 minutes and combined with NPs suspension, by dropwise-addition under vigorous stirring. The solution was allowed to react for 1 h in room temperature. To remove the HS-PEG-NH_2 excess and exchange the water into 50 mM phosphate buffer, the particles were next passed through polyacrylamide desalting column (D-Salt, Polyacrlylamide 6000, 5 ml; Pierce) following manufacturer instructions. Approximately 1 ml solution of PEG-covered particles was collected. To achieve around 10-fold molar excess of the cross-linker to amine groups on NPs, 5 mg of sulfo-SMCC were dissolved in 100 µL 50 mM phosphate buffer and added to the NP-PEG-NH_2 solution. The reaction was allowed for 30 minutes at room temperature. To remove unreacted cross-linker the particles were, again, passed through polyacrylamide desalting column. Approximately 1 ml of nanoparticle containing solution was collected. Finally, to the particle suspension CPP-Cys was added (from a prior prepared stock solution containing T-CEP) the final concentration of 10 µM peptide in the solution. After 2 hours of incubation at room temperature, the excess peptide was removed by passing the sample through the polyacrylamide desalting column. To make sure that the created construct does not contain agglomerates, NP-PEG-CPP were extruded through a 50 nm pore size membrane. Lastly, the created NP-PEG-CPP molecules were concentrated by spinning down (30 min at 10k rpm) and excess buffer removal. The prepared particles were kept refrigerated.

Preparation of NP-CPP: 60 µL of 20 nm AgNPs were added to 940 µL of 10 µM CPP-Cys solution (prepared from the prior stock containing T-CEP). The peptide was allowed to react with NPs for 1 h at room temperature, with gentle shaking. To

remove CPP-Cys excess sample was spun down (30 min at 10k rpm) and the NP pellet was washed three times with phosphate buffer. The NP-CPP conjugates were next sonicated for 15 minutes. The prepared particles were kept refrigerated.

NP concentration determination was performed by anodic stripping voltammetry (ASV) on an electrochemical workstation (AutoLab PGSTAT 12, Windsor Scientific), with the use of disposable, screen-printed carbon three-electrode sensors (provided by LIRANS, University of Bedfordshire), printed with C2000802D2 carbon ink and D60202D1 blue dielectric (Gwent Electronic Materials). Series of dilutions of 20 nm AgNPs ranging from 1 mg/mL to 5 µg/ml were prepared in duplicate. To 45 µl of the prepared samples 5 µL of 1M NH4SCN was added and samples were incubated for 1 h at room temperature. Samples were next placed onto the sensor surface and analyses were performed according to the protocol described by Szymanski et al. *Electroanalysis*, 2010[185]; Analytical signal, corresponding to the amount of charge produced during the stripping step, was recorded and calculated by measuring the area under the silver oxidation peak. Calculations were made using General Purpose Electrochemical System software (GPES 4.9). Based on the obtained values of the nanoparticle amount in the reference samples a standard curve was built, used further to estimate the concentration of AgNP in working solutions.

Cell transfection with NPs: Human Dermal Fibroblasts (HDFa) (ATCC number PCS-201-012,), from stock stored in in liquid nitrogen (NPL), were thawed and next seeded in 1 cm^2 chambers on glass cover slips with 1.5 mL of complete M106 media (Gibco) and antibiotics (gentamicin and amphotericin B). Cells incubated at 37°C, 5% CO_2 until at least 80% coffluency achieved. Next, growth media were removed from the cell cultures and replaced with identical media containing nanoparticles or nanoparticle conjugates. After 3 h or 6 h of incubation at 37°C, 5% CO_2, the solution with the excess (non-internalised) particles was removed and cells washed three times with 10 mM phosphate buffer. Finally, 1 ml of 1.5% glutaraldehyde in 10 mM phosphate buffer was added to the cells to fix them. That way prepared samples were next provided to Mr Bill Cooley (AHVLA, Weybridge, UK) or Mr Mark Turmaine (UCL) to be further processed in preparation for TEM imaging.

TEM images were taken by Mr Bill Cooley (AHVLA, Weybridge, UK), Mr Mark Turmaine (UCL) and Dr Angelo Bella (Bioengineering, NPL, UK) on Jeol 1010 Transmission Electron microscopes. Images were processed using Image J software.

PUBLICATIONS FROM THE PROJECT

1) **Peptidome analysis: tools and technologies;** P D Rakowska, M G Ryadnov in *Amino Acids, Peptides and Proteins*; E Farkas, M G Ryadnov; *RSC Publishing*, 2013, 38, 172-202. Reproduced by permission of the Royal Society of Chemistry.

2) **Nano-enabled biomarker discovery and detection**; P D Rakowska and M G Ryadnov; *Biomarkers in Medicine*, 2011, 5(3), 387-96. Reproduced with permission. Copyright © 2011 Future Medicine Ltd.

3) **Nanoscale imaging reveals laterally expanding antimicrobial pores in lipid bilayers**; P D Rakowska, H Jiang, S Ray, A Pyne, B Lamarre, M Carr, P J Judge, J Ravi, U I M Gerling, B Koksch, G J Martyna, B W Hoogenboom, A Watts, J Crain, C R M Grovenor and M G Ryadnov; *Proceedings of the National Academy of Sciences*, 2013, 110, 8918-8923. Copyright 2013 © National Academy of Sciences, USA.

4) **Stable isotope imaging of biological samples with high resolution secondary ion mass spectrometry and complementary techniques**, H Jiang, E Favaro, C N Coulbourne, P D Rakowska, G M Hughes, M G Ryadnov, L G Fong, S G Young, D J Ferguson, A L Harris, C Grovenor; *Methods*, 2014, 68 (2), 317-324. Copyright © 2014, reprinted with permission from Elsevier.

5) **Probing label-free intracellular quantification of free peptide by MALDI-ToF mass spectrometry**, P D Rakowska, B Lamarre, M G Ryadnov; *Methods*, 2014, 68 (2), 331-337. Copyright © 2014, reprinted with permission from Elsevier.

BIBLIOGRAPHY

1. JCBN, Nomenclature and Symbolism for Amino Acids and Peptides. *Eur J Biochem* **138**, 9 (1984).
2. R. H. Tailor *et al.*, A novel family of small cysteine-rich antimicrobial peptides from seed of Impatiens balsamina is derived from a single precursor protein. *J Biol Chem* **272**, 24480 (1997).
3. S. Sharma, R. Singh, S. Rana, Bioactive Peptides: A Review. *Int. J. Bioautomation,* **15**, 223 (2011).
4. M. Dziuba, M. Darewicz, Food Proteins as Precursors of Bioactive Peptides — Classification Into Families. *Food Sci Technol Int* **13**, 393 (2007).
5. P. Papareddy, M. Morgelin, B. Walse, A. Schmidtchen, M. Malmsten, Antimicrobial activity of peptides derived from human ss-amyloid precursor protein. *J Pept Sci* **18**, 183 (2012).
6. G. H. Hur, C. R. Vickery, M. D. Burkart, Explorations of catalytic domains in non-ribosomal peptide synthetase enzymology. *Nat Prod Rep* **29**, 1074 (2012).
7. M. Strieker, A. Tanovic, M. A. Marahiel, Nonribosomal peptide synthetases: structures and dynamics. *Curr Opin Struct Biol* **20**, 234 (2010).
8. J. L. Meier, M. D. Burkart, The chemical biology of modular biosynthetic enzymes. *Chem Soc Rev* **38**, 2012 (2009).
9. M. A. Marahiel, Working outside the protein-synthesis rules: insights into non-ribosomal peptide synthesis. *J Pept Sci* **15**, 799 (2009).
10. K. Nikolouli, D. Mossialos, Bioactive compounds synthesized by non-ribosomal peptide synthetases and type-I polyketide synthases discovered through genome-mining and metagenomics. *Biotechnol Lett* **34**, 1393 (2012).
11. V. T. Ivanov, A. A. Karelin, M. M. Philippova, I. V. Nazimov, V. Z. Pletnev, Hemoglobin as a source of endogenous bioactive peptides: The concept of tissue-specific peptide pool. *Peptide Sci* **43**, 171 (1997).
12. A. Karelin, E. Blishchenko, V. Ivanov, Fragments of Functional Proteins: Role in Endocrine Regulation. *Neurochem Res* **24**, 1117 (1999).
13. A. J. Kastin, W. Pan, Concepts for biologically active peptides. *Curr Pharm Des* **16**, 3390 (2010).
14. P. Y. Ong *et al.*, Endogenous antimicrobial peptides and skin infections in atopic dermatitis. *N Engl J Med* **347**, 1151 (2002).
15. T. R. Hata, R. L. Gallo, Antimicrobial Peptides, Skin Infections, and Atopic Dermatitis. *Semin Cutan Med Surg* **27**, 144 (2008).
16. T. Schuerholz *et al.*, The anti-inflammatory effect of the synthetic antimicrobial peptide 19-2.5 in a murine sepsis model: a prospective randomized study. *Critical Care* **17**, R3 (2013).
17. L. Wei *et al.*, Structure and Function of a Potent Lipopolysaccharide-Binding Antimicrobial and Anti-inflammatory Peptide. *J Med Chem,* **56**, 3546 (2013).
18. Simon Jäger, E. F. Stange, J. Wehkamp, Antimicrobial Peptides in Gastrointestinal Inflammation. *Int J Inflamm* **2010**, (2010).
19. R. Ramos *et al.*, Wound healing activity of the human antimicrobial peptide LL37. *Peptides* **32**, 1469 (2011).

20. L. Steinstraesser *et al.*, Host defense peptides in wound healing. *Mol Med* **14**, 528 (2008).
21. H. J. Schluesener, S. Radermacher, A. Melms, S. Jung, Leukocytic antimicrobial peptides kill autoimmune T cells. *J Neuroimmunol* **47**, 199 (1993).
22. M. Gilliet, R. Lande, Antimicrobial peptides and self-DNA in autoimmune skin inflammation. *Curr Opin Immunol* **20**, 401 (2008).
23. J. E. Meyer, J. Harder, Antimicrobial peptides in oral cancer. *Curr Pharm Des* **13**, 3119 (2007).
24. S. Liu *et al.*, Enhancement of cytotoxicity of antimicrobial peptide magainin II in tumor cells by bombesin-targeted delivery. *Acta Pharmacol Sin* **32**, 79 (2011).
25. J. S. Mader, D. W. Hoskin, Cationic antimicrobial peptides as novel cytotoxic agents for cancer treatment. *Expert Opin Investig Drugs* **15**, 933 (2006).
26. S. Lien, H. B. Lowman, Therapeutic peptides. *Trends Biotechnol* **21**, 556 (2003).
27. A. M. Papini, The use of post-translationally modified peptides for detection of biomarkers of immune-mediated diseases. *J Pep Sci* **15**, 621 (2009).
28. J. V. Price *et al.*, On silico peptide microarrays for high-resolution mapping of antibody epitopes and diverse protein-protein interactions. *Nat Med* **18**, 1434 (2012).
29. B. Zhang *et al.*, An integrated Peptide-antigen microarray on plasmonic gold films for sensitive human antibody profiling. *PLoS ONE* **8**, (2013).
30. F. Real-Fernández *et al.*, Ferrocenyl glycopeptides as electrochemical probes to detect autoantibodies in multiple sclerosis patients' sera. *Peptide Sci* **90**, 488 (2008).
31. E. Kondo *et al.*, Tumour lineage-homing cell-penetrating peptides as anticancer molecular delivery systems. *Nat Commun* **3**, 951 (2012).
32. B. Lamarre, J. Ravi, M. G. Ryadnov, GeT peptides: a single-domain approach to gene delivery. *Chem Commun* **47**, 9045 (2011).
33. P. D. Rakowska *et al.*, Nanoscale imaging reveals laterally expanding antimicrobial pores in lipid bilayers. *PNAS* **110**, 8918 (2013).
34. L. Ryan *et al.*, Anti-antimicrobial Peptides: Folding-mediated Host Defence Aantagonists. *J Biol Chem* **288**, 20162 (2013).
35. P. D. Rakowska, M. G. Ryadnov, in *Amino Acids, Peptides and Proteins* E. Farkas, M. Ryadnov, Eds. (RSC Publishing, 2014), vol. 38, pp. 172-202.
36. R. Aebersold, M. Mann, Mass spectrometry-based proteomics. *Nature* **422**, 198 (2003).
37. B. Domon, R. Aebersold, Options and considerations when selecting a quantitative proteomics strategy. *Nat Biotech* **28**, 710 (2010).
38. D. Nedelkov, U. A. Kiernan, E. E. Niederkofler, K. A. Tubbs, R. W. Nelson, Investigating diversity in human plasma proteins. *Proceedings of the National Academy of Sciences of the United States of America* **102**, 10852 (2005).
39. C. S. Olver, T. L. Webb, L. J. Long, H. Scherman, J. E. Prenni, Comparison of methods for depletion of albumin and IgG from equine serum. *Veterinary Clinical Pathology* **39**, 337 (2010).
40. A. Posch, J. Martosella, N. Zolotarjova, in *2D PAGE: Sample Preparation and Fractionation*. (Humana Press, 2008), vol. 425, pp. 27-39.
41. G. Baggerman *et al.*, Peptidomics. *J Chromatogr B* **803**, 3 (2004).
42. H. Schagger, Tricine-SDS-PAGE. *Nat Protoc* **1**, 16 (2006).

43. HPLC of Peptides and Proteins. Methods and Protocols (Aguilar, M.-I. (ed.), in "Method in Molecular Biology", Vol. 251 (Walker, J., Series Editor), Humana Press, 2004, 413 p., $99.50 (Hardcover)). *Biochem* **69**, 1172 (2004).
44. K. K. Han, M. Davril, M. Moczar, E. Moczar, Partial characterization of peptide fragment purified by isoelectrofocusing after organo alkaline hydrolysis of bovine ligamentum nuchae elastin. *Paroi Arterielle* **7**, 77 (1981).
45. B. Borowicz, J. Domaniewski, Analysis of the low molecular weight nuclear polypeptide by isoelectrofocusing of nuclear proteins first separated by gel electrophoresis in SDS. *Arch Vet Pol* **34**, 241 (1994).
46. H. D. Schulz-Knappe P Fau - Zucht *et al.*, - Peptidomics: the comprehensive analysis of peptides in complex biological mixtures. *Comb Chem High Throughput Screen* **4**, 207 (2001).
47. J.-F. Poulin, J. Amiot, L. Bazinet, Simultaneous separation of acid and basic bioactive peptides by electrodialysis with ultrafiltration membrane. *J Biotech* **123**, 314 (2006).
48. G.-C. Yu, J.-T. Li, H. U. I. He, W.-H. Huang, W.-J. Zhang, Ultrafiltration Preparation Of Potent Bioactive Corn Peptide As Alcohol Metabolism Stimulator In Vivo And Study On Its Mechanism Of Action. *J Food Biochem* **37**, 161 (2013).
49. Y. An, R. Goldman, in *The Low Molecular Weight Proteome,* H. Bäckvall, J. Lehtiö, Eds. (Springer New York, 2013), vol. 1023, pp. 13-19.
50. T. R. Kline *et al.*, A high-yield method to extract peptides from rat brain tissue. *Anal Biochem* **315**, 183 (2003).
51. O. Chertov *et al.*, Organic solvent extraction of proteins and peptides from serum as an effective sample preparation for detection and identification of biomarkers by mass spectrometry. *Proteomics* **4**, 1195 (2004).
52. M. Tucholska, A. Florentinus, D. Williams, J. G. Marshall, The endogenous peptides of normal human serum extracted from the acetonitrile-insoluble precipitate using modified aqueous buffer with analysis by LC-ESI-Paul ion trap and Qq-TOF. *J Proteomics* **73**, 1254 (2010).
53. L. P. Aristoteli, M. P. Molloy, M. S. Baker, Evaluation of Endogenous Plasma Peptide Extraction Methods for Mass Spectrometric Biomarker Discovery. *J Proteome Res* **6**, 571 (2006).
54. Y. Zhao *et al.*, Fully automatable two-dimensional hydrophilic interaction liquid chromatography–reversed phase liquid chromatography with online tandem mass spectrometry for shotgun proteomics. *J Sep Sci* **35**, 1755 (2012).
55. S. O. Siu *et al.*, Fully automatable two-dimensional reversed-phase capillary liquid chromatography with online tandem mass spectrometry for shotgun proteomics. *Proteomics* **11**, 2308 (2011).
56. S. E. Ong, L. J. Foster, M. Mann, Mass spectrometric-based approaches in quantitative proteomics. *Methods* **29**, 124 (2003).
57. X. Chen, L. Sun, Y. Yu, Y. Xue, P. Yang, Amino acid-coded tagging approaches in quantitative proteomics. *Expert Rev Proteomics* **4**, 25 (2007).
58. L. Dayon, J. C. Sanchez, Relative protein quantification by MS/MS using the tandem mass tag technology. *Methods Mol Biol* **893**, 115 (2012).

59. L. M. Miller *et al.*, A label-free mass spectrometry method for relative quantitation of β-tubulin isotype expression in human tumor tissue. *Proteomics – Clinical Applications* **6**, 502 (2012).
60. Y. J. Kim, P. Zhan, B. Feild, S. M. Ruben, T. He, Reproducibility assessment of relative quantitation strategies for LC-MS based proteomics. *Anal Chem* **79**, 5651 (2007).
61. S. E. Ong *et al.*, Stable isotope labeling by amino acids in cell culture, SILAC, as a simple and accurate approach to expression proteomics. *Mol Cell Proteomics* **1**, 376 (2002).
62. T. Geiger *et al.*, Use of stable isotope labeling by amino acids in cell culture as a spike-in standard in quantitative proteomics. *Nat Protoc* **6**, 147 (2011).
63. A. Emadali, M. Gallagher-Gambarelli, [Quantitative proteomics by SILAC: practicalities and perspectives for an evolving approach]. *Med Sci* **25**, 835 (2009).
64. O. A. Mirgorodskaya *et al.*, Quantitation of peptides and proteins by matrix-assisted laser desorption/ionization mass spectrometry using (18)O-labeled internal standards. *Rapid Commun Mass Spectrom* **14**, 1226 (2000).
65. Stewart, II, T. Thomson, D. Figeys, 18O labeling: a tool for proteomics. *Rapid Commun Mass Spectrom* **15**, 2456 (2001).
66. D. Kovanich *et al.*, Applications of stable isotope dimethyl labeling in quantitative proteomics. *Anal Bioanal Chem* **404**, 991 (2012).
67. M. Sethuraman *et al.*, Isotope-coded affinity tag (ICAT) approach to redox proteomics: identification and quantitation of oxidant-sensitive cysteine thiols in complex protein mixtures. *J Proteome Res* **3**, 1228 (2004).
68. F. Turecek, Mass spectrometry in coupling with affinity capture-release and isotope-coded affinity tags for quantitative protein analysis. *J Mass Spectrom* **37**, 1 (2002).
69. S. Wiese, K. A. Reidegeld, H. E. Meyer, B. Warscheid, Protein labeling by iTRAQ: a new tool for quantitative mass spectrometry in proteome research. *Proteomics* **7**, 340 (2007).
70. K. Aggarwal, L. H. Choe, K. H. Lee, Shotgun proteomics using the iTRAQ isobaric tags. *Brief Funct Genomic Proteomic* **5**, 112 (2006).
71. C. Evans *et al.*, An insight into iTRAQ: where do we stand now? *Anal Bioanal Chem* **404**, 1011 (2012).
72. W. Zhou, L. A. Liotta, E. F. Petricoin, The spectra count label-free quantitation in cancer proteomics. *Cancer Genomics Proteomics* **9**, 135 (2012).
73. K. A. Neilson *et al.*, Less label, more free: approaches in label-free quantitative mass spectrometry. *Proteomics* **11**, 535 (2011).
74. V. Brun, C. Masselon, J. Garin, A. Dupuis, Isotope dilution strategies for absolute quantitative proteomics. *J Proteomics* **72**, 740 (2009).
75. M. Bronstrup, Absolute quantification strategies in proteomics based on mass spectrometry. *Expert Rev Proteomics* **1**, 503 (2004).
76. K. Kito, T. Ito, Mass spectrometry-based approaches toward absolute quantitative proteomics. *Curr Genomics* **9**, 263 (2008).
77. F. Burlina, S. Sagan, G. Bolbach, G. Chassaing, A direct approach to quantification of the cellular uptake of cell-penetrating peptides using MALDI-TOF mass spectrometry. *Nat Protoc* **1**, 200 (2006).

78. R. Q. Wu, X. F. Zhao, Z. Y. Wang, M. Zhou, Q. M. Chen, Novel Molecular Events in Oral Carcinogenesis via Integrative Approaches. *J Dent Res* **90**, 561 (2011).
79. E. Schadt, B. Zhang, J. Zhu, Advances in systems biology are enhancing our understanding of disease and moving us closer to novel disease treatments. *Genetica* **136**, 259 (2009).
80. D. Cai *et al.*, A molecular-imprint nanosensor for ultrasensitive detection of proteins. *Nat Nanotechnol* **5**, 597 (2010).
81. Y. Cui, Q. Wei, H. Park, C. M. Lieber, Nanowire Nanosensors for Highly Sensitive and Selective Detection of Biological and Chemical Species. *Science* **293**, 1289 (2001).
82. J. W. Ndieyira *et al.*, Nanomechanical detection of antibiotic-mucopeptide binding in a model for superbug drug resistance. *Nat Nanotechnol* **3**, 691 (2008).
83. A. L. Andrade, D. M. Souza, M. C. Pereira, J. D. Fabris, R. Z. Domingues, Catalytic effect of magnetic nanoparticles over the H2O2 decomposition reaction. *J Nanosci Nanotechnol* **9**, 3695 (2009).
84. P. Baptista *et al.*, Gold nanoparticles for the development of clinical diagnosis methods. *Anal Bioanal Chem* **391**, 943 (2008).
85. S. Eustis, M. A. el-Sayed, Why gold nanoparticles are more precious than pretty gold: noble metal surface plasmon resonance and its enhancement of the radiative and nonradiative properties of nanocrystals of different shapes. *Chem Soc Rev* **35**, 209 (2006).
86. G. Yurkov, A. Fionov, Y. Koksharov, V. Koleso, S. Gubin, Electrical and magnetic properties of nanomaterials containing iron or cobalt nanoparticles. *J Inorg Mater* **43**, 834 (2007).
87. M.-E. Aubin-Tam, K. Hamad-Schifferli, Structure and function of nanoparticle–protein conjugates. *Biomed Mater* **3**, (2008).
88. Y. Liu *et al.*, Synthesis, stability, and cellular internalization of gold nanoparticles containing mixed peptide-poly(ethylene glycol) monolayers. *Anal Chem* **79**, 2221 (2007).
89. L. Maus, J. P. Spatz, R. Fiammengo, Quantification and reactivity of functional groups in the ligand shell of PEGylated gold nanoparticles via a fluorescence-based assay. *Langmuir* **25**, 7910 (2009).
90. F. Porta *et al.*, Gold nanoparticles capped by peptides. *Mater Sci Eng B* **140**, 187 (2007).
91. D. H. Geho, C. D. Jones, E. F. Petricoin, L. A. Liotta, Nanoparticles: potential biomarker harvesters. *Curr Opin Chem Biol* **10**, 56 (2006).
92. M. M.-C. Cheng *et al.*, Nanotechnologies for biomolecular detection and medical diagnostics. *Curr Opin Chem Biol* **10**, 11 (2006).
93. K. Shrivas, H.-F. Wu, Modified silver nanoparticle as a hydrophobic affinity probe for analysis of peptides and proteins in biological samples by using liquid-liquid microextraction coupled to AP-MALDI-ion trap and MALDI-TOF mass spectrometry. *Anal Chem* **80**, 2583 (2008).
94. Y. F. Huang, H. T. Chang, Analysis of adenosine triphosphate and glutathione through gold nanoparticles assisted laser desorption/ionization mass spectrometry. *Anal Chem* **79**, 4852 (2007).

95. H. Y. Lin, W. Y. Chen, Y. C. Chen, Iron oxide/tantalum oxide core-shell magnetic nanoparticle-based microwave-assisted extraction for phosphopeptide enrichment from complex samples for MALDI MS analysis. *Anal Bioanal Chem* **394**, 2129 (2009).
96. S. D. Sherrod, A. J. Diaz, W. K. Russell, P. S. Cremer, D. H. Russell, Silver nanoparticles as selective ionization probes for analysis of olefins by mass spectrometry. *Anal Chem* **80**, 6796 (2008).
97. K. A. Stumpo, D. H. Russell, Anion Effects on Ionization Efficiency Using Gold Nanoparticles as Matrices for LDI-MS. *J Phys Chem C* **113**, 1641 (2009).
98. A. Housni, M. Ahmed, S. Liu, R. Narain, Monodisperse Protein Stabilized Gold Nanoparticles via a Simple Photochemical Process. *J Phys Chem C* **112**, 12282 (2008).
99. J. D. Keighron, C. D. Keating, Enzyme:nanoparticle bioconjugates with two sequential enzymes: stoichiometry and activity of malate dehydrogenase and citrate synthase on Au nanoparticles. *Langmuir* **26**, 18992 (2010).
100. L. Maus, O. Dick, H. Bading, J. P. Spatz, R. Fiammengo, Conjugation of peptides to the passivation shell of gold nanoparticles for targeting of cell-surface receptors. *ACS Nano* **4**, 6617 (2010).
101. N. L. Rosi, C. A. Mirkin, Nanostructures in biodiagnostics. *Chem Rev* **105**, 1547 (2005).
102. P. D. Rakowska, M. G. Ryadnov, Nano-enabled biomarker discovery and detection. *Biomark Med* **5**, 387 (2011).
103. A. Luchini *et al.*, Smart Hydrogel Particles: Biomarker Harvesting: One-Step Affinity Purification, Size Exclusion, and Protection against Degradation. *Nano Lett* **8**, 350 (2007).
104. C. Fredolini *et al.*, Concentration and preservation of very low abundance biomarkers in urine, such as human growth hormone (hGH), by Cibacron Blue F3G-A loaded hydrogel particles. *Nano Res* **1**, 502 (2008).
105. C. Longo *et al.*, Core-shell hydrogel particles harvest, concentrate and preserve labile low abundance biomarkers. *PLoS ONE* **4**, (2009).
106. E. Cerasoli *et al.*, MiS-MALDI: microgel-selected detection of protein biomarkers by MALDI-ToF mass spectrometry. *Mol Biosyst* **6**, 2214 (2010).
107. Y. Hoshino *et al.*, Design of Synthetic Polymer Nanoparticles that Capture and Neutralize a Toxic Peptide. *Small* **5**, 1562 (2009).
108. L. H. Cazares, J. I. Diaz, R. R. Drake, O. J. Semmes, MALDI/SELDI protein profiling of serum for the identification of cancer biomarkers. *Methods Mol Biol* **428**, 125 (2008).
109. R. John *et al.*, In vivo magnetomotive optical molecular imaging using targeted magnetic nanoprobes. *PNAS*, (2010).
110. M. D. Rowe, D. H. Thamm, S. L. Kraft, S. G. Boyes, Polymer-modified gadolinium metal-organic framework nanoparticles used as multifunctional nanomedicines for the targeted imaging and treatment of cancer. *Biomacromolecules* **10**, 983 (2009).
111. M. D. Rowe, D. H. Thamm, S. L. Kraft, S. G. Boyes, Polymer-Modified Gadolinium Metal-Organic Framework Nanoparticles Used as Multifunctional Nanomedicines for the Targeted Imaging and Treatment of Cancer. *Biomacromolecules* **10**, 983 (2009).

112. A. Bella *et al.*, Conformationally constrained mimetics of laminin peptide YIGSR as precursors for antimetastatic disintegrins. *J Med Chem* **52**, 7966 (2009).
113. M. F. Leber, T. Efferth, Molecular principles of cancer invasion and metastasis (review). *Int J Oncol* **34**, 881 (2009).
114. E. Ruoslahti, Specialization of tumour vasculature. *Nat Rev Cancer* **2**, 83 (2002).
115. I. H. El-Sayed, X. Huang, M. A. El-Sayed, Surface Plasmon Resonance Scattering and Absorption of anti-EGFR Antibody Conjugated Gold Nanoparticles in Cancer Diagnostics: Applications in Oral Cancer. *Nano Lett* **5**, 829 (2005).
116. I. H. El-Sayed, X. Huang, M. A. El-Sayed, Selective laser photo-thermal therapy of epithelial carcinoma using anti-EGFR antibody conjugated gold nanoparticles. *Cancer Lett* **239**, 129 (2006).
117. H. J. K. Ananias, M. C. van den Heuvel, W. Helfrich, I. J. de Jong, Expression of the gastrin-releasing peptide receptor, the prostate stem cell antigen and the prostate-specific membrane antigen in lymph node and bone metastases of prostate cancer. *The Prostate* **69**, 1101 (2009).
118. N. Chanda *et al.*, Bombesin functionalized gold nanoparticles show in vitro and in vivo cancer receptor specificity. *PNAS* **107**, 8760 (2010).
119. K. A. Brogden, Antimicrobial peptides: pore formers or metabolic inhibitors in bacteria? *Nat Rev Micro* **3**, 238 (2005).
120. M. T. Lee, W. C. Hung, F. Y. Chen, H. W. Huang, Mechanism and kinetics of pore formation in membranes by water-soluble amphipathic peptides. *PNAS* **105**, 5087 (2008).
121. Y. Yu, J. A. Vroman, S. C. Bae, S. Granick, Vesicle Budding Induced by a Pore-Forming Peptide. *J Am Chem Soc* **132**, 195 (2009).
122. A. Mecke, D. K. Lee, A. Ramamoorthy, B. G. Orr, M. M. Banaszak Holl, Membrane thinning due to antimicrobial peptide binding: an atomic force microscopy study of MSI-78 in lipid bilayers. *Biophys J* **89**, 4043 (2005).
123. K. Matsuzaki, S. Yoneyama, K. Miyajima, Pore formation and translocation of melittin. *Biophys J* **73**, 831.
124. K. J. Hallock, D. K. Lee, A. Ramamoorthy, MSI-78, an analogue of the magainin antimicrobial peptides, disrupts lipid bilayer structure via positive curvature strain. *Biophys J* **84**, 3052 (2003).
125. S. Qian, W. Wang, L. Yang, H. W. Huang, Structure of transmembrane pore induced by Bax-derived peptide: Evidence for lipidic pores. *PNAS* **105**, 17379 (2008).
126. R. Mani *et al.*, Membrane-dependent oligomeric structure and pore formation of a β-hairpin antimicrobial peptide in lipid bilayers from solid-state NMR. *PNAS* **103**, 16242 (2006).
127. L. Yang, T. M. Weiss, R. I. Lehrer, H. W. Huang, Crystallization of Antimicrobial Pores in Membranes: Magainin and Protegrin. *Biophys J* **79**, 2002.
128. Y. Fang, S. Cheley, H. Bayley, J. Yang, The heptameric prepore of a staphylococcal alpha-hemolysin mutant in lipid bilayers imaged by atomic force microscopy. *Biochem* **36**, 9518 (1997).
129. L. Song *et al.*, Structure of Staphylococcal α-Hemolysin, a Heptameric Transmembrane Pore. *Science* **274**, 1859 (1996).

130. A. W. Thompson *et al.*, Unicellular Cyanobacterium Symbiotic with a Single-Celled Eukaryotic Alga. *Science* **337**, 1546 (2012).
131. M. L. Kraft, P. K. Weber, M. L. Longo, I. D. Hutcheon, S. G. Boxer, Phase separation of lipid membranes analyzed with high-resolution secondary ion mass spectrometry. *Science* **313**, 1948 (2006).
132. C. P. Lechene, Y. Luyten, G. McMahon, D. L. Distel, Quantitative Imaging of Nitrogen Fixation by Individual Bacteria Within Animal Cells. *Science* **317**, 1563 (2007).
133. S. E. Senyo *et al.*, Mammalian heart renewal by pre-existing cardiomyocytes. *Nature* **493**, 433 (2013).
134. H. Jiang *et al.*, Stable isotope imaging of biological samples with high resolution secondary ion mass spectrometry and complementary techniques. *Methods* **17**, 00042 (2014).
135. F. H. C. Crick, The packing of -helices: simple coiled-coils. *Acta Crystallogr* **6** 689 (1953).
136. G. Grigoryan, A. E. Keating, Structural specificity in coiled-coil interactions. *Curr Opin Struct Biol* **18**, 477 (2008).
137. E. Vives, P. Brodin, B. Lebleu, A truncated HIV-1 Tat protein basic domain rapidly translocates through the plasma membrane and accumulates in the cell nucleus. *J Biol Chem* **272**, 16010 (1997).
138. D. E. Leckband, C. A. Helm, J. Israelachvili, Role of calcium in the adhesion and fusion of bilayers. *Biochem* **32**, 1127 (1993).
139. N. Kucerka *et al.*, Structure of Fully Hydrated Fluid Phase DMPC and DLPC Lipid Bilayers Using X-Ray Scattering from Oriented Multilamellar Arrays and from Unilamellar Vesicles. *Biophys J* **88**, 2626 (2005).
140. S. M. Kelly, T. J. Jess, N. C. Price, How to study proteins by circular dichroism. *Biochim Biophys Acta* **10**, 119 (2005).
141. D. T. Clarke, Circular dichroism and its use in protein-folding studies. *Methods Mol Biol* **752**, 59 (2011).
142. A. Rodger, How to study DNA and proteins by linear dichroism spectroscopy. *Sci Prog* **91**, 377 (2008).
143. M. R. Hicks, J. Kowalski, A. Rodger, LD spectroscopy of natural and synthetic biomaterials. *Chem Soc Rev* **39**, 3380 (2010).
144. M. Zasloff, Antimicrobial peptides of multicellular organisms. *Nature* **415**, 389 (2002).
145. M. A. Schmitt, B. Weisblum, S. H. Gellman, Interplay among Folding, Sequence, and Lipophilicity in the Antibacterial and Hemolytic Activities of α/β-Peptides. *J Am Chem Soc* **129**, 417 (2006).
146. C. P. Lechene, G. Y. Lee, J. C. Poczatek, M. Toner, J. D. Biggers, 3D Multi-isotope Imaging Mass Spectrometry Reveals Penetration of ¹⁸O-Trehalose in Mouse Sperm Nucleus. *PLoS ONE* **7**, e42267 (2012).
147. M. L. Kraft *et al.*, Quantitative analysis of supported membrane composition using the NanoSIMS. *Appl Surf Sci* **252**, 6950 (2006).
148. W. Römer *et al.*, Sub-cellular localisation of a 15N-labelled peptide vector using NanoSIMS imaging. *Appl Surf Sci* **252**, 6925 (2006).

149. R. L. Wilson *et al.*, Fluorinated Colloidal Gold Immunolabels for Imaging Select Proteins in Parallel with Lipids Using High-Resolution Secondary Ion Mass Spectrometry. *Bioconjugate Chem* **23**, 450 (2012).
150. P. D. Rakowska, B. Lamarre, M. G. Ryadnov, Probing label-free intracellular quantification of free peptide by MALDI-ToF mass spectrometry. *Methods* **20**, 00112 (2014).
151. T. Holm *et al.*, Studying the uptake of cell-penetrating peptides. *Nat Protoc* **1**, 1001 (2006).
152. J. P. Richard *et al.*, Cell-penetrating Peptides: A Reevaluation Of The Mechanism Of Cellular Uptake. *J Biol Chem* **278**, 585 (2003).
153. A. Bolhassani, S. R. Yazdi, DNA immunization as an efficient strategy for vaccination. *Avicenna J Med Biotechnol* **1**, 71 (2009).
154. J. G. Huang, T. Leshuk, F. X. Gu, Emerging nanomaterials for targeting subcellular organelles. *NanoToday* **6**, 478 (2011).
155. F. Burlina, S. Sagan, G. Bolbach, G. Chassaing, Quantification of the cellular uptake of cell-penetrating peptides by MALDI-TOF mass spectrometry. *Angew Chem Int Ed Engl* **44**, 4244 (2005).
156. C. T. Dollery, Intracellular drug concentrations. *Clin Pharmacol Ther* **93**, 263 (2013).
157. C. A. Lipinski, Drug-like properties and the causes of poor solubility and poor permeability. *J Pharmacol Toxicol Methods* **44**, 235 (2000).
158. R. Trehin *et al.*, Cellular internalization of human calcitonin derived peptides in MDCK monolayers: a comparative study with Tat(47-57) and penetratin(43-58). *Pharm Res* **21**, 33 (2004).
159. I. A. Ignatovich *et al.*, Complexes of plasmid DNA with basic domain 47-57 of the HIV-1 Tat protein are transferred to mammalian cells by endocytosis-mediated pathways. *J Biol Chem* **278**, 42625 (2003).
160. E. Vives, J. P. Richard, C. Rispal, B. Lebleu, TAT peptide internalization: seeking the mechanism of entry. *Curr Protein Pept Sci* **4**, 125 (2003).
161. E. Vives, Cellular uptake of the Tat peptide: an endocytosis mechanism following ionic interactions. *J Mol Recognit* **16**, 265 (2003).
162. A. D. Frankel, C. O. Pabo, Cellular uptake of the tat protein from human immunodeficiency virus. *Cell* **55**, 1189 (1988).
163. L. K. Andersen *et al.*, Cell volume increase in murine MC3T3-E1 pre-osteoblasts attaching onto biocompatible tantalum observed by magnetic AC mode atomic force microscopy. *Eur Cell Mater* **10**, 61 (2005).
164. T. Imaizumi *et al.*, Effect of human basic fibroblast growth factor on fibroblast proliferation, cell volume, collagen lattice contraction: in comparison with acidic type. *J Dermatol Sci* **11**, 134 (1996).
165. E. A. Nance *et al.*, A Dense Poly(Ethylene Glycol) Coating Improves Penetration of Large Polymeric Nanoparticles Within Brain Tissue. *Sci Transl Med* **4**, 149ra119 (2012).
166. H. Otsuka, Y. Nagasaki, K. Kataoka, PEGylated nanoparticles for biological and pharmaceutical applications. *Advanced Drug Delivery Reviews* **55**, 403 (2003).
167. E. Koren, V. P. Torchilin, Cell-penetrating peptides: breaking through to the other side. *Trends Mol Med* **18**, 385 (2012).

168. G. T. Hermanson, in *Bioconjugate Techniques (Second Edition)*. (Academic Press, New York, 2008), pp. 276-335.
169. J. Manson, D. Kumar, B. Meenan, D. Dixon, Polyethylene glycol functionalized gold nanoparticles: the influence of capping density on stability in various media. *Gold Bull* **44**, 99 (2011).
170. J. V. Jokerst, T. Lobovkina, R. N. Zare, S. S. Gambhir, Nanoparticle PEGylation for imaging and therapy. *Nanomedicine* **6**, 715 (2011).
171. H. Otsuka, Y. Nagasaki, K. Kataoka, PEGylated nanoparticles for biological and pharmaceutical applications. *Adv Drug Deliv Rev* **55**, 403 (2003).
172. J. Suh *et al.*, PEGylation of nanoparticles improves their cytoplasmic transport. *Int J Nanomedicine* **2**, 735 (2007).
173. A. Mayer, M. Antonietti, Investigation of polymer-protected noble metal nanoparticles by transmission electron microscopy: control of particle morphology and shape. *Colloid Polym Sci* **276**, 769 (1998).
174. O. Balmes, J. O. Malm, N. Pettersson, G. Karlsson, J. O. Bovin, Imaging atomic structure in metal nanoparticles using high-resolution cryo-TEM. *Microsc Microanal* **12**, 145 (2006).
175. A. Coutinho, L. M. S. Loura, M. Prieto, FRET studies of lipid-protein aggregates related to amyloid-like fibers. *J Neurochem* **116**, 696 (2011).
176. B. M. Bulheller, A. Rodger, J. D. Hirst, Circular and linear dichroism of proteins. *Phys Chem Chem Phys* **9**, 2020 (2007).
177. S. E. Jin, J. W. Bae, S. Hong, Multiscale observation of biological interactions of nanocarriers: from nano to macro. *Microsc Res Tech* **73**, 813 (2010).
178. K. L. Moore *et al.*, NanoSIMS analysis of arsenic and selenium in cereal grain. *New Phytologist* **185**, 434 (2010).
179. S. K. Pandey, C. R. Suri, M. Chaudhry, R. P. Tiwari, P. Rishi, A gold nanoparticles based immuno-bioprobe for detection of Vi capsular polysaccharide of Salmonella enterica serovar Typhi. *Mol Biosyst* **8**, 1853 (2012).
180. P. Botella *et al.*, Multifunctional hybrid materials for combined photo and chemotherapy of cancer. *Dalton T* **41**, 9286 (2012).
181. I. Coin, M. Beyermann, M. Bienert, Solid-phase peptide synthesis: from standard procedures to the synthesis of difficult sequences. *Nat Protoc* **2**, 3247 (2007).
182. B. J. H. Kuipers, H. Gruppen, Prediction of Molar Extinction Coefficients of Proteins and Peptides Using UV Absorption of the Constituent Amino Acids at 214 nm To Enable Quantitative Reverse Phase High-Performance Liquid Chromatography−Mass Spectrometry Analysis. *J Agric Food Chem* **55**, 5445 (2007).
183. M. P. Mingeot-Leclercq, M. Deleu, R. Brasseur, Y. F. Dufrene, Atomic force microscopy of supported lipid bilayers. *Nat Protoc* **3**, 1654 (2008).
184. C. Fernandez-Lopez *et al.*, Highly controlled silica coating of PEG-capped metal nanoparticles and preparation of SERS-encoded particles. *Langmuir* **25**, 13894 (2009).
185. M. Szymanski, A. P. F. Turner, R. Porter, Electrochemical Dissolution of Silver Nanoparticles and Its Application in Metalloimmunoassay. *Electroanal* **22**, 191 (2010).